UNIVERSITAT DE BARCELONA

Development of a nano sensor for direct-electric free-label detection of DNA's hybridization and single nucleotide polymorphism

Rosa Letizia Zaffino

Aquesta tesi doctoral està subjecta a la llicència ***Reconeixement 3.0. Espanya de Creative Commons***.

Esta tesis doctoral está sujeta a la licencia ***Reconocimiento 3.0. España de Creative Commons***.

This doctoral thesis is licensed under the ***Creative Commons Attribution 3.0. Spain License***.

DEVELOPMENT OF A NANO SENSOR FOR DIRECT-ELECTRIC FREE-LABEL DETECTION OF DNA'S HYBRIDIZATION AND SINGLE NUCLEOTIDE POLYMORPHISM

ROSA LETIZIA ZAFFINO

Memoria presentada por optar al titúlo de Doctor

Programa de doctorado en
Nanociencias y Nanotecnologías

Departamento de Electrònica
Universitat de Barcelona

Director
Dra. Mònica Mir

Tutor
Prof. Josep Samitier

Barcelona, 2015

Rosa Letizia Zaffino: *Development of a nano sensor for direct-electric free-label detection of DNA's hybridization and single nucleotide polymorphism,* Memoria presentada por optar al titúlo de Doctor, ©

Science is the ultimate pornography, analytic activity whose main aim is to isolate objects or events from their contexts in time and space. This obsession with the specific activity of quantified functions is what science shares with pornography.

—J.C. Ballard, *The Atrocity exhibition*

ABSTRACT

The search for analytical tools suitable for wide-scale application of DNA analysis is an hot research topic, although thanks to well-established microarray based technology, analysis of DNA sequences and SNP detection can be worked out through a fairly laboratory routine.

DNA analysis has nowadays become of increasing interest for several different purposes, mainly thanks to the successful employment of microarray technology, characterized by high sensitiveness and high-throughput analysis, which rapidly advanced genetics leading to development of many fields of application of DNA analysis, which keeps high the trend in alternative technologies, which could overcome inherent limitations of microarrays technology.

In this regard, many efforts have been spent to study electrochemical/-electrical based detection strategies by means of which it could be possible to accomplish sensitive analysis by using portable equipments, cheaper and more practical than optical ones, and with scalable-devices compatibles with standard microelectronic processing.

Emerging nano-probes with increased chemical-physical properties are considered with growing interest in DNA biosensors as ideal candidates to enhance electrochemical/electrical based detection systems. Among these, nano-gaps adjusted to fit DNA, or in general analyte molecules sizes, are very promising because they can enable direct electrical detection schemes, thus providing a straightforward electronic analogue of the successful DNA microarray standard.

Electrical properties of DNA have been the principal focus of many experimental and theoretical research, since early experimental founding confirmed an old hypothesis, for its relevance in the biological function of DNA, being related both with damage and base repair, but also for the appealing potential for biosensor and, in general, in bioelectronic applications.

Thanks to its peculiar interactions, it allows versatile manipulations of the structure, compared to other organic and synthetic polymers which have been considered for such purposes. Even though many questions still are open on electrical properties of DNA, it is generally accepted that DNA's conductivity is intimately linked with details of the sequences involved, its length and the overall environment in which molecule is found. The sensitivity to structure's alteration, as that induced by the presence of a mutation, confirmed by experimental and theoretical works allows to exploit DNA electrical properties for biosensor applications.

Relying on this agreed description of DNA electrical properties features, the general aim of this thesis was to explore the possibility of developing a platform for the direct transduction of DNA hybridization event based on a nano-gap device and electrical signaling enabled by long range electron transport through DNA molecules.

In order to achieve this objective we faced several issues of relevance for current scientific and technological development. The thesis is organized in five chapters, namely: "DNA analysis ", "DNA charge migration", "Nano-sensors: Fabrication and Characterization", "Capture Probes selective addressing on nano-gap electrodes", "DNA detection in nano-gap sensors" , and "General Conclusions".

The first chapter gives a broad overview of the technologies applied in DNA analysis methods with the objective of establishing the background to the proposal of this work, and to define the aim in light of existing results in the attempt of improving current field state-of-art. By largely analyzing benefit and drawbacks of proposed analytical systems we could fix the targets of our works. These will be explicitly commented and outlined at the end of this chapter, where a schematic of the conceived system and its working principles are detailed.

The second chapter contains a large review of DNA charge migration literature, treating both experimental and theoretical background developed regarding this issue with the proposal of introduce the current understanding of this phenomenon. Thanks to this analysis we will be able to agree platform design, and its realization, which is then further treated in the following chapter.

In chapter three we presents technology processing and characterization methods explored to fabricate our nano-gaps system further used in electrical detection of DNA. Each process applied is briefly introduced on a general ground and it is further detailed to met our need. Similarly we introduce the different techniques applied in order to characterize fabrication results, by means of which we will be able to validate sensor processing strategy.

In chapter four we deal with the problem of achieve selective assembly of the CPs used on each nano-gap electrodes. Results from three applied processes, namely standard SAM adsorption from solution, electrochemical stripping and E-field driven immobilization are compared by means of electrochemical characterization, in such a way to determine the best strategy.

In chapter five we discuss measurements considered and results obtained in order to demonstrate the feasibility of the platform realized for the label-free detection hybridization of DNA and SNP. This will be performed by considering several optimization testing, and in case of need, by using a signal amplification strategy based on gold nanoparticles (GNP) and gold enhancement treatment.

General conclusions on the presented work are finally outlined in the last chapter.

PUBLICATIONS

Some ideas and figures have appeared previously in the following publications:

- R.L.Zaffino, W.A. Pardo, M.Mir, J.Samitier, Electrochemical DNA bio-sensor at the nanoscale, published in "Biosensors and Cancer" King's College London, Science Publishers 2012., ISBN: 978-1-57808-734-1 06/2013.
- R.L.Zaffino, M.Mir and J.Samitier, Label-free detection of DNA hybridization and single point mutation in a nanogap biosensor, Nanotechnology 25 (2014) 105501.
- R.L. Zaffino, T. Galan, W. A. Pardo, M. Mir, J. Samitier, Nanoprobes for enhanced electrochemical DNA sensors, Wiley Interdisciplinary Reviews Nanomedicine and Nanobiotechnology, DOI:10.1002/wnan.1344, 05/2015.
- R.L. Zaffino, D.Mauri, M. Mir, Analysis of electric field influence in nano-gap electrodes applications, under review for Electrophoresis.

CONTENTS

LIST OF FIGURES

LIST OF TABLES

ACRONYMS

DNA Deoxyribonucleic Acid

RNA Ribonucleic Acid

PNA Polipeptide nucleic Acid

CP Capture probe

SNP Single Nucleotide polimorphism

ET Electron Transfer

CT Charge Transport

LoRET Long range electron transfer

SEM Scanning Electron Microscopy

OM Optical Microscopy

SOI Silicon on Insulator

FIB Focus Ion Beam

TOF-SIMS Time of flight Secondary Ion Mass Spectrometry

AFM Atomic Force Microscope

SPM Scannelling Probe Microscope

STM Scanning Tunnelling Microscope

RIE Reactive Ion Etching

PVD Physical Vapor Deposition

CVD Chemical Vapor Deposition

PDMS Polydimethylsiloxane

PMMA Polymethylmethacrylate

DDI Double Deionized

SCC Saline Sodium Cytrate

EDTA Ethylenediaminetetraacetic acid

PBS Phosphate Buffer Saline

TCEP 2-carboxylethyl phosphine hydrochloride

LOD Limit of Detection

UV Ultra Violet

GNP Gold Nano Particle

NT Nano Tube

CNT Carbon Nano Tube

SWNT Single Walled Nano Tube

NW Nano wire

ISFET Ion Sensitive field effect transistor

FET Field Effect Transistor

SAM Self Assembled Monolayer

HF Hartree-Fock

DFT Density Funcional Theory

QMD Quantum Molecular Dynamic

CV Cyclic Voltammetry

DPV Differential Pulse Voltammetry

DEP Dielectrophoresis

WE Working Electrode

RE Reference Electrode

CE Counter Electrode

DC Direct Current

1

DNA ANALYSIS

The helical embrace of nucleic acids in the deoxyribonucleic acid (DNA) molecule is the place where nature encodes the alphabet and the rules to accomplish the complexity of life. A simple language, built with 4 letters alphabet is sufficient, and in some case also redundant, to provide the great variety of living organisms, and especially to guarantee one of the most peculiar feature of life, i. e. its reproducibility.

Since discovery of its structure, almost sixty years ago, on the back of parallel micro-nano technology advancements, our knowledge over DNA molecule and on the complex mechanisms regulating transmission of genetic information, has rapidly grown. Sensitive and high-throughput DNA analysis, based wether on detection of specific DNA sequences, than on that of precise sequence variations prompted by introduction of DNA microarrays technologies, boosted Genetics, and flourished related fields and applications.

DNA analysis technologies have advanced fast following a similar evolution as that fixed by Moore law for micro-chip. In this chapter we will give a wide overview of DNA analysis methods evolutions, including most recent advancements reached by nano-probes enhanced systems of detection. This will delimitate the technological framework of the thesis, and the challenges faced by the proposals of the work, which are stated at the end of the chapter with the general description of the proposed system, and the specific objectives targeted in each stage of its realization.

1.1 THE DNA MOLECULE: A BRIEF PORTRAIT

Firsts evidences of DNA arose in 1869, during the war of Crimea. While working with the cells extracted by the bondages of injured soldiers, the physician Friedrich Miescher observed the existence of a large molecule, inside the nucleus that he called nuclein. Few years later, he also argued the implication of nuclein in the transmission of genetic information [24].

Although, the scientific community was, at that time, firmly convinced that proteins accomplish for this function, and rejected the hypothesis. It was not until the 40's that the role of DNA in the transferring of cell's genetic information was finally showed by Averin, and his colleagues [3].

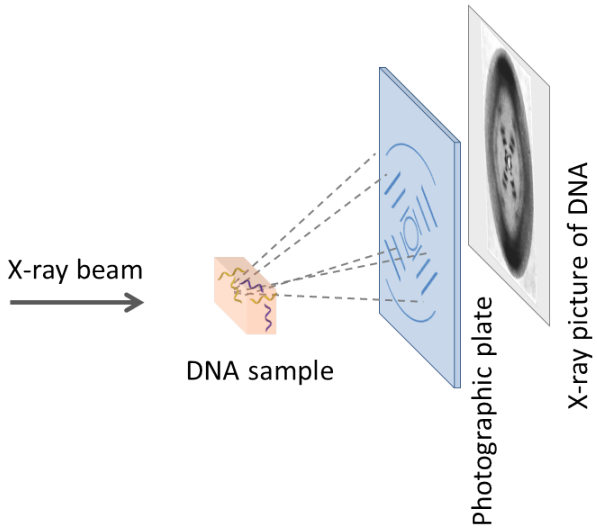

Figure 1: Schematic of the experimental system used to obtain X-ray DNA characterization, showing top view projection of 3D molecular double helix structure.

The intense studies of these years culminated in 1953 with the work by Watson and Crick on the structure of DNA [51]. Thanks to the X-Ray diffraction image taken by Rosalind Franklin [88] one year before Fig. 1, and the brilliant intuition of Watson and Crick about the specificity of interaction between complementary bases, allowed accounting for all the data and observations on DNA in the elegant, and simple, double helix model. The structure of DNA is represented by right-handed oriented

double-helix, today known as B-DNA, the form of DNA which is the most predominant in nature.

DNA's popularity, fifty years after the elucidating of it structure, goes well beyond the border of scientific context. The peculiar geometry of DNA, the *MonnaLisa* of science, as it has been baptized, has in fact inspired also many art works during the years [68]. Nucleotides in the DNA helix are arranged in such a way that a major groove alternates to a minor, being characterized for having 10 nucleotides per turn, 3,4 nm long Fig. 2.

The molecule is characterized by a highly negative charge density, which attracts through electrostatic interactions, the positive charged water ions present in solution, thus contributing to structure stability. The global negative charge present in DNA comes from the phosphate groups exposed on its backbone. The alternating repetition of nucleotides, formed by a sugar and a base, gives rise to the specific sequence, which codes genetic information.

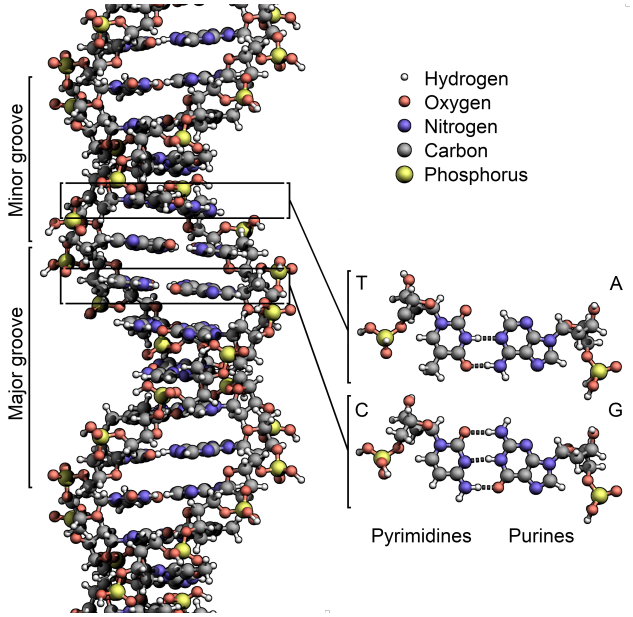

Figure 2: Double-helix DNA structure: major and minor DNA groove, characterized by different length sizes according nucleotides base-pairing.

Nucleotides are held together by hydrogen bonds that confer to the molecule a stable configuration. However, it conformation, or it 3D struc-

ture is finally determined by the environment, and in particular by the salt concentrations.

As a consequence of this, alternative DNA forms, namely the A-DNA and Z-DNA, there exist and where observed in dehydrated DNA sample, and at high salt concentrations [38], [127]. The A-DNA is much similar to the common B-DNA: it is also right-handed, but with 11 bases per turn which results in a more compact, and shorter, double helix. On the other side, the Z-DNA is left-handed with 12 bases per turn and a repetition each 2 base pairs.

The huge amount of hydrogen bonds between complementary bases assures the stability of DNA. While the stacking interactions between bases, and the electrostatic coulomb repulsions of phosphate groups on the backbone, determines the overall flexibility of the molecule, measured through persistence length, which is the parameter used to characterize the flexibility of macro-molecules. This is strongly dependent by the ionic strength of the environment, and it is an indicator of the molecule stability against environment's induced perturbations. DNA'mechanical properties are of particular relevance for its biological function. In fact, transcriptions and replication requires, as first step, the denaturation (unwinding and separation) of the double helix, followed by annealing or re-naturalization, as it is called the spontaneous pairing to a complementary RNA sequence.

DNA is the common denominator of living systems, as such, DNA nucleotides sequence detection is of primary importance for the understanding of life mechanisms, and for the diagnosis of different diseases. To access the genetic information contained in the genes of a given species, and among different individuals of the same, allows to study the relationships between genes and phenotypes, relevant also for evolutionary biology research, or between genes and diseases which constitutes a central issue for the development of pharmaco-genomic, and genetic medicine.

In the early '80, fingerprinting of DNA by sequencing detection was moving its first steps.

This technology has been applied to the identifications of accident victims or for forensic applications, as in the case of crimes attributions, or to solve paternity issues. Prompted by the strategic importance that the detection of specific DNA sequence has with respect several fields, the

development of technologies suitable, and sensitive, for the detection of specific DNA sequences, has catalyzed lot of research in the past decades.

A great impulse was given by Human Genome Project, an international scientific flagship undertaken with the proposals of sequencing the entire human genome, under which rapid development of sensitive DNA biosensors integrated in dense microarray systems, allowing multiplexed parallel analysis. A general overview on DNA analysis technologies, and a state of art in the field will be presented in the following sections.

1.2 DNA ANALYSIS: BIOSENSORS

According the standard definition, provided by the IUPAC recommendations [39], a biosensor is "a device that uses specific biochemical reactions mediated by isolated enzymes, DNA, immune-systems, tissues, organelles, or whole cells to detect chemical or biochemical compounds usually by electrical, thermal or optical signals".

A basic biosensor assembly includes, a molecular receptor, the bio-interface, a physical transducer and a processor as schematized in Fig. 3. These devices are used to detect molecules by means of the biological reaction following selective capture of the target and formation of the complex target-analyte at the bio-interface; the physical transducer provides a method to translate this event into a detectable signal.

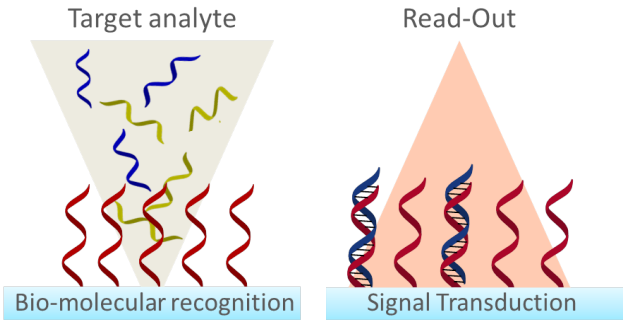

Figure 3: Schematic of biosensor working: target-probe capture on bio-molecular recognition interface trigger detection, after proper signal transduction.

The efficiency of molecular recognition level, or bio-interface, of a biosensor strongly contributes to the enhancement of its response, and for this

reason much efforts are still devoted to the study and optimization of biological interfaces for application in biosensors. The phenomenon of spontaneous biomolecules self-assembly, through which it is possible to produce functional system at a solid (metallic) surface, has been of fundamental importance for the stable immobilization of the bio-receptors on biosensor surface.

Biosensors applied to DNA analysis use as recognition signal the hybridization between two complementary ssDNA which is driven by the base-pair interaction, proper of nucleic acid. The molecular recognition element of a DNA biosensor is formed by immobilized oligonucleotides on the sensor surface. Binding of ssDNA probes on a substrate can be achieved by means of several surface chemistry reactions, mainly based on self-assembling: absorption of thiol terminated oligo-probes on gold surface, which will be treated in chapter 4, is among the most common used.

The nature of the transduction element used plays an important role to determine the strategy of immobilization. According to the physic-chemical mechanisms exploited by the transducer, DNA biosensors classify in optical, electrical-electrochemical, and mass-sensitive. DNA biosensors based on these different transduction mechanisms have been developed [122].

Most optical DNA biosensors are based on monitoring of the fluorescent signal change from a label compound attached to the target after polymerase chain reaction (PCR) amplification, which is detected after the hybridization of target with the probe [32].

Fluorescent read-out systems are very sensitive, with detection limits as low 10^7 $molecules/cm^2$ [28]. Such strategy is successfully applied by gene-chips microarray allowing thousands of probe sequences parallel analysis, as we will discuss further in section.

In order to overcome inherent limitation of fluorescent based detection, as image corruption from photo-bleaching of dyes, or loss of sensitivity due to cross-talking, alternative optical read-out have been explored, as for example in Surface Plasmon Resonance (SPR) based detection [26].

A laser source is used to excite the electrons present at a thin metal layer, interfaced between a high, and a low, refractive index material Fig. 4.

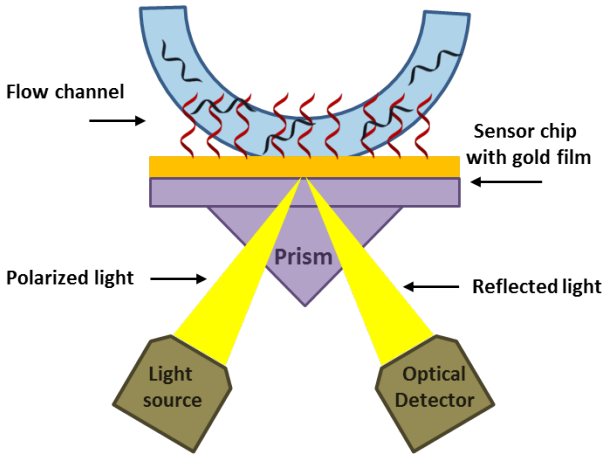

Figure 4: Scheme of a SPR biosensor

The onset of resonance, occurring at a certain diffraction angle, results in the reduction of reflected light, and allows measuring the layer properties. This technique has been largely employed for the real-time study of molecular interactions, by monitoring the shift of SPR signal. The change of SPR signal is due to the binding of delivered molecules, complementary to proper immobilized

DNA receptors, on the SPR substrate. It permits to calculate equilibrium and kinetic constants, underlying energetics of the interaction. Its involvement in biosensor applications follows straightforwardly, but developed systems are mainly restricted to research applications. A remarkable feature of the SPR based detection is that it does not rely on the use of reporter molecules, in contrast to the fluorescent optical read-out. Although, in order to obtain competitive platforms, the amplification of signal by means of PCR is needed in both optical sensors.

Mass-sensitive devices exploit the mass-transfer associated to ligand-receptor biochemical reactions. They rely uniquely on gravimetric (mass) measurement, and can be thus used for label-free detection. In the case of DNA hybridization, although it is easy to figure out that the formation of dsDNA is accompanied by a mass increase, it is not hard to imagine that an ordinary balance, although the most sensitive, cannot work out this job.

The high-sensitivity required for this measurement is achieved by using a Quartz Crystal Microbalance (QCM), Fig. 5.

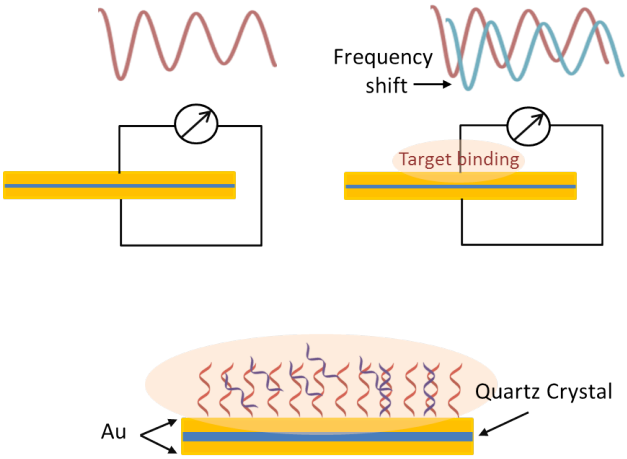

Figure 5: Scheme of a QCM biosensor

Quartz Crystal is a piezoelectric material which experiences a mechanical deformation following the application of a voltage. Under an alternating current, the quartz behaves like a mechanical resonator with a proper resonance frequency depending also by the crystal thickness, and which can be determined with high accuracy. Mass-addition on the crystal surface alters the resonator thickness resulting in a shift of the resonance frequency which can be correlated to the mass-change, which leads to its quantification.

Bio-molecular interactions detection by probing of acoustic wave change is implemented in Surface Acoustic Wave sensors (SAW). This kind of sensor, generates a mechanical wave by means of electrical signal, which is influenced by the immobilized biomolecules on its surface. The device then transduces this wave back into an electrical signal, and the changes in amplitude and phase are reported in relation to the quantity of molecules on the surface.

Both QCM and SAW offers high sensitivity. However, the full set-up required is quite complex and not suited for commercial DNA diagnostic applications, being set aside just for research use.

Electrical, and electrochemical based, biosensors offer the unique advantage that the recognition signal is electrical at its origin, in such a way that the signal transduction is high simplified, with consequent reduction of overall complexity and costs of process realization. In these devices,

hybridization detection is achieved by means of monitoring the current changes at controlled potentials following the formation of dsDNA on a proper surface.

Moreover, these devices are easily to adapt for miniaturization, and compatible with standard CMOS fabrication technologies, which mades of the electrical/electrochemical based read-out, a very attractive one for wide-scale DNA applications. High-sensitive analysis by scalable affordable devices is, by far, the most important requirement for the development of biosensors useful for wide-scale, and point-of-care, tailored applications.

For this reason, considerable efforts have been devoted to the development of electrical/electrochemical DNA biosensors. A review of the systems explored in this field will be given in the following.

1.2.0.1 *Microarrays*

A microarray is a 2D composition of biosensors on a solid substrate that permits the multiplexing of a large amounts of bio-receptors in the same assay, using high-throughput screening, and parallel detection, of all the biosensors integrated in the array [45].

This technology exploits a hybridization's detection protocol, in which sequence specific DNA detection, is achieved through the fluorescent emission of the label dyes, provided on target's molecules, activated following the hybridization with specific probes, immobilized on the surface Fig. 6, thus triggering detection. By exploiting the possibility of attaching nucleic acid on different substrates, and thanks to the great efforts spent into the development of sensitive scanning technologies, microarray are nowadays ables to express very high analytical performances, with increased throughput of results, by parallel and multiplexed detection of samples.

Since their introduction, microarrays have been intensively applied in therapeutic and biomedical applications. Genomic research and, in general, the field of DNA-based diagnostic applications, are among that's which have received more benefits from the introduction of this technol-

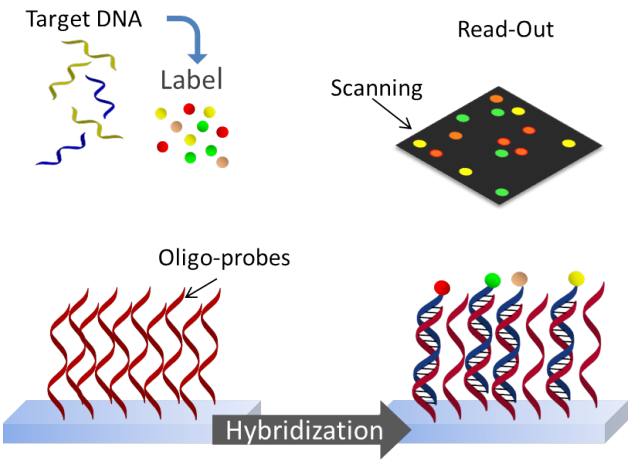

Figure 6: Steps involved in DNA analysis by Microarray.

ogy. In fact, microarrays were initially especially designed for sequencing, and gene expression monitoring, analysis.

Nowadays their applications are wider, being also used for SNP analysis, genomic diseases, drug discovery and development, forensic analysis, military defense, food analysis, and detection of genetically modified organism, among others.

The ability for multi-sample and multiplexed detection, allowing to perform many and long experiments in just one step assay, has further extended the use of this technology to many other emerging field, such as Protein Microarrays (applied for proteins function, personalized medicine, protein interaction, drug discovery and development), Tissue Microarrays (target/biomarkers discovery), Low Complexity Microarray, Carbohydrate Microarrays. Although the increasing number of applications, gene expression still covers the great part of microarray market.

Along with the development of advanced manufacturing techniques, and thank to the increase of scanner's resolution, denser microarrays allowing to locate more features, in the same space, have been developed. Parallel to this development, techniques for multiple-tiling have been also proposed [37], [73].

Although improvements, it is considered that the microarray technology already approached its maturity. Microarray's density is not only

bounded from below by topology cues, but also by the inherent limit posed by the optical scanning detection.

1.3 ELECTROCHEMICAL SENSORS FOR DNA ANALYSIS

Observation of DNA electro-activity boosted many research devoted to develop biosensors based on electrochemical detection methods, Fig. 7. Poor results coming from first attempts of direct electrochemistry of nu-

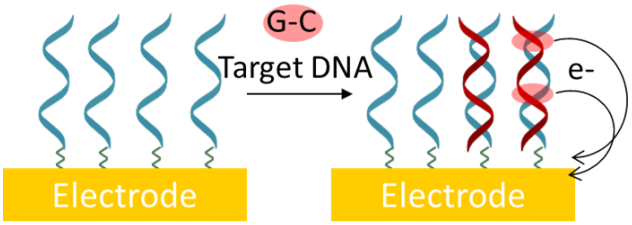

Figure 7: Schematic of direct electrochemical DNA sensor

cleic acids rapidly soften the initial expectations. Out-coming signals of guanine redox base residues, not only, were irreversible, but required also high applied potentials leading to a higher background compromising a clear detection. As a way to overcome this difficulty, other bases, such as ionosine, which oxidizes at different applied potentials, were involved to substitute guanine in the probe sequence, but reporting similar problems [81].

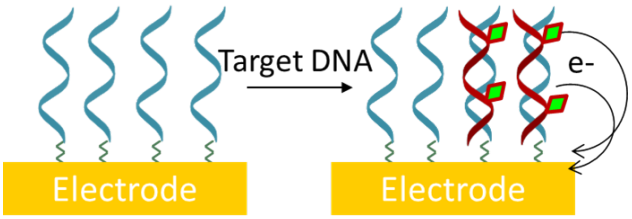

Figure 8: Scheme of electrochemical detection by using a redox active label.

In the early '80, the Palecek's group initiated investigations with DNA modified electrodes [80] based on the strong adsorption of DNA at metallic surfaces. Thanks to the self-assembly process, the electrodes could be

easily functionalized just by immersion in a solution containing nucleic acids, during short times. Modified electrodes were analyzed by adsorptive stripping analysis, a voltametric based methodology introduced by the same group [82]. This strategy improved detection sensitivity of direct electrochemical systems by several orders of magnitudes allowing also volume sample reduction.

In the following years, in order to improve signal-to-noise ratio of such systems, proper redox indicators for application in DNA biosensors were started to be studied Fig. 8.

The interaction of DNA with small molecules, able to intercalate along DNA structure or of DNA groove, was used for this purpose. Berg was pioneering in this field, starting seminal studies on the interaction of DNA with electro-active, not-covalently bounded, intercalators,
DNA groove binders [6], Fig. 9. Covalently linked redox labels have been

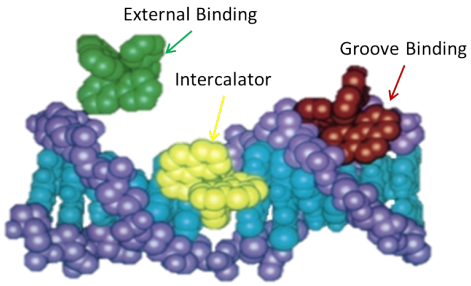

Figure 9: Binding modes to a DNA molecules

also widely applied in electrochemical DNA biosensors. In this case the label is introduced mainly by two different strategies. PCR offers the proliferation of millions of starting DNA target copies, and permits analyte labelling, by introducing one of the amplification primer, already labelled.

Another widespread method is the use of a sandwich platform, Fig. 10.

In this kind of assay, the target's analyte is captured between two specific DNA probes in a sandwich-like order, with the target bound from one side, by the capture probe immobilized on the substrate. The target is then sandwiched with another labeled probe added in a subsequent incubation. The label is activated after complexing with the target DNA thus leading to its detection. This strategy is useful to increase the signal-to-

noise ratio by increasing the signal obtained with the label. For this pur-

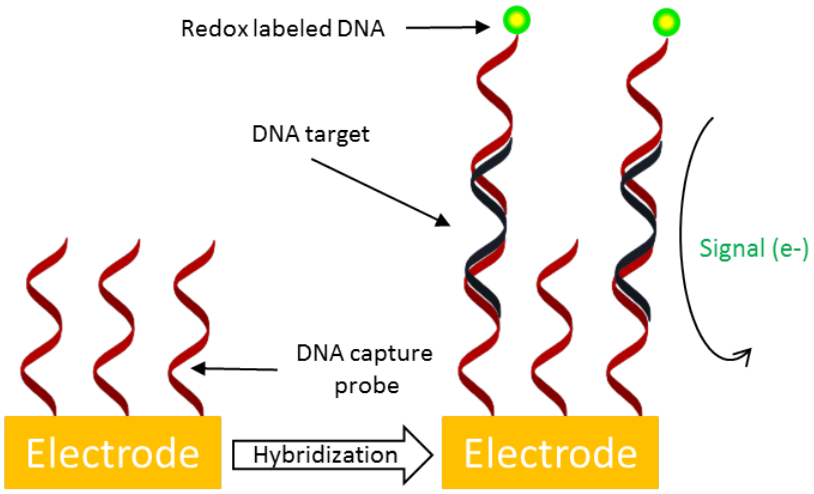

Figure 10: Scheme of electrochemical detection in a sandwich sensor assembly.

pose similar detection schemes, enzymes (horseradish peroxidase and alkaline phosphatase) [27], and redox molecules (ferrocene and ruthenium) are the principal electrochemical labels involved in the existing platforms [113].

Device employing a redox-active marker, and based on monitoring the changes in current peaks of the redox species bound at the target (or probe), was also developed. Once the duplex is formed, the whole system is exposed to a solution of the indicator, so that the hybridization signal is proportional to the surface concentration of this latter. Redox-indicators with similar detection strategy have been explored after this strategy was proposed. In these platforms, the efficiency is linked to the properties of used marker. Among these, the possibility of reversible electron transfer at low applied potentials, and the ability to differentiate between ssDNA (probe) and dsDNA (target-probe compound), are the most important.

Versatility of DNA conformational structure helped in the construction of original platforms not able for other type of bio-receptors. It has been used to develop a reagent-less electrochemical device allowing pico molar limit of detection (LOD).

This biosensor involves a ferrocene-labeled DNA, molecular beacon-likes, with a stem-loop structure which is assembled at a gold electrode,

and analyzed by standard electrochemical analysis based on Cyclic Voltamperometry (CV). The stem-loop oligonucleotide carries a thiol functional group at the side, where it is immobilized on gold, and a ferrocene group at the opposite one, Fig. 11. The conformational change, following hybridization, is used in the sequence-specific detection of DNA [33].

The loop is closed by few complementary bases in the opposite side of the immobilized capture probe, keeping the ferrocene redox molecule close to the electrode. Ferrocene is found at a different distance from the gold surface before and after hybridization, so that the rate of electron transfer differs consequently.

The ferrocene marker is closer to the electrode surface in absence of the complementary target. When this latter is added, the stem-loop spontaneously disrupt to a rigid-rod-like structure which has the ferrocene at a larger distance from the electrode surface. An incubation time of 30 minutes is sufficient to permit the sensitive, and selective, detection of DNA at concentrations as low as 10 pM. The reusability of this biosensor, after

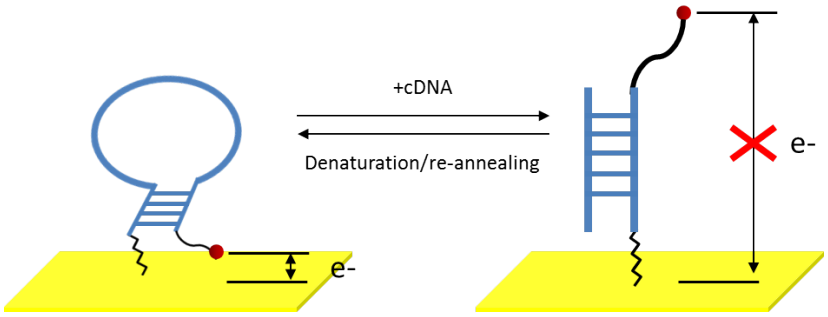

Figure 11: Scheme of electrochemical detection by conformational DNA change after hybridization.

a denaturalization step, followed by recharge of the target, is also proved by recovering the 80% of initial current.

The LOD of this assay is lower than that reported for solid-state optical molecular beacon, and it is only surpassed in an electrochemical biosensor based on catalytic enzymatic amplification approach (0,5 pM). In this latter case, the device is not reusable and it involves reagents. Unfortunately, this LOD applies to a PCR amplified DNA, it is not sufficient in the case of not-amplified samples.

During the '90, biosensors for DNA analysis relying on DNA mediated long range charge transfer (CT) were considered [54] prompted by numerous experiments, initiated in these years, and aimed at investigating DNA's electrical properties. Despite hypothesis that π-stacked DNA bases electronic system could offer a conduit for long range charge transfer was almost contemporary to the discovery of it structure [108], only thirty years first experimental evidence arose, thanks to the systematic experimental work following pioneering studies of Barton 's group at Caltech.

By using the redox chemistry of transition metal complexes, they proved that the rate for photo-induced electron transfer, between two metallic complexes covalently bounded Fig. 12 to DNA, was two orders of magnitude faster in presence of intercalating molecules [56].

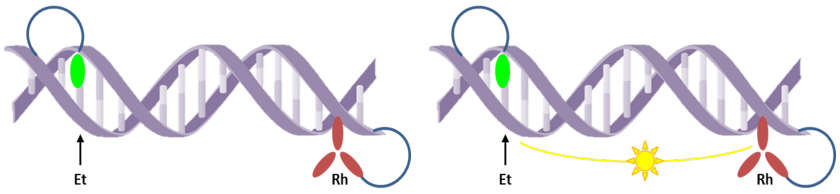

Figure 12: Electron transfer rate through DNA by quenching of fluorescence between intercalators: ethidium and rhodium intercalators covalently bounded to a DNA molecule (on the right); quenching of fluorescence between covalently bounded DNA intercalators.

Further, it was showed that the chemistry of DNA mediated CT is very sensitive to different variations in the DNA base stacking, and that this mechanism could be exploited by repair proteins to localize a single point mutation over the entire genome [14].

A part for its relevance for the understanding DNA's biological functionality, the fact that alterations of the π stacked pairing cause attenuation of the electrochemical current, provides a direct method to detect single base mismatch in a biosensor.

DNA hybridization biosensors which exploit the long range electron transfer through double-stranded DNA to a redox intercalators Fig. 13, have been reported [128]. These platforms explore the use of two different anionic intercalators, 6-anthraquinone di-sulphonic acid and 2-anthra

quinone mono-sulphonic acid, which has a lower negative charge [130]. These intercalators were useful to detect DNA hybridization and mismatching, even in presence of mixed DNA targets. The assembly of this biosensor follows the standard steps of DNA electrode modifications. First, thiolated ssDNA probes are immobilized, and spaced by mercaptohexanol (MCH), on a gold electrode via the sulfur-gold affinity. Afterwards, the functionalized electrode is exposed to a solution of the ssDNA target. After the hybridization, the chip is immersed in a solution containing the redox intercalators. Electrochemical analysis methods, CV and Osteryoung Square Wave Voltamperometry, is then employed to characterize the system.

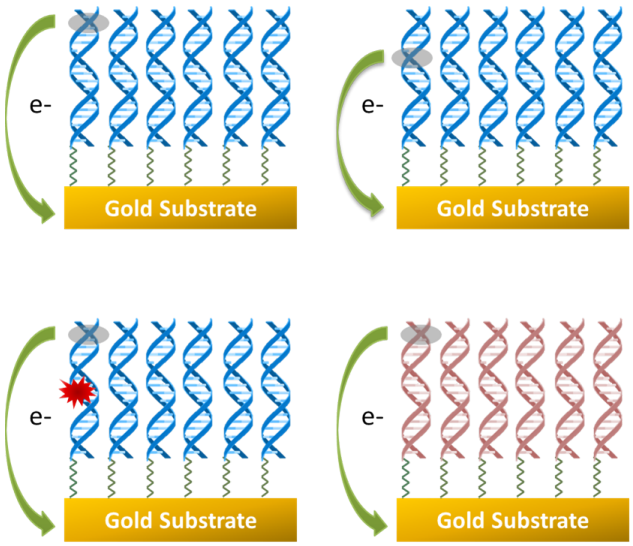

Figure 13: Electrochemical detection of DNA through long range ET.

In absence of the complementary target, no detectable redox peaks were obtained. Very low peaks current were registered after hybridization to a G-C and an A-T mismatched sequence. On the contrary, the hybridization with complementary target was followed by a net increase of the peaks current, which is consistent with the long range electron transfer through the DNA duplex. Reduction of the overall assay time is reported in the case of less negatively charged, 2-antraquinone mono-sulphonic acid (AQMS) intercalators. Although, the global assay time of this platform was still excessively long, being 6.5 hours and no very low LOD.

The emergence of different nano-structures and nano-materials, with increased physic-chemical properties, is promising, combined to the analytical power offered by electrochemical methods, to overcome limitations shared by available technologies.

1.4 ELECTROCHEMICAL NANO-SENSOR FOR DNA ANALYSIS

1.4.1 *Nanoscale: advantages for electrochemical detection*

The possibility of manipulating matter at the nanometer scale, as well than our ability to create nano-scaled systems is no more the futuristic vision contained in the popular talk by Richard Feynman "There is plenty of room at the bottom" in 1959, nor the science-fiction scenario described in Drexler's 1987 book "Engines of creation". It is a capability at our hand, and nowadays we are able to control several processes, which permit to fabricate functional nano-structures and to develop new nano-materials with increased properties, which can be well characterized thanks to the broad availability of characterization methods with improved sensitivity.

The emergence of nano-structures and nano-materials with tailored and increased physic-chemical properties, thanks to the extraordinary high value of the surface-area-to-volume ratio, is considered of particular relevance for the problem of biomolecules detection. Shrinking down the size of the probes in order to fit that of the analyzed molecules enhances the efficiency of their coupling, and opens to the possibility of achieving fast response time with low sample volumes and small target concentrations, through label-free detection strategies.

For this reason, inside the broader field of nano-technologies, nano-biotechnologies has, since ever, attracted major interests for their potential role to achieve one of the paradigms of contemporary science, nano-medicine.

From the perspective of DNA analysis, the involvement of nano-biotechnologies, with increased probe-target interactions, it is expected to end with long sample's treatment, such as the amplification of DNA by PCR, which is a common, preliminary and mandatory step, used in the

existing platforms. They could be also offer the key to develop detection strategies with overall reduced time, complexity and costs analysis.

The performances of nano-scaled biosensors are supposed to be by far better than that of macro-biosensors. The advantages inherent to high aspect ratio geometry of nano-scaled probes for biosensor applications were established by means of a simple diffusion-capture, analytical solvable, model which describes the kinetics of absorption of biomolecules at the nano-sensor surface in presence of solvation effect [76], [77].

The model considers the three possible geometry in which nano-probes comes and are usually arranged in biosensor systems, from the two-dimensional planar FET geometry to the one-dimensional of a nanowire based device, and the spherical one shared by nano-particles as represented in Fig. 14. Although simple, this model allows accounting for a series of reported experimental observations.

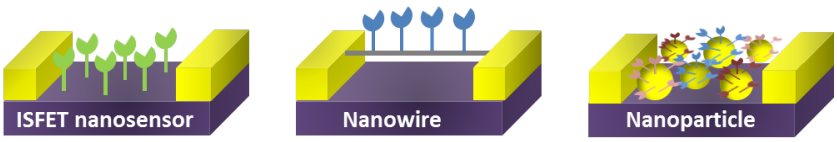

Figure 14: Three standard configurations for nano-probes based electrochemical DNA sensors: classical ISFET, Nanowire, and GNPs based FET.

The active area of a biosensor is in general a critical parameter to determine its performance, this is true also in the case of nano-scaled biosensors, for which the detection limits are as higher as the highest is the active area of the device.

This is maximized for high surface-area to volume ratio, and it is well-known that 1D nano-wires share extraordinary aspect-ratio compared to other geometry. But the screening effects in such small nano-devices could have negative effects arising from ions contained in solution which affect the incubation time required to achieve the same sensor response.

When these effects are accounted, the detection limit in the case of the nanowire geometry is two-three order of magnitudes higher than that of a planar ISFET for the same required time of 100 s. Improved performances are allowed by the nano-sphere geometry with a limit of detection of 100 fM Fig. 15. These conclusions sustain to the enthusiasms raised by the use

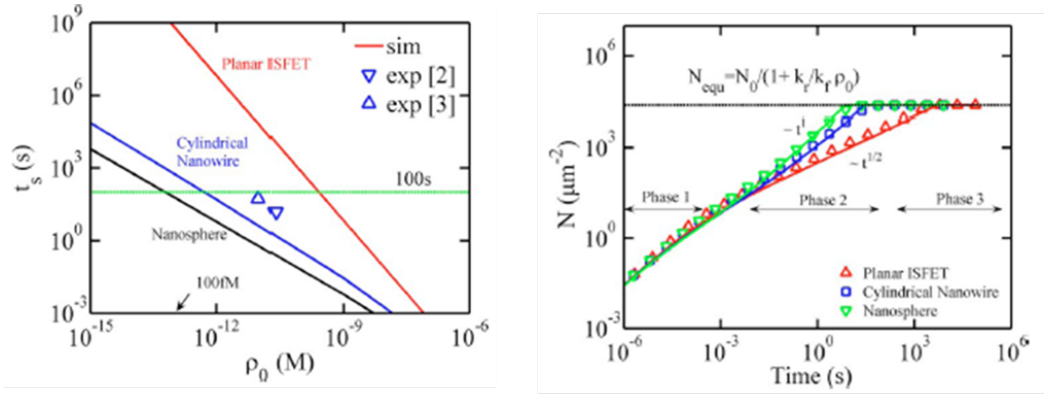

Figure 15: Comparison of analysis performances achievable according the different nano-probes geometry considered in [76].

of nano-probes to enhance the ability of detection of analytical systems. Indeed, they pick also the focus on the need of developing functionalization schemes, at low ionic strength, to reduce the effects of the electrostatic screening, but the settling time.

In the following, we will review some of the electrochemical based nano-devices which have been so far proposed for DNA analysis.

1.4.2 *Nanowire and Nanotube based systems*

Nano-wires (NW) and nanotubes (NT) with their extraordinary length-to-width ratio, exceeding 10^7, are the thinner structures at work. Despite the nano-metric diameter, NW and NT can be long up to centimeters in such a way to reach such notable length-to-diameter aspect ratio. Moreover, the growth process of NWs, contrary to that of NTs, can be nowadays well controlled so that the electrical, as well as the optical properties, can be adequately custom-tuned (Fig. 16).

SiNW can be obtained both by $top-down$ and $bottom-up$ fabrication processes. In the former, photolithography is used to transfer the desired pattern on a thin film of material deposited on a substrate. Bottom up processes, as will be deeply discussed chapter 3, include chemical vapor-solid-liquid- growth (CVLS) and self-assembly. CVLS processes made use of a catalyst to drive the growth along a specific direction in a confined

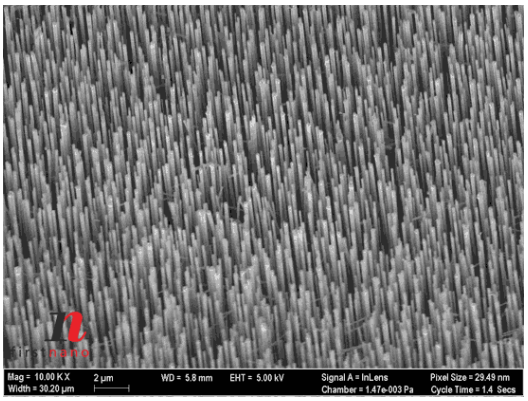

Figure 16: A "forest" of alined SiNW.

area: a little drop of the catalyst, acting as a nucleation center, is saturated by the atoms of the specie to be growth provoking its precipitation, which results in a one-dimensional growth path.

Biosensors based on semiconducting nano-wires are usually arranged in FET geometry [67]. The nanowire connects the two metallic electrodes, source and drain, where currents are, respectively injected and collected, thus working out the gate's role through the modulation of its conductance. The depletion, or accumulation of the charges on its surface, according the sign of the applied gate potential, induces a conductance change which turns on/off the electronic device.

This could be fruitfully explored for biomolecules detection. In fact, the binding of a charged analyte species to the nanowire surface plays the role of an applied gate potential which determines a conductance change directly related with the concentration of the analyte. The efficient charge transfer between the surface-anchored analyte and the NW (or NT) is, indeed, favored by the one-dimensional geometry. The functionalization of the nanowire with a molecular receptor, which selectively binds to the analyte, makes of the same target molecule the electrical gate for its own detection.

Carbon Nano Tubes (CNTs) arise in two forms: single walled nano tube (SWCNT) or multi walled nano tube (MWCNT). They can be pictured out as narrow graphene sheets rolled up to form a continuous tube. For this reason, they have very similar physic-chemical properties with graphene, as for example, the high atomic-scale perfection, which is at the origin of

the conductions abilities and mechanical stability found in this material. Higher melting point, and increased resistance to applied tensions, are also expressed in comparison with metals.

The atomic structure and the diameter size influence their electrical behavior which can range from that of a ballistic conductor to that of a semiconductor. These properties derive from the completely covalent sp2 bonding that is characteristic of the defect-free graphene sheet [112].

Sharing diameters as low that 1nm, SWCNTs are among the smallest available nano-structures. Their size is similar both to that of the individual biomolecules, and to the range of electrostatic screening lengths of meaning in the physiological environment.

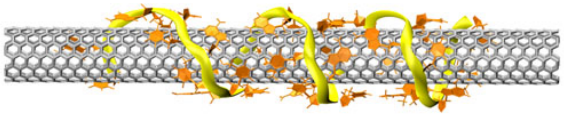

Figure 17: A ssDNA wrapping CNT.

CNT (as well as SWCNT) are arranged in a FET configuration for sensing applications [61]. This can be obtained by embedding the CNT in a dielectric, between a top gate and a ground plane, with two metallic electrodes, as a source and a drain [69]. When compared to conventional semiconductor FET, devices based on CNT have superior electrical characteristics, higher charges mobility and chemical inertness. Although the poor chemical activity, acid induced oxidation of the carbon generates surface groups that makes possible to integrate biomolecules on the CNT, and to explore their use in electrochemical nano-scaled biosensor.

Experimental observations, supported by theoretical studies, show that ssDNA strongly interacts with SWCNT. According to Molecular Dynamic (MD) simulations, ssDNA binds to the external surface of uncharged, or positively ,charged SWCNT on a time scale of a few hundred picosec-

onds [31], Fig. 17. Adsorption of ssDNA from a solution on a SWNT, of adjusted diameter, arises from the interaction between the exposed DNA hydrophobic sites with the hydrophobic (graphene) surface of SWNT.

The formation of a hybridized dsDNA compound, at the CNT surface, induces a negative charge which changes the gate conductance allowing its electrical detection. The encapsulation of ssDNA was also shown experimentally using a radio frequency field to stretch ssDNA, followed by a dc electrical field to electrophoretic applied to drive the ssDNA inside the SWNT [71].

1.4.3 *CNT-FET biosensors*

A CNTFET based electrical, real-time and label-free, biosensor for the ultra-sensitive detection of DNA hybridization, and SNP, employing a SAM of peptide nucleic acid (PNA) probes has been developed by Kerman and colleagues [57].

PNAs are synthetic polymers in which the phosphate and deoxyribose of the DNA backbone is replaced by a polypeptide. These are frequently exploited in genetic sensors as they provide better stability with respect the ionic strength, since they are not charged, and improved resistance to degradation by proteases and nucleases.

The problem of maintaining low ionic strengths is crucial in FET because they respond to changes in the surface charge, and increased ionic strength comprises the electrical double layer around the wires. Indeed, electrical neutrality expressed by capture probes thanks to the low initial charge on FET reduces device's background, which combined with lack of charge repulsion, results in improved performance for hybridization, compared to standard DNA probes [58]. Despite these favorable characteristics, their application is limited by the high synthesis costs.

In this platform, biomolecules are not immobilized directly at the SWNT surface, as it is usually done. The backside of the device is connected to the gate electrode by means of a micro-fluidic channel through which biomolecules solution are easily delivered. By monitoring the conductance change after delivering of the complementary target, the device is tested useful for the label-free and real-time detection of 11-mer oligonu-

cleotide sequence with a LOD of 6.8 fM. In control experiments, the specificity of the biosensor is proved by using a blank solution followed by a single mutated DNA and a no-complementary strand.

The sensing mechanisms of CNT-FET, although several studies faced this issue, is still lacking [21]. Among proposed mechanisms, they are: the electrostatic gating to the change in the gate coupling, the changes in the carriers mobility, and the unconventionally Schottky barrier (SB) effect [44].

In [131] the source-drain current (I) versus the gate voltage potential (Vg) curves for a large number of SWCNT-FET devices, immersed in an electrolyte solution, for both hole and electrons transport, were experimentally.

For all them, the electrostatic gating, and/or SB, mechanisms were individuated as the principle sensing mechanism. The increased reproducibility of the results obtained by fit analysis, based on the assumption of electrostatic gating mechanism along the bulk of the SWCNT, instead of SB modulation at the contacts, points out the relevance of the electrode-SWCNT contact, with respect to the channel doping, to establish the sensing mechanism.

Similar conclusions were been also reached theoretically by calculating the transistor characteristics in the framework of the semiclassical WKB (Wentze, Kramers and Brillouin), an approximation standardly involve in quantum-mechanical calculations and particularly useful to calculate tunneling currents [96].

According this analysis, whenever there is a consistent SB at the NT-contacts, the latter operates as a SB-FET modulating contact resistance, with improved performances in the case of sharper contacts, which enhance the electrical field. Only for very small SB values, the NT-FET device operated as standard one, or by modulation of the electrostatic potential in the channel.

1.4.4 *SiNW based nano-sensors*

Semiconductor nano-wires based on silicon bridges enable the efficient charge transfer between the surface-attached DNA and the nanowire, and

can be thus used for DNA biosensors. Despite CNT, SiNWs can be prepared by exploiting either a "bottom-up" than a "top-down" fabrication approach. Indeed, their electrical properties are highly reproducible, and tunable, during the growth process, which can be well controlled.

The effectiveness of SiNW-FET based biosensor was first demonstrated by Ham and Lieber [43], which developed a device for the direct electrical ultra-sensitive detection of DNA mismatching applied to detect two different mutations of the cystic fibrosis transmembrane receptor, which is manifested in this disease.

This SiNW biosensor employs p-type SiNWs, synthesized using the gold nano-cluster catalyzed chemical vapor deposition (CVD) method. Also in this case, a PNA SAM is implemented as biosensor interface. The increase of the conductance, reported after the addition of fM concentrations of mutated DNA, is consistent with the increase of the negative surface charge density due to the binding of DNA to the NW surface.

A very low detection limit, down to 10 fM, is achieved in a totally label-free and real-time manner. By introducing proper antibody molecules on the SiNWs surface, the same group demonstrated the efficiency for the label-free real-time, multiplexed detection of protein cancer markers, with ultra-sensitive performances.

Label-free electrical detection of DNA hybridization has been shown also for a SiNW-FET biosensor as that of Fig. 18.

A reliable and scalable fabrication technique for producing uniform, and well aligned SiNW, was applied in [35]. Arrays of SiNW were obtained by combining deep ultraviolet lithography, and self-limiting oxidization, on silicon-on-insulator (SOI) wafer, isolated against electrical contacts in aqueous solution by micro-fluidic channels, embedding the SiNW arrays. PNA capture probe, immobilized on the SiNW surface via the silane chemistry, are used.

By monitoring the device resistance, after immersion in the hybridization buffer with different complementary DNA concentrations, this platform allows the ultra sensitive detection of DNA, with a LOD of 0.10 fM. Increase of the resistance is generally reported after exposure of the device to the complementary DNA sample, although if different settling times are required by varying sample concentration, with increased set-

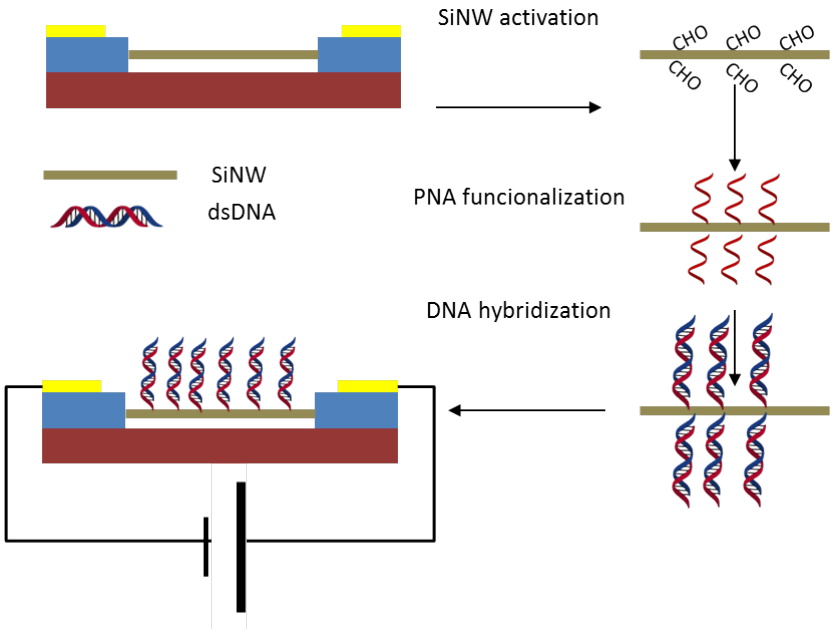

Figure 18: Schematic of the SiNW-based sensor used for the ultra-sensitive detection of DNA hybridization.

tling times at lower concentrations. By comparing this result with that obtained by switching to the neutral buffer solution, the authors concluded that the reported changes in the resistance are consequence of the DNA hybridization, which decreasing the carrier concentrations on the surface of the n-type SiNW, gives rise to a field effect on the NWs, leading to the detection.

1.4.5 *Gold Nanoparticle (GNP) based nano-sensors*

Medical applications of gold compounds, in particular of colloidal gold (the name given to a suspension containing gold nano-particles), are very old dated. They were first reported between the fourth and fifth centuries B.C., by Chinese, Arabic and Indian scientists [100].

Although, its use in standard biology research arose only in the '70, when it was first employed, as an immune-chemical marker in conjugations to antibodies for the electron microscopy visualization of the Salmonella [89]. Since then, a lot of research has focused on the synthesis,

and optimization of GNPs [29] for different applications. GNPs shape, size, and chemical-physical properties, can be in fact easy tailored at the taste of researchers by controlled synthesis processes.

The gold surface, indeed, provides an inherent biocompatible support on which the well-known, and versatile, surface chemistry allows to play several biomolecules functionalization strategies, Fig. 19. Target binding

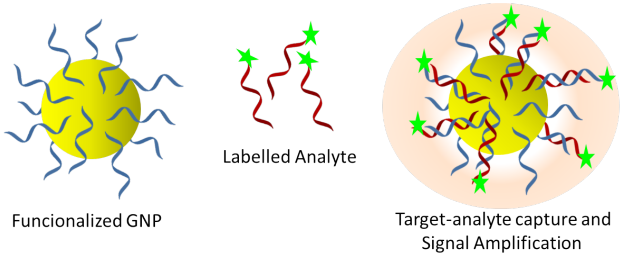

Figure 19: Schematic of target-probe signal amplification with specific functionalized GNP.

events at the nanoparticle surface, can produce changes both on the optical and/or the electrical properties, in such a way that GNPs can be explored as useful interfaces for constructing electrochemical biosensors [123].

At low concentrations, ranging from the attomolar to pico molar range, GNPs signal can be amplified by means of silver-enhancement treatment, which improves sensitivity [124].

The silver-enhancement treatment promotes the selective and catalytic deposition of silver-metal in the presence of gold. This technic has been explored to develop a nano-sensor for the efficient discrimination of not-complementary DNA, relying on the magnetic properties of the used nanoparticles [134].

In this platform, biotynlated-DNA probes are bound to streptadivin-coated magnetic latex spheres. Hybridization is followed by the formation of the biotyn-streptadivin couple and the catalytic silver precipitation on gold labels detected by applying potentiometric stripping analysis.

The removal of not-hybridized DNA is achieved by means of magnetic separation, which allows an efficient minimization of not specific binding, thus increasing the efficiency of the hybridization response. A LOD of 10

pg for 50 µg/L after a hybridization time of 20 minutes can be achieved by exploring this technique. Lower detection limits are expected for longer hybridization times.

A similar GNP based array to detect DNA hybridization was shown by Park and colleagues [83], schematic of this assay is shown in Fig. 20.

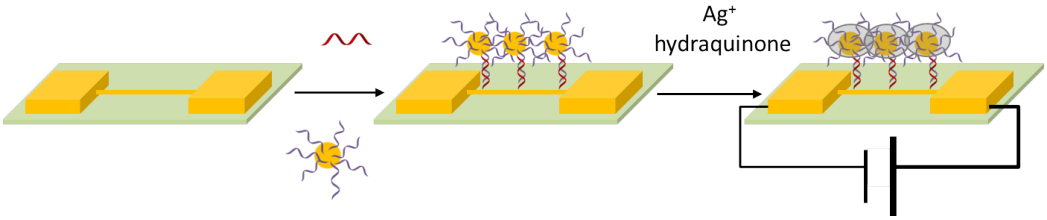

Figure 20: Scheme of DNA hybridization electrical detection according the standard silver-enhancement treatment, usually explored in a GNP based sensors.

In this device, a short oligonucleotide capture probe is located between the micro-electrodes gap, while a longer target oligonucleotide in solution is provided with recognition elements complementary to the capture probe, and labeled with GNPs.

Following target-binding, gold nanoparticles fill the micro-electrode gap, and undergo a silver-enhanced treatment with a photographic developing solution, that uses GNPs to promote the reduction of Ag (I) and hydro-quinone, to increase the sensitivity of the device. Micro-electrodes, far apart 20 µm, were obtained by standard photolithography on SOI wafer functionalized with succinimidyl4-melamidophenil-butyrate, and left incubating during 24 hours.

After treatment with the target and nanoparticles, the array undergoes silver-enhancement procedure with the photographic solution. Hybridization detection is then achieved by monitoring the gap resistances at increased time-exposures of the silver enhancement, with complementary and mutated strands. The deposition of silver is turned on by the nanoparticles and thus by the hybridization event. In the control experiments carried out with denaturalized strands, no detectable signals were measured.

Two different array formats, which also rely on the use of magnetic beads to trigger the direct electrochemical detection of the GNP tags on

a magnetic graphite-epoxy composite electrode, were explored by Castaneda *et al*. [19].

The two alternative designs explored, a so-called two strands assay format and a sandwich one, were proven to be effectives in the hybridization detection of breast cancer (BRCA1), and of cystic fibrosis gene.

In the former case, the capture probe is immobilized onto biotinylated paramagnetic beads. After immobilization, the hybridizing solution containing the target is added and all the molecular assembly exposed to a solution containing streptavidin-coated GNPs. The detection is carried out by direct differential pulse voltamperometry (DPV), through which the GNPs tags in the conjugate are measured.

A similar protocol in the case of the sandwich-based proposes an alternative array design. Here, a further hybridization step is necessary to conjugate the target wit the probe, attached to the paramagnetic beads, and to a second biotinylated probe need for signaling with streptavidin-coated GNPs. In both cases, the device showed great discrimination efficiency in control experiments performed with a three base mismatched sequence and a non complementary strand. Clear current DPV peak increase was reported only in presence of the complementary strand, with a sensitivity of 600 nM.

1.4.6 *Nano-gap based sensors*

Nano-gaps, a pair of electrodes separated by an insulating thickness (usually air) having nano-metric size, are emerging as one of the most attractive, between available nano-devices, for applications in the direct electrical detection of biomolecules interactions.

In general, they are useful for the investigation of molecules electrical behavior, and for this they have been applied to study charge transport mechanisms in biomolecules [65]. In comparison with other methods usually involved in this field, such the STM's based approach, nano-gaps provide a simpler platform to implement conductance measurements, and of other electrical parameters of molecules. Electrical properties of nano-gaps can be, in fact, determined by applying standard electrical set-up,

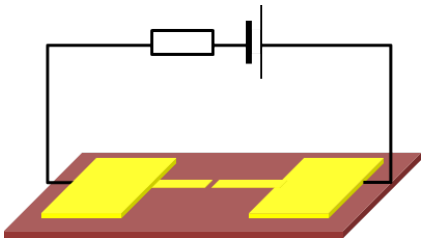

Figure 21: Typical arrangement of a nano-gap for direct electrical characterization of biomolecules.

portable and more friendly-use instrumentation, compared with that implied by other measure protocols Fig. 21.

Nano sensors for DNA detection based on a nano-gap electrodes configuration, have been considered. They explore the formation of DNA nano-

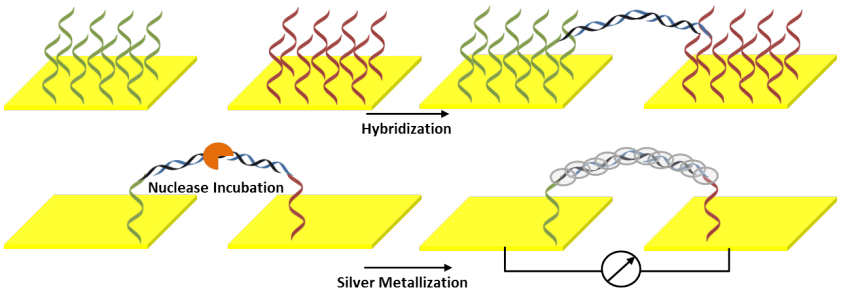

Figure 22: Hybridization assay of planar nano-gap sensor.

wires, which connect the nano-gap. DNA nano-wires, inside a nano-gap, have been obtained both by electrostatic trapping of dsDNA, and by electrodes modification by DNA bio-receptors specific to different DNA target regions, in such a way that DNA nano-wires bridges nano-gaps through specific interaction of complementary base-pairs during hybridization.

Nano-sensors based on nano-gap electrodes with both vertical [94], as well as planar [101] geometry have been so far developed, and shown ables to detect DNA hybridization and SNPs, Fig. 22, Fig. 23.

In both of these platforms, two gold electrodes, separated by a distance of about 60 nm, are functionalized with two short capture probes (CPs), which are thiolated ssDNA chosen antisymmetric each other, and in such a way to have the last 20 bases complementaries to a target ssDNA.

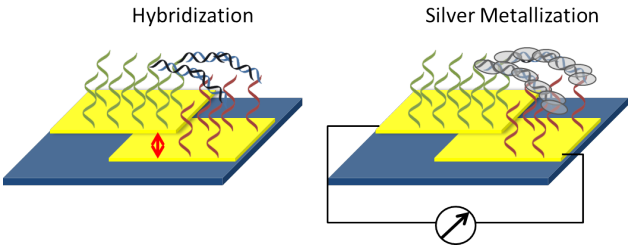

Figure 23: Detection scheme for the vertical nano-gap sensor.

The size of nano-gaps is adequate to fit that of the target DNA. In both systems, the DNA nano-wires formed after target hybridization with the immobilized CPs, are metallized by adding 1.4 nm GNPs, which enables the hybridization transduction by analysis of the current-voltage (I-V) curves across the nano-gaps. Elimination of mismatched duplexes, and of free capture probes strands, is achieved by incubating the system with nuclease enzyme. Both nano-sensors have been proven useful for SNP and genotyping applications achieving rapid response and pico molar LODs.

1.5 AIM OF THE THESIS PROJECT

As general objective of this thesis, we conceived an improved design of the nano-gaps which allows label-free DNA hybridization detection through the enhancement of long range DNA charge transport, favored by the configuration considered Fig. 24.

In the proposed system, two gold electrodes are facing a nano-gap at a separation distance within 50 nm. The non-active sensor area is blocked with a nano-metric thickness of passivation layer leaving opened only the area for the immobilization of molecular probes, and electrical conduction. By this way, only the sensing area is functionalized with bio-receptors, and all the hybridized target is used for signal transduction.

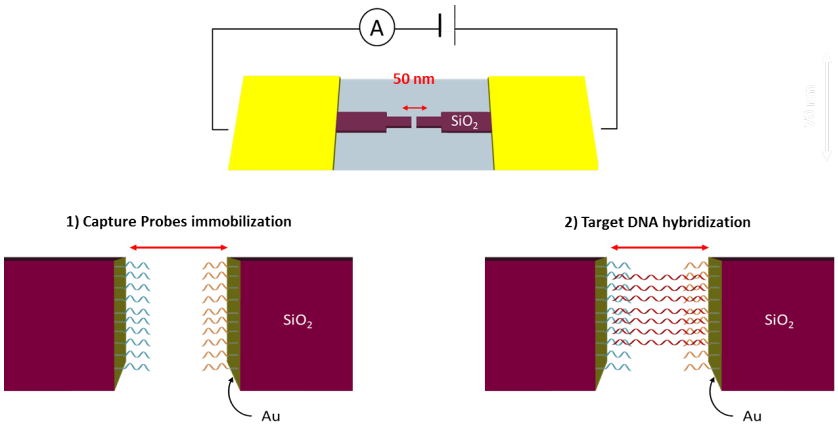

Figure 24: Working scheme in our nano-sensor.

Two antisymmetric molecular receptors, provided with a thiol terminal, are immobilized inside the vertical walls of the planar nano-gap through the well-known sulphur-gold affinity. Nano-gap geometry, with the two electrodes distributed face-to-face, allows the formation of straight DNA nano-wires, bridging the nano-gap.

This configuration, with respect that exploited in [94], [101] favors the ordered orientation of the π-stacked bounds of the DNA bases, see Fig.25 which improves the long range electron transport through the DNA molecu le, thus providing a direct tool for its detection by monitoring current-voltage response of the nano-gaps. The platform was demonstrated with a selective response, only obtained when the fully-complementary target

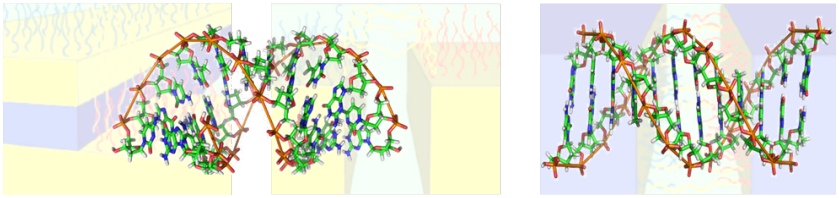

Figure 25: Improvement of DNA charge transport in our platform.

is incubated in the sensing area. The specific objectives carried out to this purpose are the next.

- A deep study of the theory behinds DNA charge migration will be performed in order to design a nano-sensor device highly efficient, which do not requires doping or labelling process in order of establishing reliability of electrical detection of the nano-sensor, according current understanding of the phenomenon, by means of available nano-fabrication and characterization methods.

  Further, it was used to perform a phenomenological model to estimate the charge transfer rates for the molecular system considered, by which under the hypothesis of wire-like conduction it will be possible to obtain nano-gap conductivity values.

- Fabrication of nano-gap electrodes arrays suitable for low conductivity measurements, giving rise to high reproducible sizes necessary to produce repeatable and comparable experiment results. Fulfillment of above requirements, through simple processing routines, with the potential for mass-scale production and inherent cost reductions. Each process involved in nano-gap manufacturing, will be properly characterized.

- Bio-functionalization of vertical nano-electrodes in a selective manner in a two electrode conforming a gap at nano-metric distances. The electrodes surface functionalization will be tested and characterized with selected techniques considering the limitations brought in such a nano-metric vertical devices.

- Detection of electron transport trough DNA, due to a specific hybridization of the complementary DNA target with the immobilized

capture probes on the nano-gaps electrodes. The small size of the device as well as the low current of the system will be faced with appropriate equipments, and a reliable characterization methodology established.

- Optimization of the biosensor platform by testing the selectivity of the system with mismatched capture probe to test the specificity of the nano-device signal, by proving nano-sensor regeneration for further use, and its ability to quantitative measurements.

2

CHARGE MIGRATION ALONG DNA

The debate around electrical properties of DNA is an old-standing ones which dates backs to 1962, when Eley and Spivey raised up the hypothesis that base stacks could act as a one-dimensional path for charge transfer.

Of relevance both for biological and technological implications, the possibility of DNA long range electron transfer received a renewed interest, when its implication in damage and repair process emerged by the experimental observation of induced oxidative guanines damage transferred far away from the oxidant, which could be explained by assuming long range electron transfer through DNA. Results observed in these early experiment, claiming for the possibility of *chemistry at distance* and molecular wire-like DNA electrical conduction, brought the field of interest of the phenomenon beyond biological context, being of relevance for the development of bioelectronics.

In this chapter, the problem of DNA charge migration will be deeply treated by examining, and discussing, the experimental and theoretical background leading to current understanding of this process. Based on standard description of the phenomenon, we developed a phenomenological model, in order to have rough estimation of charge transfer rates, and conductivity values, for the molecular system considered in our application, constituted by a DNA bridge embedded between two metallic electrodes.

2.1 GENERAL OVERVIEW

Hypothesis of emerging DNA electrical properties was pushed by the similarity of DNA's structure, in particular from the resembling of base pairs stacking in DNA structure with that of some organic salts Fig. 26, as the Bechgaard salt. This salt can show metallic conductions, and the electronic structure analogy of DNA was used to postulated the hypothesis of a semi-conductive behavior of the molecule.

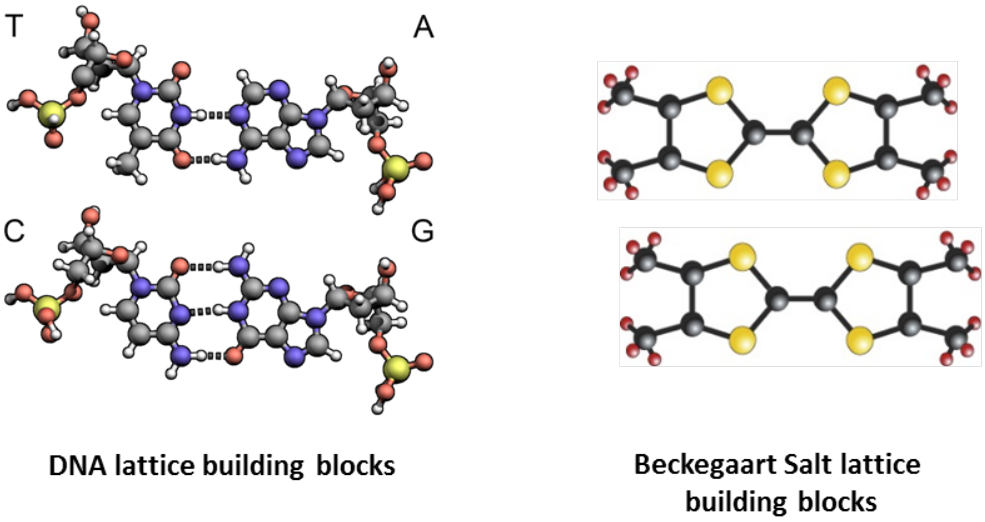

Figure 26: DNA lattice structure compared with that of organic salt showing metallic behavior.

Electronic behavior of DNA was supposed to emerge for the presence of delocalized electronic π systems, having low-lying π type free orbitals, on all the four DNA's bases. These latter are aromatic entities having the atomic p_z orbitals perpendicular to the plane of the base, in such a way that delocalized π-band can be formed across the different bases, with an energy gap between the π -bonding and π-anti bonding orbitals, of about 4 eV [16]. In the case of strong coupling between the bases, this could lead to the appearing of extended electronic states, along the backbone, with a narrower energy gap, which would results into a metallic conduction state, for the limiting case of a vanishing gap.

The formation of such extended metallic states in DNA molecules, promoted by the overlapping of the π and the anti-π bands, would result especially dependent from the system spatial configuration, with the twist angle and the base stack distance separation, playing the role of principal parameters, and as consequence, it is expected to be particularly sensitive to the sequence details, and the environment conditions.

Charge migration refers, in general, both to holeand to excess of electrons migration, so that it can occur both on reduced and oxidized strands of DNA. Hole's transfer is the migration (change of position) of a positive charge along an oxidized DNA's strand.

The ideal charge carrier candidates for hole migration are the purine bases characterized by having lower oxidation potentials in vitro [98], [109], compared to that of pyrimidines, which are favored as carriers in the case of electron transfer ($E_0 = 1,3V; 1,4V; 1,6V; 1,7V$ vs normal hydrogen electrode (NHE) for G,A, C and T) [109].

Guanines are the lowest oxidation potential basis and most of the first studies on DNA charge migration pertain to radical transfer in solutions Fig. 27. Only recently, analogous process of charge's migration has been observed involving adenines [40].

Almost thirty years later the hypothesis of Eley and Spivey, the issue of DNA charge migration come back in the scientific scenario, as renewed interest was brought especially from the work started by Barton's group at Caltech. In the '90 they performed a series of experiments [56] in which they were studying the photo-induced oxidative reduction of guanines, as a function of length, and base stacking of the DNA's bridge intervening between the photo-oxidant and the damage site Fig. 27.

According to their observations, the presence of DNA resulted in increased electron transfer rates over long distances. The observation of exceptionally high electron transfer rates over a range of r=19-26 Å, lead the authors to claim for the possibility of a molecular wire like conductivity of DNA.

The rate of electron transfer measured in these experiments were, in fact, in contrast not only with that recovered in similar measurements, but were also not compatible with the predictions of standard electron

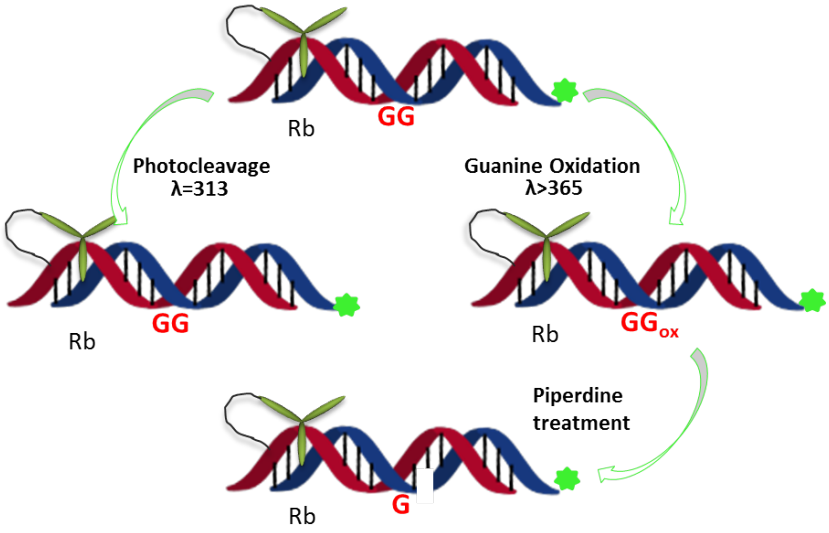

Figure 27: Long-distance Photo-induced guanine damage

transfer theory. According this, for donor-bridge-acceptor (DBA) systems, the rate of process is given:

$$R = \exp^{-\beta L} \tag{1}$$

and it is characterized by an exponential distance-dependence. On the contrary, obtained results provided evidence for longer electron transfer, than that accessible to the decaying state of [41], and with yields independent from the distance.

After work of Barton and colleagues, many kinds of experiments were undertaken to provide a more systematic characterization of the electron transfer rate with respect the sequence details, and the related alterations on the π stack; and to establish reliable direct measurements of DNA conductance.

As soon as new experiments were performed, results still more divergent begun to emerge, bringing new questions about the possible mechanisms of charge migration in DNA.

The debate raised up especially after the starting of direct conductance measurements of DNA molecules. Here, molecule conductivity is directly obtained by analyzing the electrical response of an opportunely tailored circuit embedding the molecules, immobilized between two electrodes.

Several approach to measure DNA conductivity were developed, which we will review in the following reporting very different kinds of electrical behavior:

- insulator at room temperature [25],[110]
- true wide band-gap semiconductor at all temperatures [86]
- Ohmic or nearly Ohmic at room temperature [34]
- induced superconductivity [53];

It could be useful to remind that electron transfer is not electron's transport; while the former is decay of an excite state, and involves high energies (eV), the latter becomes relevant at small V, and it is characterized by another length-dependence, which can be determined through conductivity measurements. While electron transfer is usually reserved to indicate processes involving single-step charge migration, electron transport refers to multi-step processes. Although this, they can occur in the same medium.

Bearing the difference in mind, the emerging evidence is that both, the electron transfer and the electron's transport through DNA are no trivial processes. Observed rates of electron transfer are not ever in agreement with the standard description of this process. On the other side electron transport properties of the DNA appear still more elusive considered on the basis of measured conductances.

An analysis of experimental and theoretical backgrounds in DNA charge migration will be extensively given in the rest of this chapter. Electron transfer and transport (conductivity) DNA measurements are presented and discussed. Also we introduce, on a general ground, theoretical approach usually applied to model the mechanisms of DNA charge migration.

2.2 EXPERIMENTAL BACKGROUND

2.2.1 *Electron Transfer measurements*

Photochemical and photo-physical experimental methods have been largely applied to study rates of electron transfer in DNA assemblies. These rely on use of labelling DNA with proper electron acceptors and donors, through which it is possible to measure the rate for molecular electron transfer by the fluorescence quenching of the reporter molecule.

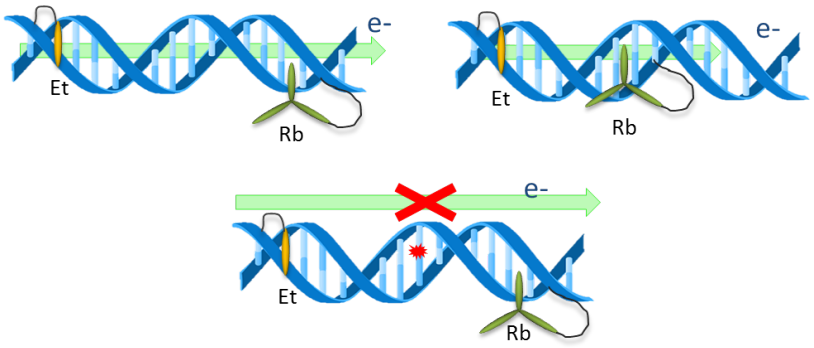

Figure 28: Electron transfer between metallo-intercalators bound to DNA in function of their relative distance, and in presence of a mismatched base-pairs.

Also, electrochemical analysis has been used, in this context, to evaluate the influence provided by an intervening DNA stack, in the electron transfer to a DNA modified surface of redox reporters, which are ables to intercalate within the base-stacking Fig. 28.

In the above cited experiment by Barton [55], two intercalators, one of which is a classical donor molecule, the ethidium-bromide, while the other is a metallic acceptor intercalators, a phenanthrequinone diimine phenanthroline ruthenium, were labelled with methylene tethers and attached to a DNA molecule of about 10-14 base pairs. The measurement of electron transfer rate is realized indirectly by means of the fluorescence emitted, which is analyzed by Time Correlated Single Photon Counting and steady-state techniques. When the excited ethidium molecule is at-

tached to DNA, quenching of fluorescence is observed, over distances ranging from 17 to 36 Å.

The authors suggested that fluorescence's quenching was due to the leaking of charge on the excited donor molecule, along the length of DNA, to a nearby acceptor molecule. The DNA mediated electron transfer process observed was also found to be slight dependent on the distance but very sensitive to the base stacking, since a large decrease in the fluorescence's quenching occurred after the introduction of base stacking perturbations to the system.

This observation is especially relevant, highlighting the importance of base stacking in DNA mediated charge migration. Also it provides a method which could be used in DNA biosensing based on the long range charge migration properties of the molecule. Results obtained at Caltech were claimed with enthusiasms by the researchers involved. But, on the other side, they were received with some skepticism by the scientific community. As consequence, many experiments were undertaken in the following years animated to shed light on the question.

One of the criticisms that were moved against the experiment of Barton and colleagues was the lack of a systematic determination of the distance dependence of the ET, which was questioned both on the theoretical and the experimental ground. A more systematic study of the distance dependence in DNA mediated ET was performed by Lewis et al. [66] soon after. In their work, Lewis and colleagues studied the distance dependence of

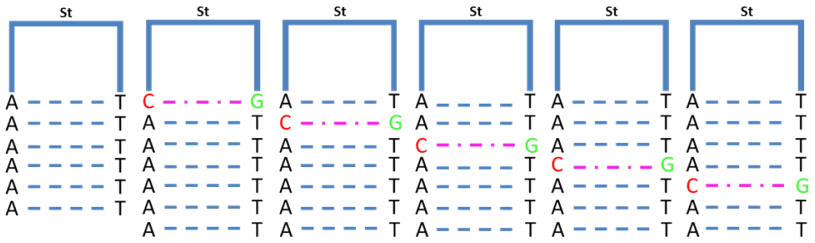

Figure 29: The series of stilbene hairpirins used in experiment by Lewis to study electron transfer distance dependence.

the photo-induced label ET, for a family of synthetic hairpirin having the two nucleotides arms connected by means of a stilbene-carboxamide's bridge. Once prepared, the hairpirins were modified by the introduction

of a G-C base pair, see Fig. 29, acting as a charge acceptor at different locations with respect the stilbene bridge. By studying the fluorescent, and the transient absorption spectra, the authors established that no ET occurs for the parent hairpirin T6-St-A6, while distance dependent fluorescence's quenching, and the formation of a stilbene anion SA radical, was found to arise for the hairpirin, where a G-C base pair was introduced.

In particular, they found that when a GC pair was directly attached to the SA's bridge, the fluorescence of photo-excited SA was quenched, with decreased rates of fluorescence's quenching for increased distance, between the SA's bridge and the acceptor pair. By means of a kinetic analysis, they were able to conclude that DNA was more effective for ET than proteins, and other organic compounds, known to be conducting. Although, the rate of ET was lower than that expected for a molecular wire.

Giese *et al*. [40] measured the efficiency of charge transfer of a GGG triplet across a bridge of $nAT(n = 1-3)$ from which it was shown that the amount of charge transfer dropped down by a factor of 8, for each interplaying AT bridge, between the guanines. For greater sequences, having n >4, the ET distance dependence was weaker and found to vanish for longer sequences. They accounted for these results by assuming that, as the bridge length increases, there is a switching between coherent unistep tunneling and thermal hopping processes enabling charge transfer.

2.2.2 *Conductivity measurements*

Unlike the measurement of molecular ET rates, that of molecular conductance is implemented by using a two-point contact set up, in which the molecule is embedded between the contacts. As we will see in the following, this is the standard set-up also involved for the direct measurements of the electrical properties of DNA's molecules, Fig. 3.

One of the first direct measurements of electrical conduction along DNA's molecule was performed at Basel University by Fink and Schonenberger [34]. They conceived a sophisticate experimental set up involving a low energy electron point source (LEES) microscope, in order to mini-

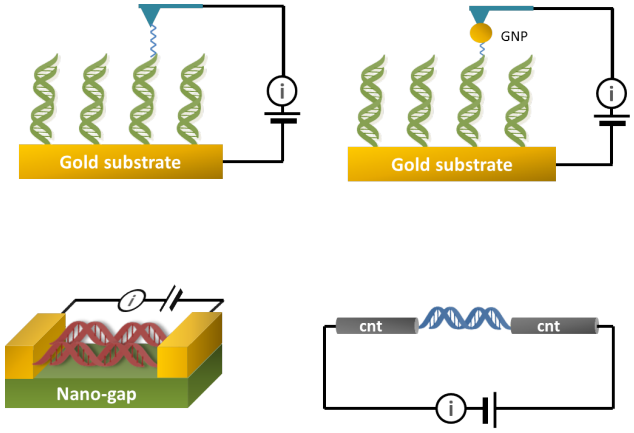

Figure 30: Typical set-ups used to implement molecular electron transport measurements based on analysis of electrical properties of the molecular junction formed by embedding molecule between two conductive probes.

mize the eventual sample damaging. This kind of technique was already efficiently applied to test elongated molecular objects.

In this experiment, drops containing DNA's molecules are placed on a gold-covered carbon foil, carrying holes of about 2 μm of diameter, scanned by means of the LEES. Ropes, formed by DNA's molecules inside the holes, are then broken by a tungsten tip through which a bias voltage is applied for its analysis. The I-V characteristics measured in the experiment, Fig. 31, show the linear profile typical of conducting polymers, with an upper resistance's value of 2.5 Ω, for a DNA sample of about 600 nm. This is the length of samples considered containing approximatively 50000 base pairs, and it comes from the Lambda Phage virus.

The possibility that ionic currents support such high conductivity, was ruled out by running experiments in vacuum, although it was not possible to exclude the contribution of ions trapped by DNA. It was also been pointed out in [25], that the LEES imaging method could contaminate the sample leading to the observed conductivity. Last, it should be also remarked that this is not a single molecule conductivity measurement, since ropes of DNA, containing lot of molecules were suspended between the contacts. On a nano-metric length scale, direct electrical measurements of shorts poly(G)-poly(C) DNA oligomers (10 nm long) [86], electrostatic

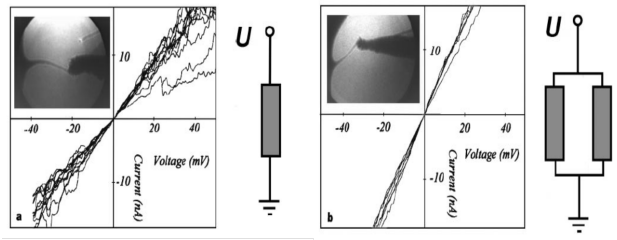

Figure 31: Picture from the LEES set-up of ref [34] with results of measured I-V characteristics.

trapped between two metal nano-gap electrodes at a distance of 8 nm, show the semiconducting behavior of Fig. 32. The profile of I-V charac-

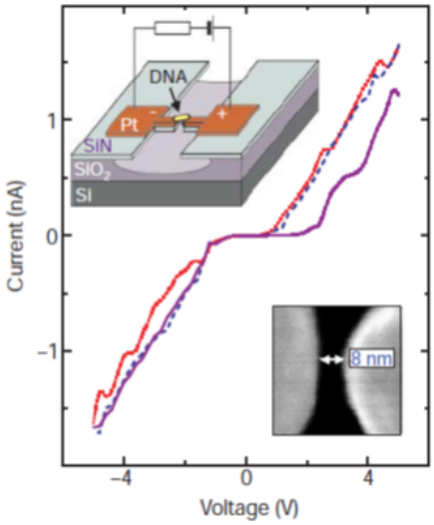

Figure 32: Set-up and results of Porath experiment.

teristics, with no appreciable conduction below a bias voltage of 1V, is in agreement with the behavior of a semiconductor with large band-gap.

It is relevant to observe that, the sequence considered in this experiment is particularly suitable for electrical transport; it contains in fact only GC pairs, which favors the overlap of π-orbitals across the bases, giving rise to a channel for the charge conduction. These results does not rule out that DNA can behave also as an insulator, and send back the problem of DNA electrical behavior, to the system's specificity and on the experimental parameters applied.

Storm et al. [110], on the contrary, reported no evidence of conducting behavior for several samples of DNA deposited between Pts micro-electrodes separated by a gap of 40 nm, Fig. 33. Molecules of different length, and structures funcionalized with thiol group (SH) in order to promote the bonding of DNA molecules at the metallic contacts, were deposited on to the micro-electrodes, fabricated by means of electron beam lithography on different substrates. These include mica and SiO_2. I-V characteristics, obtained at gate voltages ranging from -50 V to 50 V, show an insulating behavior of DNA molecules at length scales longer than 40 nm, with a lower bound resistance of 10 TΩ. Images of the DNA linking two electrodes are shown in Fig. 33, and were obtained by means of AFM. For all the analyzed molecular samples, the DNA length is ever greater

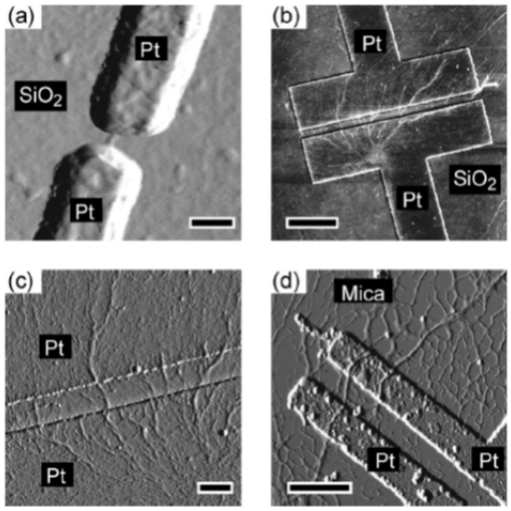

Figure 33: Pictures showing DNA molecules bridging micro electrodes as implemented in Storm experiment [110].

than the separation distance between the electrodes, and a consistent part of molecules overlaps on the electrodes, augmenting the electrical contact without contributing to the gap conduction. However, the results found on this length scale, as the same authors pointed out, do not contradict previous founding observed at shorter scale-lengths.

Another experiment designed in such a way to reduce the effect of molecule-electrodes contacts, prompted forward the hypothesis that observed DNA's conductivity was principally determined by the electrical

contacts [49]. In this set-up, the electrical properties of DNA were inferred by measuring the electrostatic force between the tip of a scanning force microscopy and the molecular sample, which is either directly absorbed to a gold electrode, on to a single-walled carbon nanotube, and finally on an insulating substrate employed to avoid contact with a conducting object. The presence of a conductor sample should decrease the oscillation frequency of the scanning probe microscope (SPM) due to molecule's polarization, providing a method for its characterization. Frequency oscillations were detected only in the presence of nanotubes attachment which lead the authors to conclude that the DNA's molecule did not show relevant DC conduction.

An interesting approach, which allows to implement single DNA molecules conductance measurements, was proposed by Barton's group [42]. They exploited the formation of amine bounds between a dsDNA's molecule to the funcionalized edges of a nano-gap obtained inside a SWNT. Being the cross section of SWNT's very similar to that of the DNA's molecule ($\sim 3\ nm^2$), it is expected that as much as one DNA's molecule will fit the nano-gap.

I-V characteristics of devices realized with well-matched DNA's molecules showed resistance values of about 0.5-1 MΩ over a length of 6 nm. These values are typical of highly oriented pyrolytic graphite which makes the author conclude that DNA behaves like aromatic graphite planes. Several control experiments were also done to contrast many issues. A 300 fold increase of the resistance was observed in devices reconnected with mismatched DNA sequence, proving evidence for the role of the base-stack integrity in transport of charges, as well as that it is supported by DNA. To further contrast this possibility, a specific cut enzyme was used to prove the on/off of conductivity of the device after its application.

In order to complete the diverging scenario emerged on the experimental ground, let's just discuss, one of the maybe more controversial experiments [53] ever performed on DNA charge transport, claiming for a proximity-induced superconductive state in DNA molecules, 16 μm longs.

In this experiment, molecules of DNA are connected between two superconducting electrodes, made of rhenium/carbon and deposited by

sputtering on a mica substrate, Fig. 34. These electrodes are characterized by a resistance of 100 Ω, they indeed undergo a superconducting transition around the temperature of 1 K. The thickness was chosen to minimize structural deformations on the suspended DNA's molecules, which could have effect on the electric transport properties of DNA. Two samples with

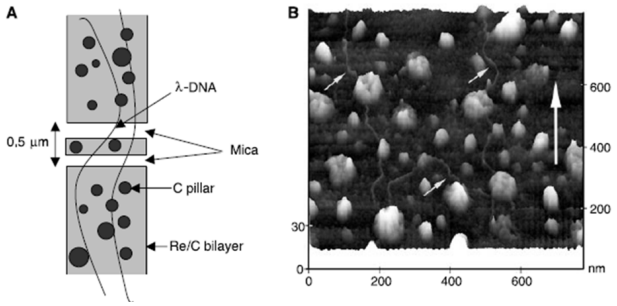

Figure 34: Results of experiment on induced superconductivity in DNA molecules. Top image shows DNA molecules bridging superconductive electrodes.

different DNA's molecules densities were prepared and characterized by means of AFM.

The authors estimate that for each one of the samples employed there were respectively about 100 and 200 DNA molecules bridging the electrodes. Exceeding DNA's molecules were eliminated by means of a low energy laser beam before charge transport measurements.

The values found for the resistance, at temperatures ranging from the room temperature down to 0.05 K, were found of 10 Ω and 40 Ω for DNA1 and DNA2, respectively.

A sharp change of the resistance in function of the temperature was observed in the case of the shorter DNA1 sample, for which an increase of about 75% in conductivity was reported at 0.05 K; in the case of DNA2, at the same temperature, only an increase of the 15% could be registered. The same overall electrical behavior was detected under dry and at biological conditions. The rather exceptional outcomes of this experiment were interpreted within the framework of proximity-induced superconductive effect, i.e. the emergence of superconducting-like correlations inside a normal conductive material due to the proximity with a superconductor one, undergoing a temperature driven transition. The power law trend

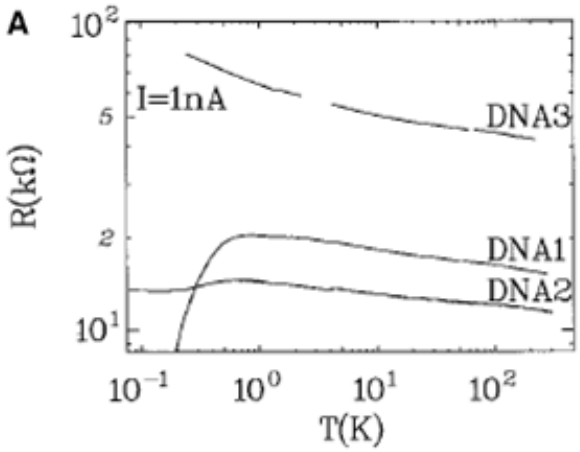

Figure 35: Results of experiment on induced superconductivity in DNA molecules.

of DNA's conductivity, see Fig. 35, observed below the transition temperature was explained through the emergence of a Luttinger's liquid like behavior inside the molecules of this sample.

The observation of such phenomenon inside DNA molecules would imply that DNA is, indeed, a conducting material characterized by a phase coherent length of the order of molecule's size, and as such, its electrical properties could be tuned to that of a very low resistance material, when connected to superconducting electrodes. A Luttinger's liquid is a 1D many-particles state which, from an historical perspective has been considered as a joke by theorists.

Only recently, we gained the possibility to experimentally realize systems really similar to that described theoretical, like carbon nanotubes, semiconducting wires, and organic crystals, and thus to observe the emergence of such phenomenon. The publication of these results, raised a lot of expectations in the scientific community waiting for further, and soundest confirmations, but there were no following works on it.

2.2.3 *Discussion*

One of the motivations, which has been invoked to account for a so huge variety of results, was argued to be in the same nature of electrical be-

havior of DNA which is promoted by the formation of a π-channel, perpendicular to the bases-stack plane. The different interaction mechanisms that DNA's molecules can establish with the substrates used, could compress the electronic structure of the molecules, and suppress the formation of such conduction channel. The role of DNA-substrates interactions to determine the overall length and 3-D structure, of DNA's molecules immobilized on a substrate, has been highlighted by many AFM based experiments, in which the vertical length of the deposited DNA's molecules, at different conditions, shows dependence from many variables.

An underlying problem, when comparing the results obtained in different experiments, is that they vary a lot each-others, not only for the kind of measurement implemented but also for the variety of the samples analyzed. In some cases, very long DNA molecules, with micro-metric lengths and arbitrary sequences, were used.

For these cases, it is hard expecting to observe another electrical behavior that the isolating one, as it is in general accepted that the efficiency of charge transport along molecular bridges decreases fast with the increase of molecules length. Also attention should be paid on the role of electrical contacts between a soft material, like biological DNA, with the metallic electrodes used for the analysis [49].

Achievement of reproducible molecule-metal interfaces for the efficient analysis of molecule's electrical properties, is still object of undergoing investigations. Even, it is difficult to relate the electrical behavior emerging from experiments with single-molecules DNA's conductivity. In many of the reviewed experiments what is actually measured is the conductivity of networks of DNA's molecules, embedded between the electrical contacts.

The emerging interrogative picture from conductivity measures reflects, in part, also the limitation inherent to a language, and a methodology, proper of solid state physics when it is applied to access and to describe, the conductivity of a molecule.

The electronic structure of a molecule, like DNA, is that of a 1D polymer formed by the repetition of given sequences, which is not necessarily periodic. The classical theory of conductivity instead classifies materials as insulating, semiconducting or conducting, according the electronic structure of the semi-infinite periodic lattice. Whether this kind of pic-

ture could be adequate to apply also to biological DNA, or in general to a molecule, is no simple to answer, and one of the principal focus of theoretical works is to solve such a question.

Another important remark is that these results compare outcomes from very different systems, in which not only the length and the sequence of the DNA molecules used may change, but in which even the experimental set-up varies, as well as the environment parameters.

Parallel to these considerations, to address the electronic properties of DNA, as well as that of other polymers, constitute still a technological challenge. To obtain single-molecules electrodes contacts, reproducible and efficient, to report the electronic properties of the molecule, against that of its environment, is object of ongoing investigations.

Only in the last decade, the field of molecular electronic studies has evolved a lot, thanks from one side to the great advancements following the introduction of STM techniques. Then, the rapid development in nano-fabrication processing technologies allows nowadays disposing of different kind of probes, adapted to fit the molecule sizes, and able to easily access the electronic parameters of a molecule: nano-gap electrodes provide an excellent example of such nano-probes.

All these considered, more reproducible, and comparable, experiments are necessary to fix the electric properties of DNA or other molecular systems. In this regards, advancements in nano-probes manufacturing and nano-characterization analysis deserves promising expectative for the development of the field.

2.3 THEORETICAL MODELS

Theoretical understanding of charge transfer and transport properties of DNA should provide a suitable model from which it could be possible to extract physical parameters to compare with experimental outcomes, to propose new experiments and to develop a reliable language of general applicability. The ultimate challenge would be to formulate a unique model to calculate reliable rates of electron transfer k and conductivity values σ.

The phenomenology resulting by the experimental studies of the electrical properties of DNA, characterized by different, and sometimes diverging observations, poses an evident difficulty also to the development of such theoretical model.

Electrical properties in bulk materials are well described by band theory of conduction, which has been at the basis of solid-state devices development too. Theoretical analysis of molecular charge migration is generally worked out by involving one of the two different frameworks [36], *ab initio* calculations, and model based calculations. Former approach, as the name would suggests, is a computational method based on first principles of quantum mechanics, thus relying on the conceptual scheme of band theory. Then, several approximation have been considered in order to solve model equations, and to determine electronic structure and energy configuration of the analyzed system. Hartree-Fock (HF), Density Funcional Theory (DFT), Tight-Binding [23] are some of the approximation frameworks involved to determine electronic band structure. In many cases, they are also used to provide a starting model description which is then refined through further modellization.

With respect HF, *ab initio* calculations based on DFT, in which the state of a system is represented by a functional depending from electron density, instead than a function of electron position, allow less computational effort. Anyway, the main issue in the application of *ab initio* methods is represented by the fact that they requires an high computational cost even in case of simple molecular systems, which yet implies the handling of a huge unit cell to implement Quantum Molecular Dynamic (QMD) calculations, demanding supercomputing facilities and long analysis times. Then, it should be noted that, independently from approximation used, solutions are found imposing periodic conditions, which are not always satisfied. In the case of biological DNA, with a random bases sequences, symmetry system is broken and such approaches, already of complex application unless in case of few bases sequences, reach limited results.

Model based calculations attempt to shift conceptual description of DNA charge migration beyond the general context of band theory by using different quantum model assumptions. Models of DNA charge mi-

gration, based on nonlinear processes [47], through the propagation of polarons [63], or solitons [97] are among these.

These models exploit the coupling of charge carriers to the vibrational degrees of freedom of the molecular electronic states, with the formation of domain walls on the dimerized DNA. Interests in nonlinear DNA's dynamic were brought when it was suggested [63] that the propagation of solitons, along DNA, could play a role in the RNA transcription. During transcription, the double helix separates locally in such a way that one strand provides the template for RNA messenger, to which the genetic information is copied.

Solitons are solitary waves that behave like particles, as the name suggests, and emerge as stable solutions of many model equations used in the analysis of nonlinear phenomena. The stability which characterizes these solutions arises from the critical balance between the nonlinearity and dispersions of the equations model. Solitons-like excitations have been found as solutions of a 1D model, the so-called Peyrard-Bishop-Dauxois (PDB) [62], employed to describe the processes of transcription, replication and thermal denaturation of DNA, for all of which, the local opening of the base pairs is the common starting process. Although this model greatly simplifies over the real complexity of the DNA molecule in solution, it was been found in good agreement with some experimental outcomes.

Polarons, instead, refer to the particle-like state compound by a charge and polarization's state, and they were firstly introduced by Landau for the problem of a charge moving in a polarizable medium.

In a 1D system, as it is DNA's molecule, polarons excitations are expected to spread over several sites rather than to be localized at specific positions. For this reason, polarons transport models have been started to be considered with interests for the analysis of DNA's charge transport. Two kinds of polarons-like excitations could emerge along a DNA chain: those due to structural distortions, and those due to the excess of charges, in the surrounding medium. In the first case, polarons arise because of the π-overlapping of coupled bases, so that when a charge is found on the base stacking, the change of spatial configuration induces the polarization, which gives rise to polarons behavior. In the other case, the same

effect is induced through the environment interaction, and in particular by the excess of charges surrounding the DNA molecule.

Polarons-likes excitations in DNA's molecules were observed in an experiment, recently performed by Barton's group [99], and inferred from the delocalization of holes wave-function.

From the point of view of theoretical works, many questions stay opened, given that no one model is able to fulfill requirements imposed to an effective theoretical description, as stated above. In the following, we will introduce standard method of calculation of charge transfer rates for a generic molecular system which has been largely used in literature to obtain parameters estimations to compare and to interpret experimental results. This will be then applied to the specific features of our system in order to have a rough evaluation of parameters value which could be observed in experiment realizations.

2.3.1 *Rate of DNA charge transfer: standard method of analysis*

Rates for charge transfer along DNA's sequences are usually estimated by describing this process according the known mechanisms of charge transfer theory for a molecular D-B-A system, relying in general as discussed before on the conceptual ground of band theory.

According this [22], [12], charge transfer could arise, on short scale-lengths by uni-step (coherent) tunneling (also referred as super exchange), or by the multistep (diffusive thermal) hopping for longer D-A separation distances, as represented in Fig. 36.

During coherent tunneling, an electron is never localized and does not exchange energy with the molecule, on the contrary in the case of multistep thermal hopping the electron is localized, so that there is energy exchange with the molecule.

For coherent tunneling, charge transfer rate for uni-step, can be determined in the framework of classical Marcus-Levich-Jortner model [41] which applies for no-adiabatic charge transfer processes:

$$K_{CT} = \frac{2\pi}{\hbar}|V_{\pm}(D, A) + V_{DA}|^2 F_{FC} \tag{2}$$

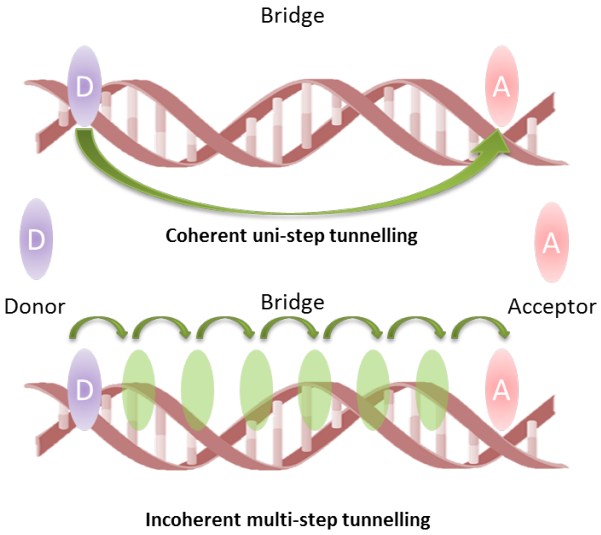

Figure 36: Mechanisms of charge transfer along DNA: Coherent Tunneling (top) and Multistep Hopping.

where $V_{\pm}(D, A)$ and V_{DA} are respectively first and second order electron coupling elements. Resembling of above equation to Fermi golden's:

$$\Gamma_{i\to f} = \frac{2\pi}{\hbar}|\langle f|H'|i\rangle|^2\rho \tag{3}$$

(where ρ is the density of final states per unit energy, and $\langle f|H'|i\rangle$ is the coupling (or overlapping) between initial and final state) which applies in quantum mechanic to calculate the probability of transition $\Gamma_{i\to f}$ from an initial, to a final (eigen)state of a system, under effect of a time-depending perturbation, as introduced by H' is evident.

Both expressions point the focus on coupling element terms to determine the rate of electron transfer, or according the analogy, initial to final state transition probabilities. For a given system, electron couplings values are principally influenced by the constraints imposed by the particular microscopical quantum model H' considered. This latter defines system components and their interactions.

By applying standard perturbation theory, and the scattering matrix formalism, it is possible to calculate first and second electron coupling terms of eq. (2):

$$V_{DA} = V_{\pm}(D, B_1)V_{\pm}(B_N, A)\frac{1}{\Delta E_{DB_1}}\prod_{j=1}^{N-1}\frac{V_{\pm}(B_j, B_{j+1})}{\Delta E_{DB_{j+1}}} \tag{4}$$

where $\Delta E_{DB_1} = E(d^+, B_j) - E(d, B_j^+)$ and $\Delta E_{DB_{j+1}} = E(d^+, B_{j+1}) - E(d, B_{j+1}^+)$ are energy gap values. It should be remarked that whole second order coupling term also depends above the separation energy between the donor and first bridge's unit, as well as on separation energies between the donor and following bridging elements.

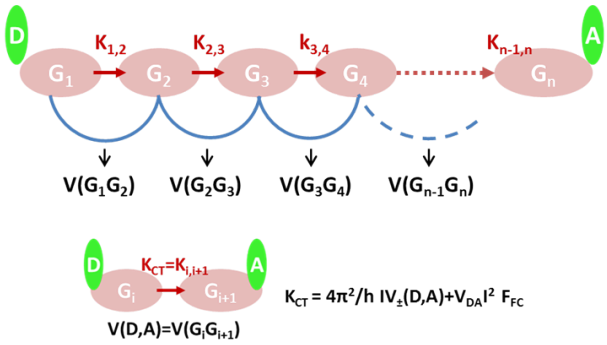

Figure 37: Mechanisms of charge transfer through multi-step hopping via elementary super exchange rates.

By equation eq. 2 it can be seen that charge migration attenuates fast in a range within the length of bridge. In case of DNA, it reduces by a factor of 10 for every 2 Å of DNA's bridge extension.

As a consequence, the single tunneling step process appears unlikely to account for long charge transfer, except over very short distances. For this reason, the interplay of multi-step hopping mechanism has been invoked to account for excepcional charge transfer rates observed in experiments.

Charge transfer rates for elementary hopping processes between adjacent sites, within the whole multi-step path, can be calculated by applying the same model, which holds for uni-step, super exchange mechanism as given by equation eq. (2). So that multi-step hopping is accomplished by a series of uni-step hopping through the individual DBA subsystems along the bridge, as illustrated in Fig. 37.

2.3.1.1 *Electronic Couplings*

Electron coupling matrix elements can be derived by applying standard perturbation theory and scattering matrix formalism. They have been estimated by several authors both for inter-strand (coupling between the two strands of a dsDNA system), and intrastrand site couplings (within the single strand) Fig. 38, by means of quantum microscopical models, which slightly differ one from the other [11], [13]. In case of hole transfer

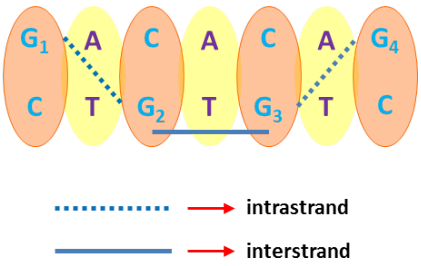

Figure 38: Inter-strand and inter-strand couplings between adjacent bases.

along DNA, they were first calculated by Dee and Bauer by means of a localized discrete jumping model in which it is assumed that charges, and in general, the excitation's migration occurs between neighboring discrete sites along the chain, with total loss of the phase coherence. The main limitation to this description is opposed by the fact that no quantum mechanical coherence (long-range) effects are taken into account. Another model, based on extended Hükel calculations of donor-acceptor electronic coupling were considered by Beratan *et. al.* [87].

In the following we will focus on the results obtained by Voityuk et al.[120] for the matrix elements of all nucleotides pair couplings. These were obtained by assuming a two-states electron transfer model for both inter-strand and intra-strand coupling. The applied method is based upon Hartree-Fock (HF) self consistent field calculations, carried out by means of the software GAUSSIAN which adopt a standard set of basis state functions, the so called $6-31 \quad G^*$. The HF approach has been shown to give results in good agreement with that obtained by means of the more complete active space-state interaction method.

In order to estimate electron couplings, the mutual positions of the four bases in the system should be carefully established. This can be stated in

DNA pair	$v_+^{(\alpha\alpha)}(X,Y)$	DNA pair	$v_+^{(\alpha\alpha)}(X,Y)$
GG	0.084	TG	0.085
GA	0.089	TA	0.086
GT	0.137	TT	0.158
GC	0.110	TC	0.076
AG	0.049	CG	0.042
AA	0.030	CA	0.029
AT	0.105	CT	0.100
AC	0.061	CC	0.041

Table 1: Matrix Elements for Intra-strand Hole Transfer between nucleo-bases pair in DNA, all values are given in *eV*.

DNA pair	$6-31G^*$	$6-311G^{**}$
GG	0.0193	0.0188
AA	0.0347	0.0307
TT	0.0032	0.0037
CC	0.0007	0.0007
GA	0.0211	0.0185
AG	0.0213	0.0237
AT	0.0163	0.0189
TA	0.0163	0.0200

Table 2: Matrix Element for Inter-strand Hole Transfer between nucleo-bases pair in DNA, all values are given in *eV*. Calculations refer to standard geometry and have been performed by using the two $HF/6-31G^*; 6-311G^{**}$ basis set

.

term of rise and twist of the helix, which in the actual case is assumed to be in the regular B-form, characterized by a rise of 3.38 Å and a twist of 36°. Idealized atomic coordinates have been derived by high resolution X-ray studies and involved to generate the examined structures. Results of this analysis are given in the Tables 1, 2.

Values collected in above tables will be used in order to estimate the values for first and second order term of the electronic couplings $V_{\pm}(DA)$ and V_{DA} necessary to evaluate the rates of charge transfer for the process, as presented in the following section.

2.4 CHARGE TRANSFER RATE FOR OUR SYSTEM

Considering this standard description of DNA charge migration, we modeled the process happening in our DNA nano-gap sensor as realized through multi-step hopping, with elementary charge hopping rates, given by the super exchange rate constant of equation eq. (2).

By assuming this hypothesis, we were able to estimate charge transfer rate of our molecular system. This approximate calculations will allows us to have an idea about the range of conductivity values of our system.

In order to implement this analysis, we considered the molecular chain formed by CP1-TW-CP2, formed after target hybridization. It alternates, electrode-to-electrode ssDNA, and dsDNA short pieces, referred ssCP1, dsCP1TW1, ssTW, dsTW2CP2, and ssCP2, as it is schematized in Fig. 39. This includes, ssCP1 comprising the first 33 single nucleotides of CP1,

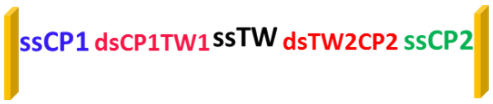

Figure 39: System model scheme applied to calculate charge transfer rate characteristic of our system.

dsCP1TW1 is the double strand formed by the remaining 20 CP1 bases after hybridization with the corresponding complementaries of TW (indicated as TW1), ssTW is target sequence which is not complemented, while dsTW2CP2, and ssCP2 are respectively dsDNA obtained by hybridization of target to the other CP, and the terminating ssCP2 sequence, Fig. 40. Each, can be thought as builded up by a certain number of DBA

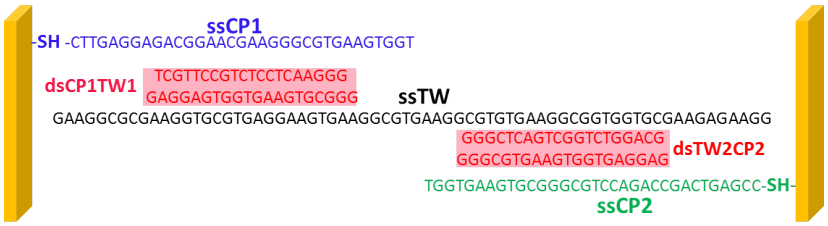

Figure 40: Sequences of the molecules involved in our model calculations.

systems like DB1B2...BNA , where D and A are donor and acceptor

states which we assume to be guanines, through B1B2...BN molecular bridge nucleo-bases. We calculated first ss's contribution (ssCP1, ssTW, and ssCP1=ssCP2), for which only inter-strand hopping can arise. We

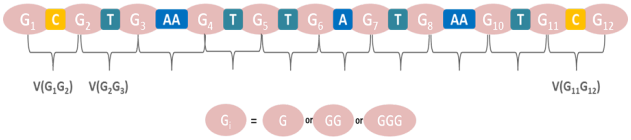

Figure 41: Schematic of charge migration for ssDNA(CP) considered

will refer to them as: ssCP1, dsCP1TW1, ssTW, dsTW2CP2, and ssCP2, where ssCP1 comprises the first 33 single nucleotides of CP1, dsCP1TW1 is the double strand formed by the remaining 20 CP1 bases hybridized to the corresponding complementaries of TW, indicated as TW1, ssTW is target sequence which is not complemented, while dsTW2CP2, and ssCP2 are respectively dsDNA obtained by hybridization of target to the other CP, terminating with ssCP2 sequence.

We calculated first ss's contribution (ssCP1, ssTW, and ssCP1=ssCP2), for which only inter-strand hopping can arise. With reference to the schematic modelization of Fig. 41, we calculated second order coupling term of each occurring GXG (where X is any of other nucleo-bases) subsystem between the first bridge site, 1, and the last 11. These reduces to:

$$2V_{GAAG} + V_{GAG} + 6V_{GTG} + 2V_{GCG} \tag{5}$$

where:

$$V_{GAAG} = |\nu(G,A)|^2 \times \frac{\nu(AA)}{\Delta E_{GA}^2} \; V_{GAG} = \frac{|\nu(G,A)|^2}{\Delta E_{GA}}$$
$$V_{GTG} = \frac{|\nu(G,T)|^2}{\Delta E_{GT}} \; V_{GCG} = \frac{|\nu(G,C)|^2}{\Delta E_{GC}}$$

In this case, it reduces to:

$$7V_{GAAG} + 2V_{GAG} + 7V_{GTG} + 2V_{GCG} \tag{6}$$

According schematic process represented in Fig. 42 we accounted for contribution along ssTW. Then, we evaluated second order electron coupling contributions along the two dsDNA segments, dsCP1TW1 and

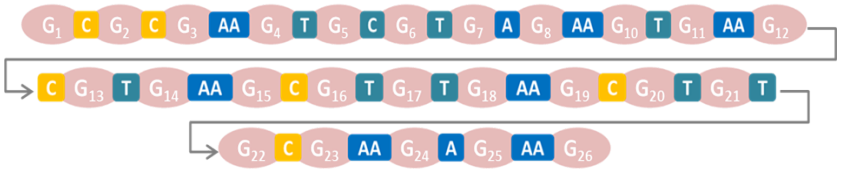

Figure 42: Schematic of charge migration for ssDNA(TW) considered

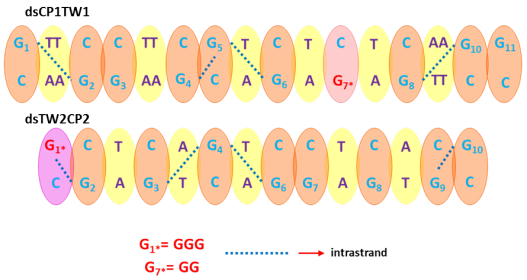

Figure 43: Schematic of charge migration for dsDNA(TW) considered.

dsTW2CP2, whose structure is schematized in Fig. 43. In this case, charges hopping can arise both by inter, than intrastrand donor acceptor couplings, through occurring A-T bridges. For each elementary subsystem, as in Fig. 44: where n is the number of A-T nucleo bases, second order

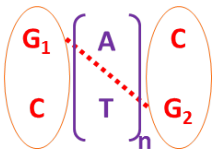

Figure 44: Elementary coupling in intrastrand hopping.

intrastrand coupling writes:

$$V(D,A) = \frac{V(G,T)[V(T,T)]^{n-1}V(G,T)}{\Delta E^{n}_{GT}} \tag{7}$$

$$V(D,A) = \frac{V(G,A)[V(A,A)]^{n-1}V(G,A)}{\Delta E^{n}_{GA}} \tag{8}$$

for hopping through A or T, respectively, so that we obtain for processes through to the sequences of Fig. 43:

$$V(\mathrm{dsCP1TW1}) = 3\left[\frac{V(G,T)^2V(T,T)}{\Delta E_{GT}^2} + \frac{V(G,T)^2}{\Delta E_{GT}}\right]$$
$$V(\mathrm{dsCP1TW1}) = 3\left[\frac{V(G,A)^2V(A,A)}{\Delta E_{GA}^2} + \frac{V(G,A)^2}{\Delta E_{GA}}\right] \tag{9}$$

and:

$$V(\mathrm{dsTW2CP2}) = 6\frac{V(G,T)^2}{\Delta E_{GT}}$$
$$V(\mathrm{dsTW2CP2}) = 6\frac{V(G,A)^2}{\Delta E_{GA}} \tag{10}$$

Then, by substituting numerical values of electronic couplings, in eq. (9), eq. (10), and reminding that, first order contributions are all equals to electronic coupling between donor and acceptor, or $V(D,A) = V(G,G)$, we could evaluate charge transfer values.

DNA strand	$K_{CT}(s^{-1})$	$g(G_0)$
ssCP	$4,49 \times 10^{12}$	$0,035G_0$
ssTW	$5,71 \times 10^{14}$	$0,044G_0$
dsCP1TW1	$9,88 \times 10^{14}$	$7,66G_0$
dsTW2CP2	$4,88 \times 10^{14}$	$3,39G_0$

Table 3: Rate for charge transfer, and corresponding conductivity values, expressed as multiple of the conductance quantum G_0

.

Results are collected in the following table Tab. 3, which includes conductivity values (expressed in function of $G_0 = 12,9 \times 10^3\Omega$). These values were obtained by applying the next equation:

$$g \approx \frac{8e}{\pi^2\Gamma_D^{(L)}\Gamma_A^{(R)}F}k_{D\to A} \tag{11}$$

where e is the elementary electron charge, and $\Gamma_{D(A)}^{L(R)}(E)$ are the widths of donor and acceptor states coupled to the metallic left, and right electrodes; F is the Franck-Condon factor, and $k_{D\to A}$ is the rate for electron transfer.

This useful relationship was derived by Nitzan [78], and provides a very practical instrument to have rough evaluation of the parameters to expect measuring in experiments. It is derived under the assumption that molecular wire actually behaves as a conductor embedded between two metallic electrodes.

From theoretical models and experimental results it is possible to give approximate values for the parameters appearing in eq. 11. Indeed, since $\Gamma^{L(R)}_{D(A)}s$ are of order of 0.5 eV one obtains: $g \cong [10^{-17}k_{D\to A}(s^{-1})]\Omega^{-1}$, which could be used to establish a criterion in order to observe a conducting behavior. For example, in the case of our current detector, which has the sensitivity of fempto-ampere, a rate of 10^3 s^{-1} to observe Ohmic behavior at 0.1 V is necessary.

Obtained rates for charge transfer are rather greater compared with that observed, for example, in fast photo induced electron transfer between metallo-intercalators bound to a 50 base-pairs DNA sequence, which is of order $\approx 10^{10}s^{-1}$. This, as well the resulting conductance values are greater than thats typical found in single walled carbon nanotubes ($2G_0$), for which a ballistic conduction model applies, should not be surprising. These latter were in fact obtained under hypothesis of a conductor-like behavior of molecular system embedded between electrodes.

Then, it is useful to remind that rates for charge transfer were estimated by assuming that hopping between two subsequent donor-acceptor sites is mediated by the super exchange mechanism, which could lead to overestimate contribution obtained over system comprising a large intercalating bridge, between proper hopping sites.

2.5 CONCLUSIONS

Being of relevance for DNA detection, as well for the development of nano-electronic devices thanks to self-assembly and base-pair recognizing properties of DNA, electrical behavior of DNA is meaningful, indeed, to clarify its biological functionality being involved in many pathological instances through oxidative DNA damage. For this, the possibility that DNA backbone could provide a medium for efficient charges migration over long molecular distances, has been intensively investigated

after early experimental evidences claiming for molecular wire-like rates of charges migration. Initial excitement, following pioneering experiment results, was progressively weakened as diverging outcomes from direct contact molecule measurements were reported by applying different, sophisticated measurement methods.

A part reflecting the intrinsic difficulties existing in making good electrical contacts to an object with a diameter of few nano-meters, this deserves for the need of reproducible, and comparable analysis systems. The cloudy experimental background poses additional challenge for the development of a suitable theoretical model, accounting for distinct results. The general approach followed by theorists has been to combine known mechanism for biomolecule charges migration, tunneling and hopping between donor and acceptor site. By means of their interplaying, it is possible to explain global features of DNA charge migration over length above that settled out by tunneling.

In this chapter, we provided a picture of mechanisms for DNA charge migration's current understanding, by revising experimental and theoretical backgrounds. Then, we developed a phenomenological model to describe charge migration along DNA sequences which will be further used to assembly and testing our devices, allowing us to evaluate migration process rates.

This model relies on the standard description of DNA charge migration based on the interplaying between tunneling and multi-step charges hopping. By exploiting electronic couplings values found in literature, generally derived by assuming microscopical quantum models and scattering theory based calculations, under the hypothesis of conductor-like behavior, it was finally possible to related calculated rates to conductance values.

3

NANOSENSORS: FABRICATION AND CHARACTERIZATION

The introduction of micro/nano-electronic systems (M/NEMS) providing the advantages of automation, portability, low sample and reagents volumes, and lower response times has already had a great impact in the field of life sciences and biomedical research. This is expected to have a growing impact even in the development of future diagnostic and therapeutic approaches, inspired by the idea of a "Smart Medicine" enabling both research, diagnostic and also therapeutic at the point-of-care.

Ability to fabricate features with micro and/or nano-scale definitions on several class of materials, allowing the possibility of smart sensors integration to build devices capable to sense, decide and react, is a relatively new achievement. This has been gained on the back of great advancements in nano-scale fabrication, and characterization techniques.

We made use of several processes typical in M/NEMS fabrication technologies in order to obtain devices, which will be used in experiments. These were characterized accordingly available methods. Fabrication, and characterization techniques enabling principles will be introduced before detailing the operation protocols followed for their application in our case. Results of fabrication were accounted by means of several characterization techniques, divided in Optical, and Electrical/Electrochemical based analysis.

3.1 BUILDING MICRO AND NANO-SCALED STRUCTURES

The fabrication of systems with micro and nano structure details definition is achieved by using different processes [10]. Nanofabrication methods are usually divided in two major categories, namely as *top − down*, and *bottom − up*, Fig. 45. The former mainly exploits transference of a

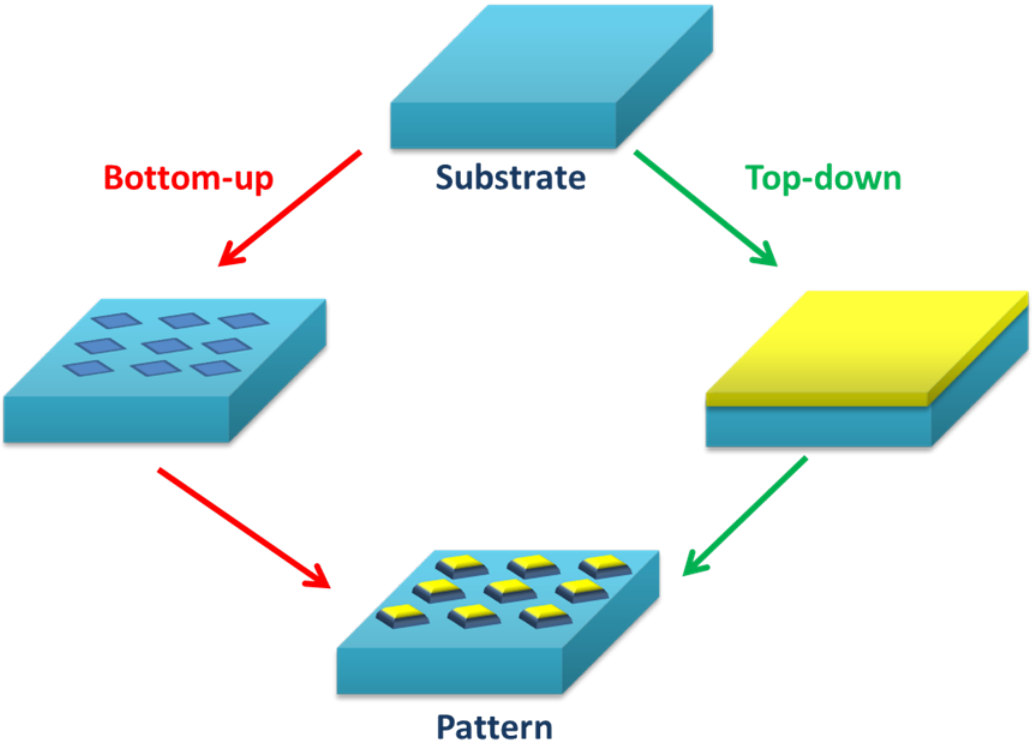

Figure 45: Bottom-up vs Top-down fabrication approach: growing up vs pattern transfer

given pattern to a specific surface, in such a way that nano-scaled structures/functional devices are finally obtained by starting from larger dimensions scaled down to desired. The latter instead explores self-assembly of atoms and molecules directed through chemical mechanism and suited technologies to build multifunctional nano-structured materials. Given the broad range availability of nano-fabrication processes, we will introduce with more details thats listed below:

- Thin film deposition, generally used to obtain thin metal layers on SOI or plastic substrates:
- Patterning (Lithography)
  - Optical Lithography
  - Advanced Lithography (E-beam, FIB, Scanning Probe Lithography (SPL), nano-imprint)
  - Alternative lithography (Soft-lithography, Imprinting Lithography)
- Materials Etching
  - Wet etching
  - Dry etching

Here we explored a top-down fabrication approach, based on standard UV photolithography, to transfer the conceived nano-gap electrodes arrays patterning on a SOI wafer metalized by a thin adhesion layer of Ti and a 70 nm thickness layer of Au.

A second photolithography, through the corresponding passivation (negative) masks, was involved in order to protect the pads, and other pattern elements, for electrical connections during SiO_2 sputtering, so that they can be finally opened by lift-off of the underlying photo-resist.

Principles, and capabilities of involved fabrication processes will be introduced in the following section. Then operational methods, which we applied to fabricate nano-gap electrodes array, are described, and results are finally discussed according the different characterization analysis.

3.1.0.2 *Photolithography*

Standard photolithography allows to easily obtain arrays of micro-patterned circuits on a huge variety of materials, with increased reproducibility of patterning details inside an array, and between different arrays, achieved through the parallel processing of many copies at the same time.

Increased reproducibility of the results, and the reduced processing time, waste of materials and equipment, allowed exploiting photolithography for mass scale production of microelectronic devices.

This is optical based process by means of which it is possible to achieve the transfer of a given pattern onto the surface of a substrate, coated with a photo-resistive polymer. Photo-resist is an organic material which is light sensitive, in particular, under light exposition photo-resist is cross-linked so that, its exposed or unexposed parts, depending on photo-resist type, whether positive or negative, have increased solubility and can be then chemically removed, leaving the desired pattern ready for further processing like evaporation, etching, and/or deposition.

In conventional lithography, light is collimated through a quartz plate supporting the patterned mask. During light exposition, quartz plate is put in proximity or in contact with the substrate, allowing resolution limit of about 1 μm with a 400 nm light. Increased resolution is made possible by projection lithography, in which a lens is interposed between mask and substrate.

In general, intrinsic bound to resolution of optical systems is posed by light diffraction, as it is accounted by Rayleigh criterion, according which the smallest distance which can be resolved by an optical detector is:

$$R = 0,61\frac{\lambda}{NA} \tag{12}$$

where:

$$NA = n \sin \alpha \tag{13}$$

is the numerical aperture of the system. In case of project alignment, this can be used to calculate line-space pitch resolution resulting in:

$$2b = K\frac{\lambda}{NA} \tag{14}$$

with $k \approx 0.3 - 0.9$ depending on the lithography system. From above eq. (14) it is seen that increasing resolution requires varying one of the parameters K, λ, or NA, as explored in advanced lithography technologies.

Wafer processing by photolithography is carried out in clean room facilities, where reduced atmospheric pollutants, and controlled environment

parameters prevent surface contaminations and assure constant working conditions. A batch-line with yellow light and protected from other light exposition is found standardly in clean rooms. A whole photolithography

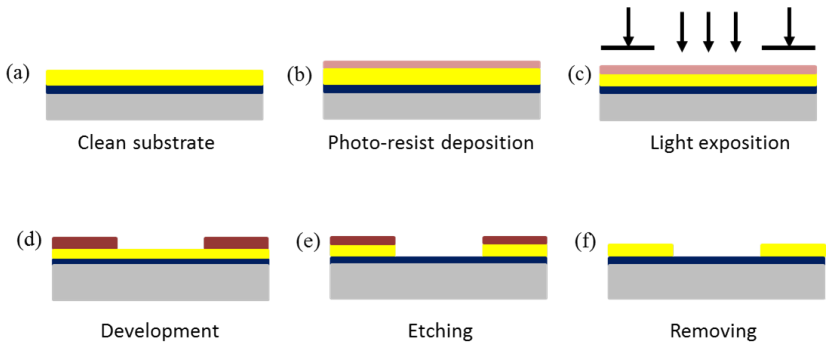

Figure 46: Processings steps in standard photo-lithography.

process accounts for the following steps, Fig. 46:

- a clean substrate, eventually metalized with desired material;
- resist coating, done with a spin coating equipment, the goal of this stage is to assure the deposition of an uniform thin film of the photoresist over whole wafer's surface;
- mask alignment; mask carrying desired pattern is placed at nanometric proximity of substrate;
- light exposure; with the proposal of transferring the pattern through a mask to the substrate coated with the photoresist: UV light is standardly employed;
- resist development; in the case of an exposed pattern it is used for the etching of unexposed parts, while in the case of an exposed pattern it is used for the evaporation of metals on the substrate, or of depositing reagents;
- etching; this is usually carried out by means of either a chemical bath or a dry etch procedure, to remove exposed metals.

This process is even achieved by starting from a cleaned substrate, which after resist development is provided by a metal layer either evaporated

and sputtered on the opened pattern area. In this case an etching step is not necessary.

3.1.0.3 *Advanced photolithography*

Inherent limitations arising in optical system due to light diffraction can be overcome, according the Rayleigh criterion eq. (12) by changing one of parameters, defining achievable pitch line distance separation eq. (14).

E-beam and FIB assisted lithography allows to extend resolution limits by varying wavelength of scanning probe, through employment of a collimated electron, and ion source, respectively. Both can be classified as direct lithography methods, because patterning is achieved without use of a mask. Overcoming diffraction light limitations makes it possible to create structure with nano-metric features. For this reason, they are considered superior lithography techniques with respect conventional photolithography.

Despite, the need for serial sample processing leads to considerably lower throughput, indeed they require use of sophisticate equipments, FIB and E-Beam systems, resulting in a rather costly technology and an overall complex processing.

3.1.0.4 *E-beam lithography*

E-beam lithography, compared to FIB, requires rather more processing, in fact it involves pattern transferring on a substrate coated with an electroactive resist, and materials etching in order to reveal patterned area [111].

Typical e-bem processing is schematized in Fig. 47.

Briefly, a high focused electron beam source is used to modify resists properties under exposition, in such a way that, in complete analogy with standard photolithography, resist solubility is affected during following development in a proper solution bath. Achievement of high resolution, high density, high sensitivity and process reliability by e-beam technology is related to many working parameters.

Principally, these are the quality of optical system, from which depends the ability of generating a high focused beam-spot; resist properties, and in general process conditions, such as working out a good thin

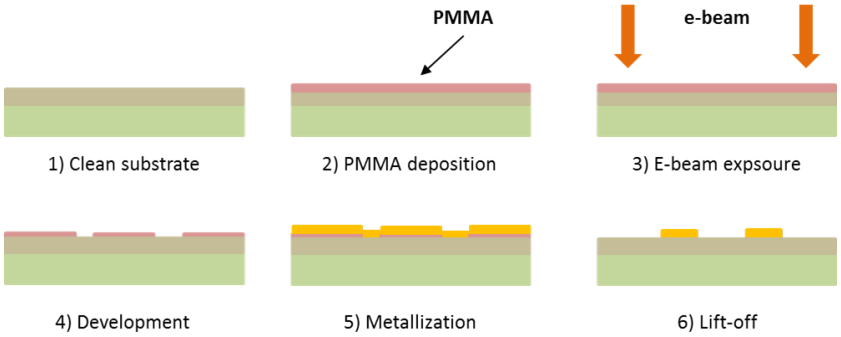

Figure 47: Processing step in e-beam assisted lithography.

resist layer, employment of well optimized development and etching parameters. Controlling interrelations between all these variables could be rather complicated, with increasing difficulty as the resolution required gets more fine.

With respect e-beam lithography, although of comparable sophisticates, lithography processing assisted by FIB is instead realized through direct material etching, under ions bombing.

3.1.0.5 *Focus Ion Beam (FIB)*

FIB is principally a method employed as a machining tool in the modification of structures allowing nano-metric definition [75].

The basic working principle of a FIB is common with that of Scanning Electron Microscopy (SEM), with the exception than an additional ions probe source is provided, allowing surface modification by erasing material at atomic level. In FIB, the sample is scanned by means of a finely focused beam of ions (generally of gallium ions), which are positively large (slow) particles, if compared with the electrons, which constitute the probe of SEM.

A scheme of FIB microscope is given in Fig. 48. By detecting the secondary electrons emitted following the interaction of scanning ion probe within the surface, it is possible both to image, and to process the sample surface.

Opposite to the electrons, ions beam interaction with a surface, results in a destructive process which cause the etching of target surface

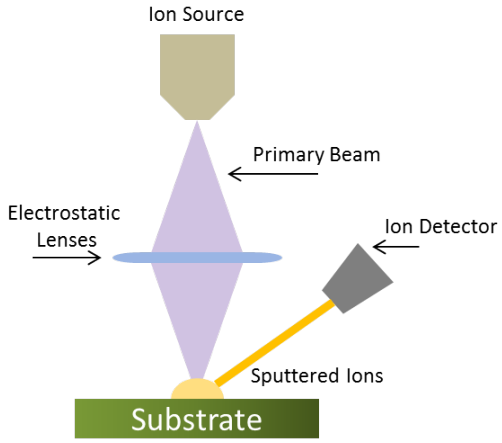

Figure 48: Scheme of a FIB equipment.

atoms, which makes it possible the use of FIB as a machining tool in nano-fabrication processes through selective material etching. Ideally, FIB permits to etch away one atomic layer, without interacting with the subsequent one.

Use of a charged probe in FIB, as well in SEM, could be an issue when treating with isolating surfaces. For this reason, in some cases a low energy electron gun is employed in order of neutralizing primary ion beam charge, providing a way for imaging the surface, without the need of a conducting mask as required sometimes by SEM, in which the screening effect, arising from charges accumulating on the analyzed substrate, is higher.

We used FIB based nano-lithography to mill nano-gaps with desired opening sizes inside the path connecting to active micro-pads electrical connections. Compared to other nano-gaps fabrication processes so far explored, like electro-migration [59], mechanical-stress [60] or other [114], the lithography based approach displays some unique advantages. Although on the nanometer scale it relies on more complex processing, it allows high aspect-ratio pattern definition with increased predictability, and reproducibility, compared to other methods. For this reason, it represents a powerful tool to fast engineer versatile nano-gap systems.

3.1.1 *Soft lithography*

Under this category are classified all lithographic processes based on printing, embossing, or replica of a mold, which usually is a patterned PDMS layer. Thanks to the remarkable properties expressed by elastometer materials, such as the wide applied polidimethylsiloxane (PDMS), allowing micro and nanometer scale detail features, soft lithography extend photo-lithography approach beyond the border of semi conductive "hard" materials. This is particularly useful to exploit prototyping of biocompatible, and flexible materials, which are especially important to develop dressible electronic devices.

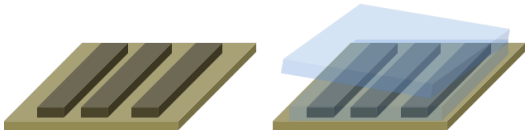

Figure 49: Replica Molding working principle

Here we focus on replica molding soft photolithography. Despite other methods, this could involve a photolithography step in which the pattern is previously transferred to a master. The mold is then obtained by peeling-off the used elastometer, Fig. 49 and it can be used to further replica.

We used this process to obtain a micro metric thin PDMS membrane to cover sample surface, leaving opened holes for pads connections, and solution delivering in proximity of nano-gaps.

This membrane, in general useful to protect device surface, was exploited to assembling nano-gap electrodes array of 1", into the holding system conceived to allows micro-fluidic integration, and parallel electrical analysis of multiple nano-gaps. For this reason, we need a very thin layer of material to favor array embedding and its stability, but keeping the reduced, and compact characteristics of the system.

3.1.2 *Wet/Dry Etching*

These two techniques are employed in order to selectively etch materials from surfaces, and can be applied to several targets. Both procedures exploit a chemical reaction in order to achieve layer etching, with the exception that in wet-etching the reaction takes place in a solution, while dry etching usually involves ion bombing, and for this reason should be worked out in a vacuum chamber.

The two processes are characterized respectively, as isotropic and aniso tropic, according attack's directionality.

In a wet process, the etching rate is the same in both horizontal and vertical directions, while in dry etching, these are distinct. While wet etching is a low cost process, easy to implement, characterized by high etch rates, and with a good selectivity for several materials, it is inadequate to define features below 1 µm.

Compared to this, dry etching could achieve definition below 100 nm, but it is more expensive and has low throughput, with respect wet-etching. It exploits the reactive feature of plasma to remove, by chemical attack, a given material.

A typical reactive ion etching (RIE) system is constituted by a vacuum chamber in which can be usually allocated one single wafer, Fig. 50. The

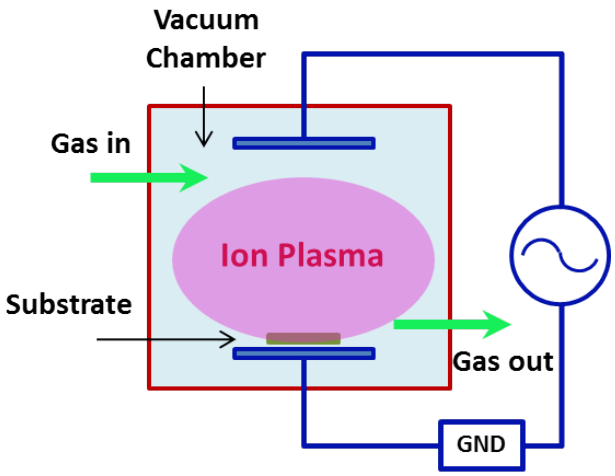

Figure 50: Schematic of RIE used for Ti etching.

high energetic ions of the plasma, generated in a vacuum chamber by

applying a radio-frequency (RF) field, react with the wafer's surface. The oscillating electromagnetic field ionizes the gas molecules giving rise to the ionic gas, or plasma. The ions, bombed on the surface, promote the reaction between active element and the material to remove.

3.1.3 *Sputtering*

Sputtering is one of the techniques exploited into NENS and MEMS applications, through which it is possible to deposit a thin film of material on a given substrate. Several protocols are available allowing to treat many materials, as well different adhesion substrates.

These can be classified in two main standards: physical vapor deposition (PVD), and chemical vapor deposition (CVD), which as the names suggest are respectively based on physical interactions, and chemical reactions.

For some materials and depending from target surface, these processes could require special environment conditions, for this CVD's usually differentiate into Atmospheric VD or simply CVD, Low Pressure VD (LPCVD) and Plasma Enhanced VD (PECVD).

During sputtering, the surface of a given target material is bombed by a high energetic ions beam which causes the emission of its atoms or molecules; the emitted particle are then deposited on the substrate of interest, by the condensation that they undergoes on the vacuum chamber walls; the source of ions can be of several kinds, as for example it is a plasma which can be obtained under specific parameters, which mainly depends from features of the deposition. Equipment used in sputtering is basically constituted by a vacuum chamber, complemented with ionic cannon. A plasma state can be induced, and then maintained, by applying Magnetotron, Radio Frequency (RF), or DC. Target material surface is fixed on a rotating plate, in order to achieve uniform particles emission to compensate the directionality ions source, Fig. 51. Among the different methods, sputtering is available for a wide range of materials, with uniform and reproducible results.

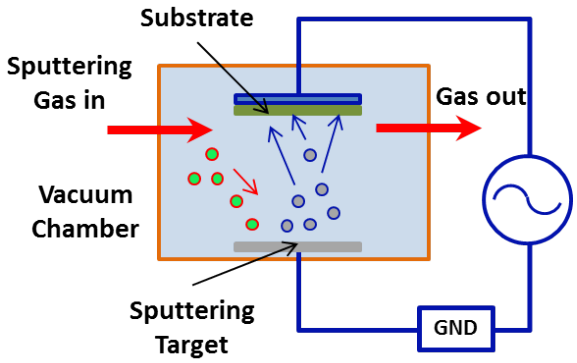

Figure 51: Working principle of a sputtering equipment.

3.2 NANO-GAP SENSORS ARRAY FABRICATION

3.2.1 *Lay-out Patterning*

3.2.1.1 *Masks Design*

Patterning lay-out was designed by using the software CleWin4.0. We considered the simple and denser array patterning of Fig. 52 for the firsts *proof of concept* experiments. Then, we conceived the bit more complex cir-

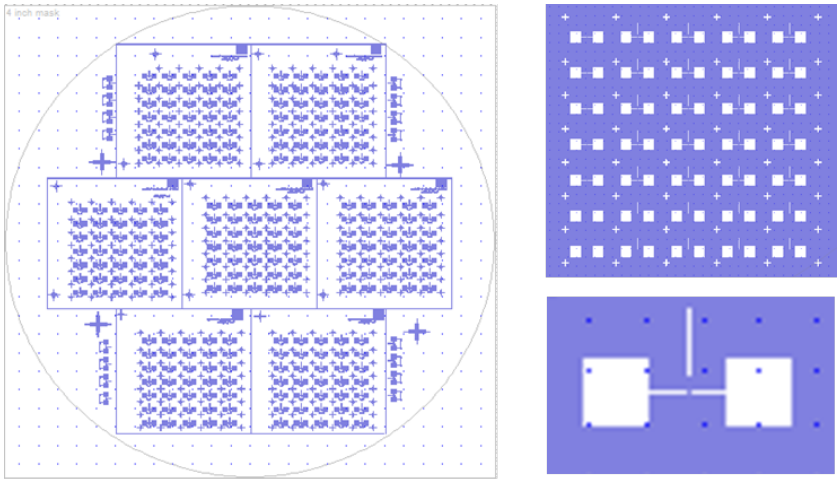

Figure 52: Cle-Win lay-out of the first electrical pattern (mask1) and of corresponding negative (passivation mask) pattern.

cuitry of Fig. 53, which allowed to readily carry out electrochemical characterization of devices. These patterns, with aspect ratio of 2.60 µm and

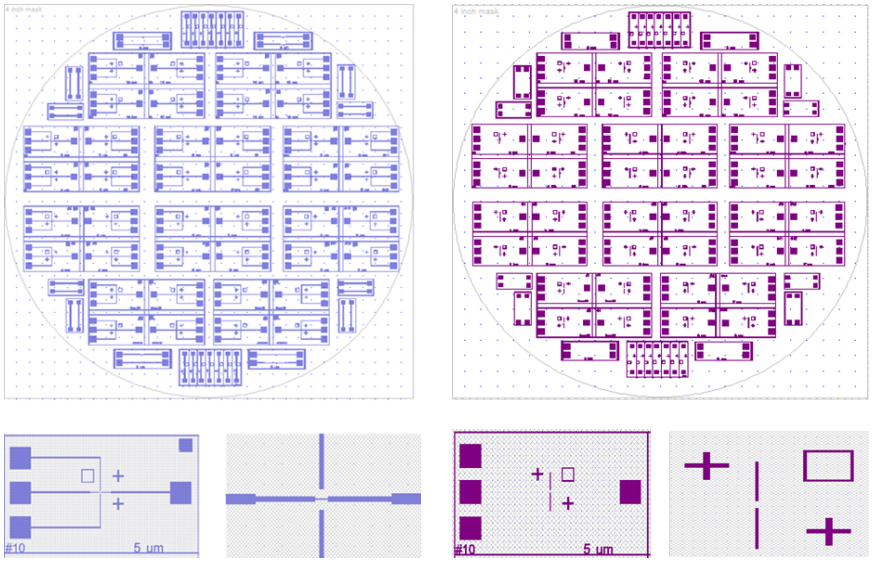

(a) Positive mask (b) Negative mask

Figure 53: Patterning lay-out used for electrochemical characterization (mask2).

23.09 µm respectively, were transferred on chromium masks by means of Direct Laser Lithography, worked out by the DWL66fs system of Heidelberg Industries, having a write head of 4 nm and a resolution of 0.6 µm.

Masks used for electrical circuit passivation were impressed by laser on acrylate acetate. This a far cheaper method which is well suited to low aspect-ratio photolithography application, as in case of our passivation routine. Chromium masks were thereafter used to pattern wafer by standard photolithography.

3.2.1.2 *Photolithography*

Wafers were furnished by the Centro Nacional de Microelectronica of Barcelone, and comprise alternating layers of Si of 1 µm of thickness, 10 nm of Ti and 70 nm of Au. Prior to photolithography they were cleaned by rinsing with acetone, ethanol, and isopropanol, then dried with a N_2's flow.

This procedure assures that the wafer's surface is free of all organic and inorganic contaminants, which could affect the uniformity of deposited photoresist layer in the following step, Fig. 54.

Figure 54: A clean substrate is covered by the photoresist in a spin coating system.

Spin Coating of the photoresist has been carried out by using the Spinner ModelWS-650MZ-23NPP/LITE of Laurell Technologies Corporation.

We used a positive photoresist, the AZ1512, spinned at a final rotation speed of 8000 rpm for 1 minute, reached through a three steps process, which, according the technical indications, should results in the deposition of 1 µm of photoresist.

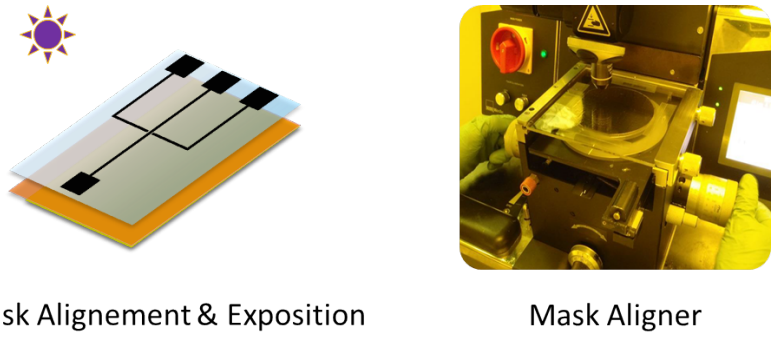

Figure 55: Pattern transferring through UV light exposition using a Mask Alignment equipment.

Once covered with the photosensitive resist, the substrate is post-baked at 95°Cfor 1 minute, to dry the excess of solvent, not evaporated during spinning.

Mask alignment and UV-light exposition were done using the Mask Aligner MJB, SUSS Microtec, Fig. 55. Light intensity was 26.5 $mWcm^2$ and it was applied for 7.2 s.

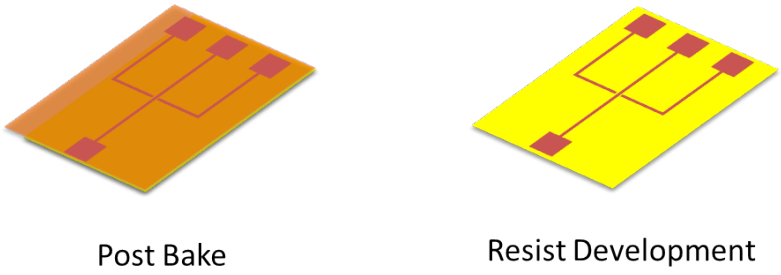

Figure 56: Developing of the resist achieve its removing from light exposed pattern.

After exposition, photoresist was developed by immersion in a bath of the AZ developer, NIF120, during 25 s, sufficient to dissolve it from exposed pattern, and to open these patterning area to the chemical attack, further used to etch the not patterned areas, Fig. 56.

3.2.1.3 *Sacrificial layers removing*

We used a wet etching bath to remove gold from exposed patterning area, followed by dry etching of the Ti underlying exposed gold.

3.2.2 *Gold Wet etching*

Gold removing from exposed pattern was achieved by a wet etching process.

Being a noble metal, gold is characterized by an electronic configuration which prevents it to easily react with the most part of elements, and chemical compounds. Gold wet etching therefore requires the use of a strong oxidizer in order to unpair the valence electrons, and of a complexing agent, which prevents the reassembling of oxidized atoms, back to the crystalline structure.

To achieve gold etching of not-patterned area, the wafer was submitted to a bath of the chemical etchant type TFA of the Transene Company, Inc.

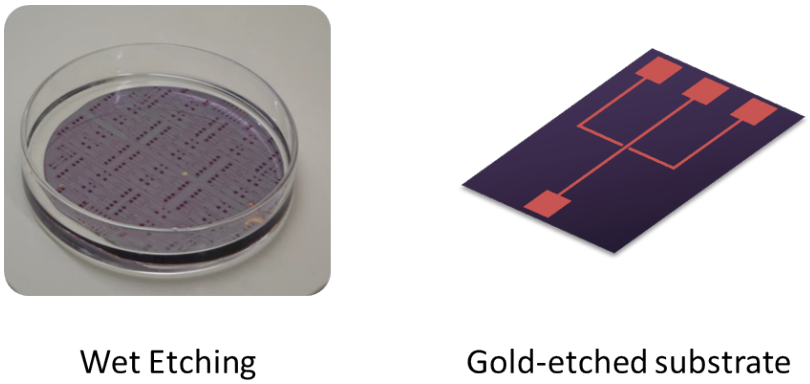

Figure 57: Wet Etch of Au layer.

Danvers MA 01923, which is characterized by a rate of 28 Å/s at 25°C, resulting in a immersion time of 25 s to etch the gold thickness of 70 nm (Fig. 57).

Once the not-patterned gold was etched, the underlying titanium layer was attacked by RIE.

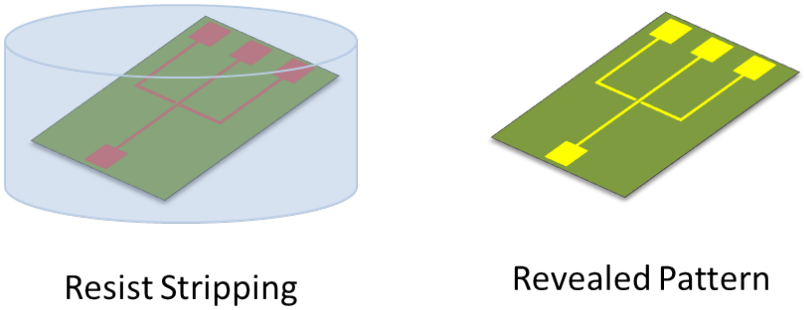

Figure 58: Resist Removing.

The RIE process was carried out by submitting the wafer to two different ion plasmas formed respectively by Cl_2, for 1 minute with a flux of 50 sccm at a nominal value of 40 mTor, with a RF power of 250 W, and by CHF_3 applied with the same parameter, with the only difference for the time of exposition, which in this case was 5 minutes.

The first plasma acts by inducing the formation of TiO_2 while, the second strips away the oxide formed during the previous step.

Thereafter RIE, photoresist removing from unexposed pattern, was finalized by immersing the wafer in a bath containing the AZ 100 Remover (from AZ Electronic Materials) for 10 minutes, Fig. 58.

3.2.3 *Lay-out passivation*

3.2.3.1 *Photolithography*

Processed wafers were thereafter submitted to a further photolithography with the proposal of achieving on selected pattern area, a protection layer of SiO_2 sputtered, by exploiting photoresist properties under UV light.

Passivation patterns, Fig. 59, were transferred from an acrylate acetate mask on the wafer coated with the positive photoresist already used, according the same process of first photolithography.

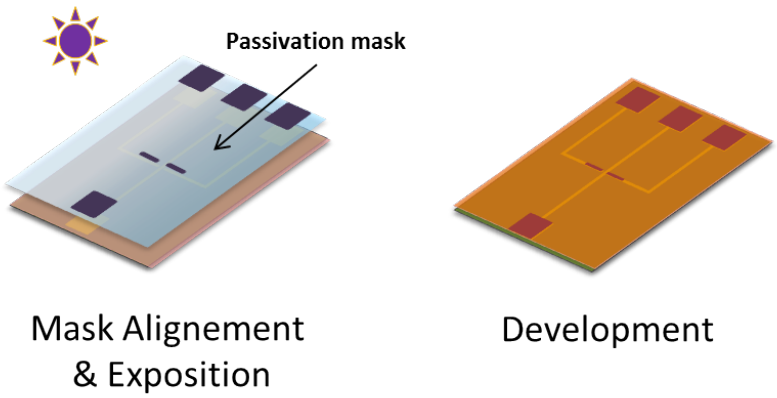

Figure 59: Photolithography through the passivation mask.

Passivation masks leave open to UV light exposition all patterning but connection pads, and the auxiliary electrodes (where present) Fig. 59, in such a way that during development, exposed resist dissolves and it is removed, while the unexposed stays, providing the desired SiO_2 protection layer, except on the pads and auxiliary electrical connections.

Chemical attack of photoresist, after sputtering with SiO_2 of whole wafer surface, makes then it possible to open pattern area to electrical connection.

3.2.3.2 *Sputtering*

Sputtering was carried out by the use of ACT ORION sputtering device, available at Institutes de Ciencies Fotoniques (ICFO); plasma's generation was achieved by applying a potential ramp of 100 W for 360 s to a gas of Argon, pumped in the chamber, were a 30 mTor vacuum environment was previously obtained.

Then, the gas of SiO_2 is also turned on, and plasma is generated by applying a subsequent potential ramp for 600 s; after plasma generation, chamber pressure was lowered down to the value of 2 mTor, in order to induce plasma's condensation on the wafer surface, and put in rotation at 20 rpm.

The times of deposition change within the material's features and the thickness, which one wishes to deposit. It was observed that in order of sputter the wafer surface with a film of SiO_2 in the range of 55 to 60 nm it was necessary a time of approximatively 55 minutes.

3.2.4 *Nano-gaps milling*

We used the nano-lithography capability of FIB to open the nano-gaps between electrode's pads, with size of 40-65 nm, corresponding approximatively to the longitude of DNA's sequences involved.

Nano-gaps depth is about 140 nm, accounted by considering SiO_2, Au, and Ti multilayer thickness, in which it is milled.

The working parameters of the ionic beam, the intensity and dwelling time were adjusted in a series of preliminary cuts, as shown in Fig. 60, in which we keep fixed beam energy (E) operating at a voltage of 30 KeV and a current intensity of 10 pA, while increasing milling times of 0.5 s starting from 3 s. Milling time slight variations, as that considered by following cuts in Fig. 60, result in different sizes. In general, resulting nano-gap sizes is influenced by more parameters than power generated by beam source.

Undoubtedly, surface roughness, in proximity of milling area, plays a leading role. Region explored in FIB optimization is rather small compared to whole wafer surface, meanings that applied beam parameters

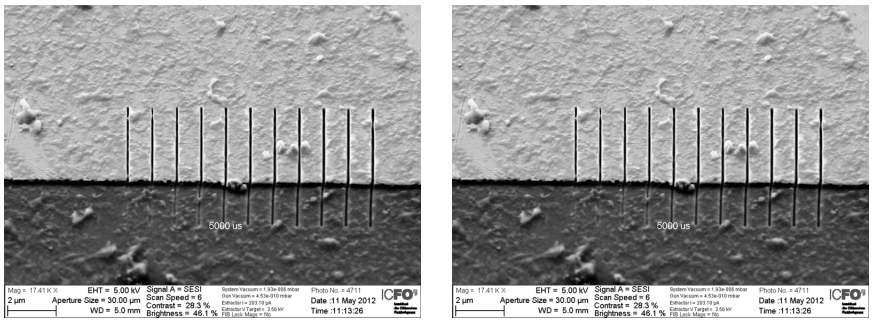

(a) FIB parameters optimization (b) Resulting nano-gaps size.

Figure 60: Dwelling time optimization.

are not effective predicables with respect final size results, because surface roughness can be mislead. By following the same reasoning, we expect that same milling times will achieve distinct nano-gap sizes for small surface roughness changes, as it is normal to observe on different area of processed wafer.

The rate of nano-gap production was on average of 2-3 nano-gaps per hour, some of thats obtained will be shown with characterization results in Fig. 131. Processing time also is even influenced by the fact that sample surface is electric isolated, in the region to be worked, and thus it is more difficult to treat under the high-conductive FIB source.

3.3 ARRAY INTEGRATION

A system providing integration of microfluidic, and accessibility to parallel nano-gaps electrical characterization, embedding 1-inch arrays between two micro-machined holdings, as it is shown in Fig. 62 was developed. A bottom PMMA piece is micro-machined to accommodate a square array, containing several test site units.

A top holder, carrying holes for probes and tubing connections, fabricated using a transparent polymeric layer, frames the underlying structure, adhered through a PDMS membrane of about 50 µm, and assembled by screw-butterflies, directed by column guides.

Holders were fabricated by following home-project design at Centro de mecanizado CIM of Universitat Politecnica de Catalunya (UPC). Gold

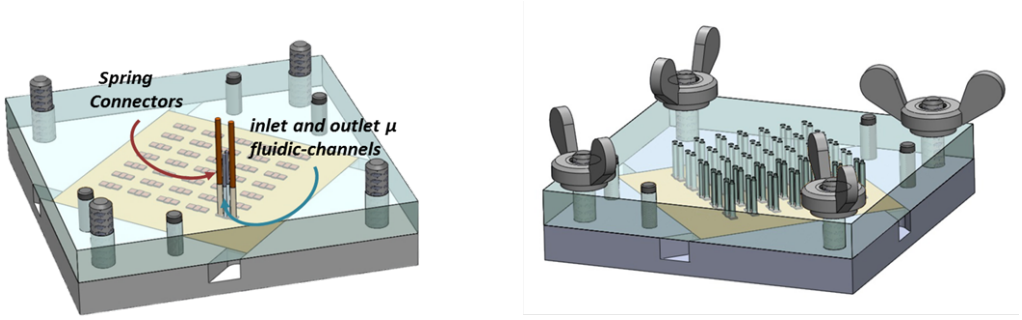

Figure 61: Holding structure, with integrated delivering accesses.

spring probes, with tip radius of 0.5 mm were glued inside top holder corresponding holes, to provide pads connections for electrical measurements.

Spring probes, although more expansive and relatively difficult to manipulate, for the sophisticated micro-machined mechanisms involved, were preferred in order to amortiguate eventual plane inclination.

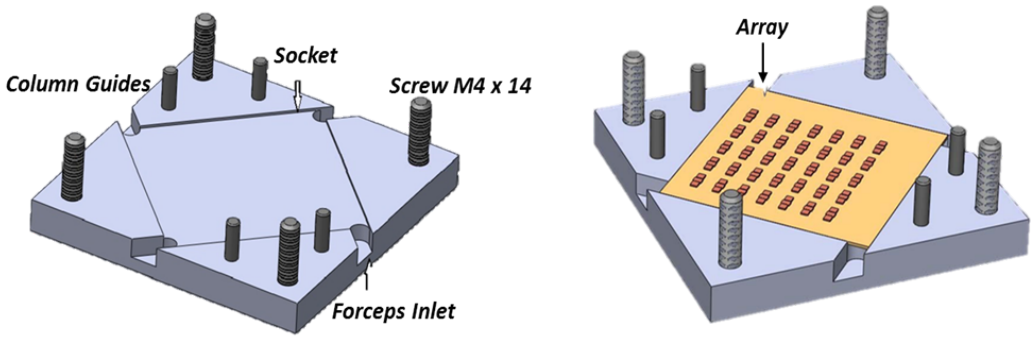

Figure 62: Bottom Holder structure

Micro-fluidic delivering probes were achieved by using common syringe needles, of 0.4 mm tip radius, wired to micro-channels after removing of terminal conical plastic, and glued through top holder spots.

Micro metric PDMS membrane, patterning, the micro-fluidic channel, was obtained by soft lithography from a SU-8 photolitho
graphed master, according following processing.

3.3.1 *SU-8 Master*

We used SU-8 based photolithography to pattern pillar structures on a glass surface, which is thereafter employed as a master to cure a film of PMDS with a thickness of about 50 μm. We used NANO™SU8-50 negative tone photoresist by Micro-Chem, standardly processed by near UV (350-400 nm) light, and allowing film thickness from 1 to 200 μ m.

Normal processing of SU8 involve: substrate preparation, spin coat, soft bake, exposition, post expose back (PEB), and develop.

Glass substrates (purchased at Corning) were activated, prior to photolithography, in a bath of piranha solution. After 10 minutes immersion, substrates were carefully rinsed with DDI water, and dried in oven at 85 °C.

Photoresist was then spin-coat at 3000 rpm during 25 s at an acceleration of 1500 rpm/s, final spin-coating parameters were achieved progressively starting from 500 rpm at 100 rpm/s during 1 s. According SU8 technical sheet data, soft bake was achieved by putting coated substrates on hot plates at 65°Cduring 5 minutes, followed by 20 minutes at 95°C.

First baking evaporated solvent residual, while second one is used to densify the film.

Thereafter, exposition was accomplish in the mask alignment system of our clean-room in hard-contact modality and by using 30 mW/cm^2 light intensity for 10 s.

SU8 development is not a critical process, and it is usually worked out by immersing cured substrates in SU8 developer starting from a minimum immersion time, and then eye-monitoring developing state by rinsing with isopropanol, which reacting with not developed area makes them appear whiter, so they can finally be developed by spotting solution on such marked zones, until they become transparent.

3.3.2 *Silanization of SU8 Mold*

Surface silanization is a process through which a silane coating is provided over an hydroxyl-group terminated substrate to bound mineral

components and organic molecules. This is usually applied to induce chemical inertness of surface, as well to stabilize adhesion of polymeric coverage on suitable silanizable substrates.

Mica, glass and metal oxides can be easily silanized having exposed hydroxyl-groups which attack and displace alkoxy-silane molecule thus ordering molecules assembling.

It is standardly applied in PDMS processing on SU8 molds, since it promotes adhesion during PDMS curing, but it avoids coupling through surface reactivity in such a way that resulting film can be easily peeled-off from master. Surface silanization can be performed both by Solid-Phase and Vapor-Phase reaction.

We made this process by using: a desiccator, the silane reagent, and an oven. We used facilities available in our laboratory. A drop of reagent was spotted on a small glass piece and putted with SU8-Mold inside desiccator for 1 hour. After that substrates are moved to oven and dried during 1 h at 80°C.

3.3.3 *PDMS film*

PDMS was obtained by using Sylgard 184 Silicon Elastomer from Dow-Corning.

We weigh out the base and curing agent of the elastomer with a ratio 10:1, and vortex the final weight (about 30 g) until achieving a homogeneous mixture. Bubbles induced by vortexing are removed by placing flask containing PDMS inside a desiccator attached to a vacuum pump. Degassing of the mixture usually late 30 minutes, anyway it can be eye-controlled.

In order to obtain desired PDMS membrane thickness, we delivered a volume sufficient to cover SU-8 Mold, which was then distributed over all mold surface by spin-coating. Parameters of this process were determined by considering that for a mixture of PDMS at 100 % thickness height is related to radial velocity by:

$$h = k\omega^{\alpha} \tag{15}$$

where $k = 22000$ and $\alpha = 0.98$ with h given in μm and ω in rpm.

According this relationship which parameters are furnished by the elastometer fabricator, and by accounting reported protocols, we finally accomplish successfully by spin-coating PDMS at 2500 rpm, with an acceleration of 1000 rpm/s for 20 s.

PDMS was then cured in oven at 85 °Cfor 2 hours. Thereafter, substrates rested till reaching room temperature.

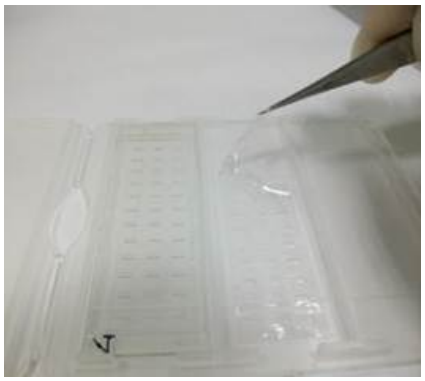

Figure 63: Master and PDMS film.

PDMS thickness was then characterized by perfilometry after scratching surface to remove membrane from substrate.

Peeling-off of this very thick PDMS film, Fig. 63, is rather a delicate task, especially in proximity of patterned area, although it can be worked out by using lot of care and patience, without the need of other materials wasting process. PDMS film is then adhered on nano-gap electrode array and all assembled with top, and bottom holder, Fig. 64.

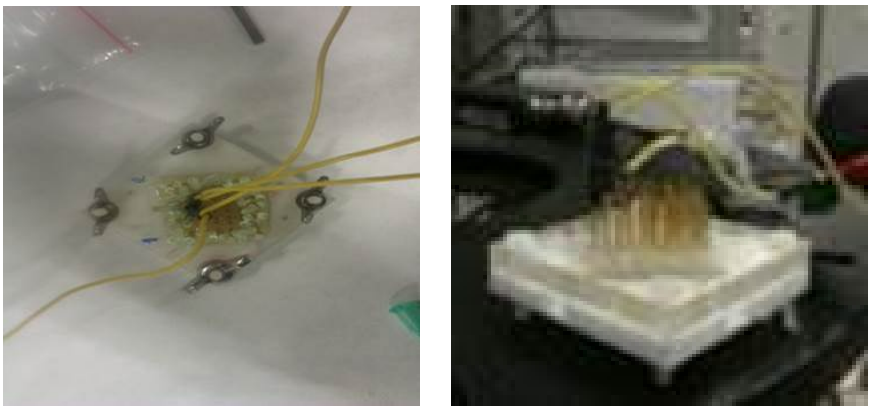

(a) Holder wiring (b) Array integration

Figure 64: Prototype of array integration with SMU.

3.4 CHARACTERIZATION OF THE FABRICATION PROCESS

3.4.1 *Optical Characterization*

At each stage of the fabrication process, we performed different analysis in order to verify the obtained results.

Optical, and electrical characterization were the principal methods applied.

Rapid checks of the expected electrical conduction over the substrate, after each step of the photolithographic process, the electric passivation and the FIB processes, were performed by means of a standard multimeter. This was useful to establish the integrity of expected electrical patterning after each processing step.

Further, a deeper analysis of the electrical behavior of the nano-gaps was conducted by measuring the I-V characteristics of the nano-sensors, under different conditions, which will be commented in the following.

3.4.1.1 *Optical Microscopy (OM)*

"Microscopy" from greek μικρου (micron) "small" and σκοπειυ (skopein) literally look at small, is the word coined by Faber of Accademia dei Lincei in 1642 for the optical instrument invented by Galileo Galiei, characterized by use of a convex and concave compound lens system.

Huygens advanced ocular system to correct light aberration standing the basis to further development of optical microscopic systems. It is worth nothing that advancing eye-vision power by use of optical systems flourished especially pushed by economical and defense reasons, when commercial interchanges was especially based on naval transport.

Light with wave-lengths in the visible spectrum (400 to 700 nm) is the probe source available to our optical vision system; accordingly, we can solve objects with size in the range between hundred meters up to 200-400 μm.

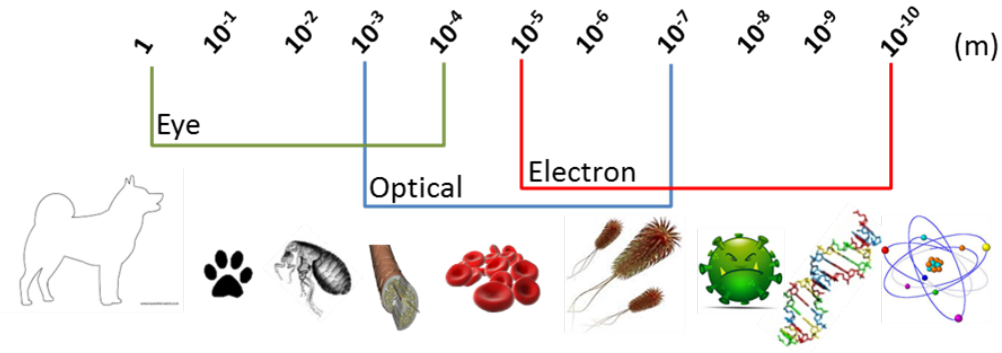

Figure 65: Scales and corresponding characterization systems.

Then, in order to get insight of matter below micrometers down to few nanometers, imaging by other probe sources, like the electron beam or X-rays, as exploited by scanning electron, and X-ray microscopy, is needed Fig. 66.

These higher energy probes, characterized by a lower spot-sizes with respect light, make it possible to partly overcome diffraction light limitations. Although, this advantage is gained under more stringent analysis conditions, as the requirement of low/high vacuum environment. Indeed, sample could suffer damage during imaging by hard-sources, and electron microscopy it is better suited for conductive samples.

Light, as employed by optical characterization systems, as microscopy, interferometry, ellipsometry is far a safer source, and this at the basis of wide-employment and availability of several methods to address distinct materials.

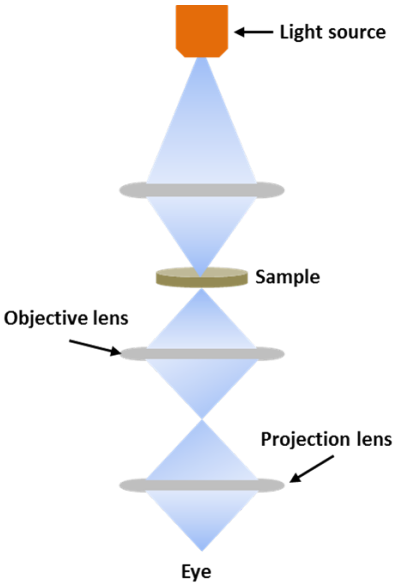

Figure 66: Schematic of an optical microscope.

To push further lower bound limit above micro-scale, optical microscopes employ a collimated visible light, and a lens system allowing magnification sample imaging. Thanks to this, they achieve, in standard configuration, resolution up to few microns Fig. 74.

Higher capability can be expressed, always by keeping light illumination, considering fluorescence based microscopy, confocal and more sophisticated techniques, like near-field microscopy.

We used optical microscopy after each stage during the photolithographic process to verify, either the results of sacrificial layers removing involved, than to prove the integrity and good transference of the pattern, as discussed in the results section.

3.4.1.2 *Interferometry*

Surface roughness profiling was performed by white light interferometry. This technique permits to obtain surface information from the interference of a reference beam and the tested beam, reflected by surface sample.

The equipment for interferometry includes, see Fig. 67, a broad-range white light source, collimated at condenser lenses, to probe and reference the sample.

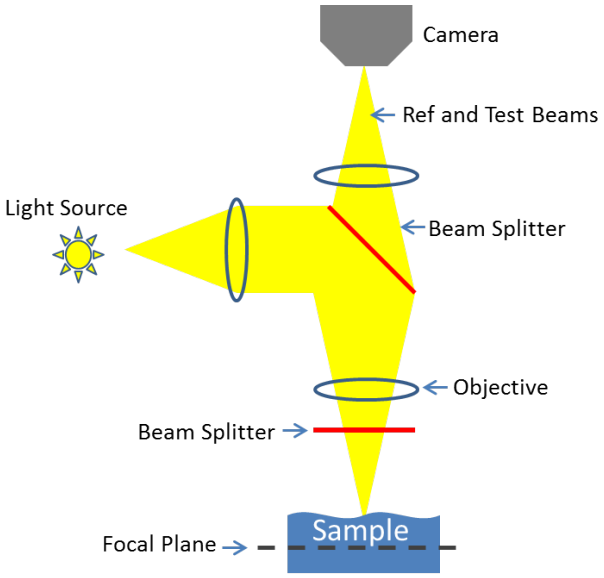

Figure 67: Schematic of an inteferometer.

A first beam splitter divides the incident source beam into reference and test beam. Former beam after mirror reflection, is recombined at the second beam splitter with the surface scattered beam (test-beam) so that interference pattern are finally detected by the CCD camera.

Interfacing traditional interferometry with current hardware and software electronics makes of nowadays white light interferometry a powerful, as well versatile, investigation tools, providing non-contact and sample safe 3D measurements of surface roughness with nano-metric resolution.

3.4.1.3 *Ellipsometry*

Ellipsometry is another optical based technique and it was used to characterize the thickness of SiO_2 passivating layer.

Ellipsometry is usually applied to characterize the surface of materials and it offers high sensitivity, also in the range of ultra-fine films (< 10nm). The high sensitivity is achieved by means of the optical probe polarization change measurement, given by the ratio of p-, and s-polarized light, reflection coefficients with wave plane of incidence, and thanks to the opportunity of exploring a wide range of incidence angle within optical range, Fig. 68.

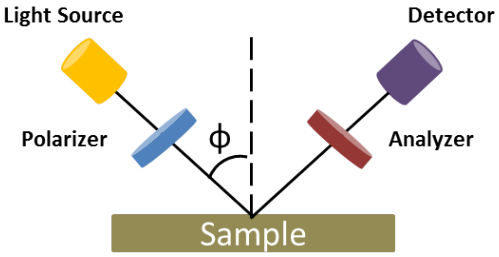

Figure 68: Ellipsometry working principle.

The physical parameters are then obtained as the best fit between a model generated from experimental data, and an optical one, which is built including all the available information about the sample, such as the expected materials and their thickness).

Ellipsometry is a quite recent technique, and devices employed are usually equipped with software which makes easy to perform both data acquisition and analysis.

3.4.1.4 *Scanning Electron Microscopy (SEM)*

Microscopy based on the use of an electron source, replacing the role of light in OM, was established in 1931 with the introduction of Transmission Electron Microscope (TEM), in which electron beam source is exploited to see "through" the sample.

Overcoming limitations posed by light physics was becoming particularly relevant at that time, when increasing interest was raising in Biology to get deeper insight inside cell structure. Electron wavelength is up to 10^5 shorter than photons one, which allows to solve object structures on comparatively smaller scale, according Rayleigh criterion. Electron Microscopes involve a technology rather more complex, and sophisticated, than standard OM.

Employment of high energy electron source requires operating under high-vacuum, or in some case under low pressure environment. Beam collimation, and driving inside the optical system, is achieved by using electrostatic and electromagnetic lenses, by means of interaction with charged probe.

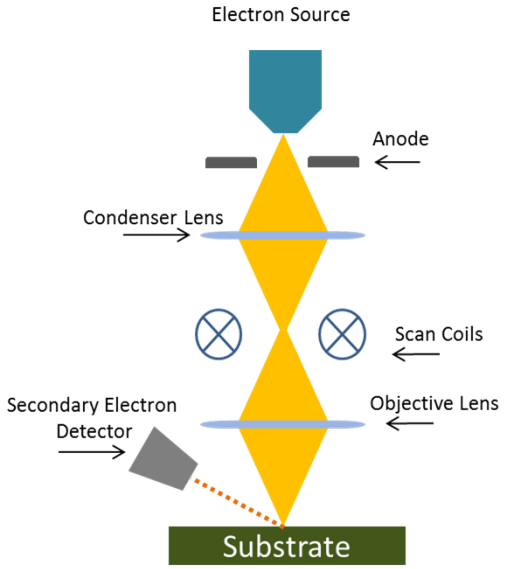

Figure 69: Working scheme of a SEM equipment.

The overall electronic system enabling electron microscopy results in very costly equipments, expansive to maintain, and requires trained personnel Fig. 69. First SEM debuted few years later TEM. Although they started to be commercialized only around 1965.

Although, they are extraordinary tools available to characterize a broad-range of materials, with increased information compared to OM, not only in relation to the resolution limit. Electron scanning of sample makes it possible to get morphology details, so that SEM images look likes as 3D-featured, which permits bulk-sample imaging.

This is understood by considering radiation emissions produced by electron-matter interaction, as schematized in Fig. 70. This depends on the energy released during scattering of primary (beam) electrons with that of bulk material met along a penetration depth, which varies in function of beam energy and sample features. According this, different kinds of electrons and photons are emitted.

In standard use, SEM detects secondary electrons, resulting from collisions with more external electronic orbitals of material atoms. As consequence these are low energy electrons, which can be collected by applying a positive voltage, done through a photo-multiplier tube.

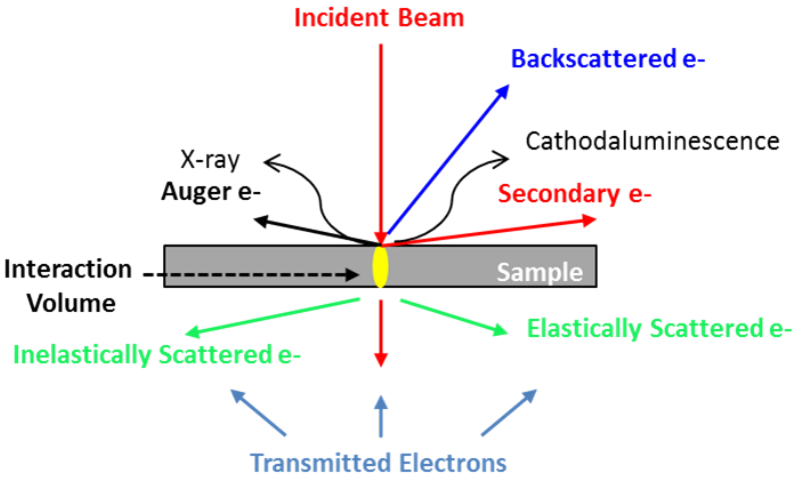

Figure 70: The different signals which are generated from e-beam-sample interaction.

We used high resolution SEM imaging during FIB parameters optimization, and in order of analyzing nano-gap sizes.

3.4.1.5 *Time Of Flight Mass Spectroscopy (TOF-SIMS)*

TOF-SIM is primary a mass-spectroscopy technique so that it is used to determine molecular atoms mass of materials sample. Moreover, it allows chemical imaging to visualize the distribution of materials sample on the surface, and as a function of the depth, through vertical profiling analysis.

Currently it is usefully applied to investigate the materials composition of unknown sample, which cannot be processed by gas chromatography, and it is versatile also for biological samples analysis, too. Although it is a based on the employment of high energy ions probe and for this reason its a sample destructive tool. So that it should be handled with care when sample safety, after analysis, constitute an issue.

System scheme is shown in Fig. 71.

TOF-SIM relies on a simple principle which is that a particle time of flight, for a given kinetic energy, depends from the particle's mass, so that

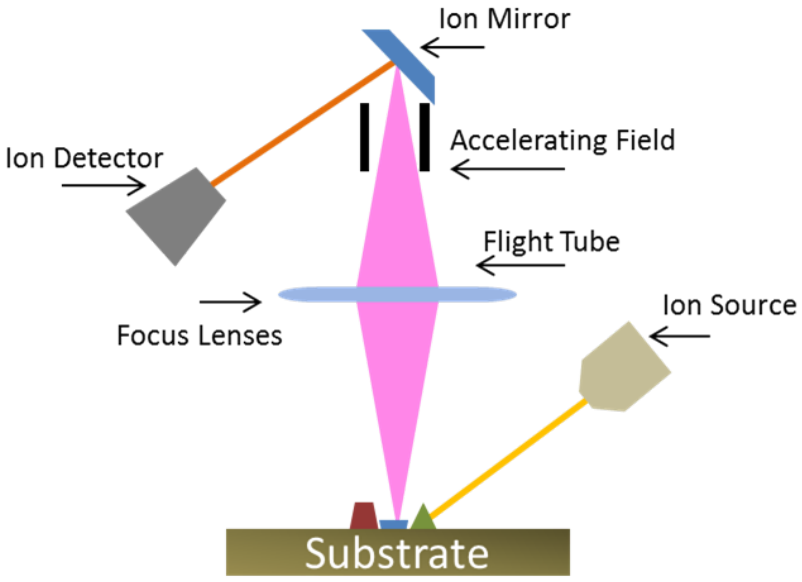

Figure 71: Schematic of a TOF-SIMS equipment.

smaller particles are faster than heavier ones, as it can be easily verified by using

$$E = \frac{1}{2}mv^2 \, v = \sqrt{\frac{2E}{m}} \tag{16}$$

which is the kinetic energy of a particle with mass, m.

In a TOF-SIMS equipment, a primary source bombs the surface of a given material in such a way to extract the ions which are then accelerated by an electrical, or a magnetic field, and are then detected after a fixed distance d. By knowing the arrival time of the ions, which is easier to measure than particle's velocity, it is possible to determine particles velocity:

$$v = \frac{d}{t} \tag{17}$$

and then, using eq. (16) their mass.

Being primarily an optical technique, TOF-SIMS analysis has the same resolution limits of optical microscopy, which stay well above the size of our nano-gaps. We used TOF-SIMS to analyze the nature of materials detectable inside the nano-gaps, right after milling and cleaning. In

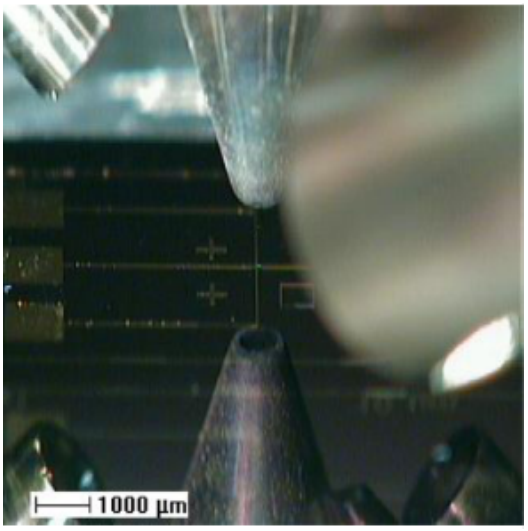

Figure 72: Region of Analysis investigated by TOF-SIMS.

particular, it was used to investigate the possibility of nano-gaps contamination by implantation of gallium ion from FIB source. These could act as doping moieties in the SiO_2 underlying nano-gaps leading to undesired semi conductive behavior of passive layer.

In order to accomplish TOF-SIMS analysis Fig. 72, larger nano-gaps, with an opening of at least 400 nm were appositely fabricated and used. TOF-SIMS was used to test the gallium ions concentrations from FIB fabrication, and in further chapters for biomolecules immobilization characterization.

3.4.2 *Optical Characterization Results*

3.4.2.1 *Lay-out Patterning and Passivation*

Chromium mask patterings and their transferring on metalized silicon wafers are shown in comparative photographic picture of Fig. 73. Optical

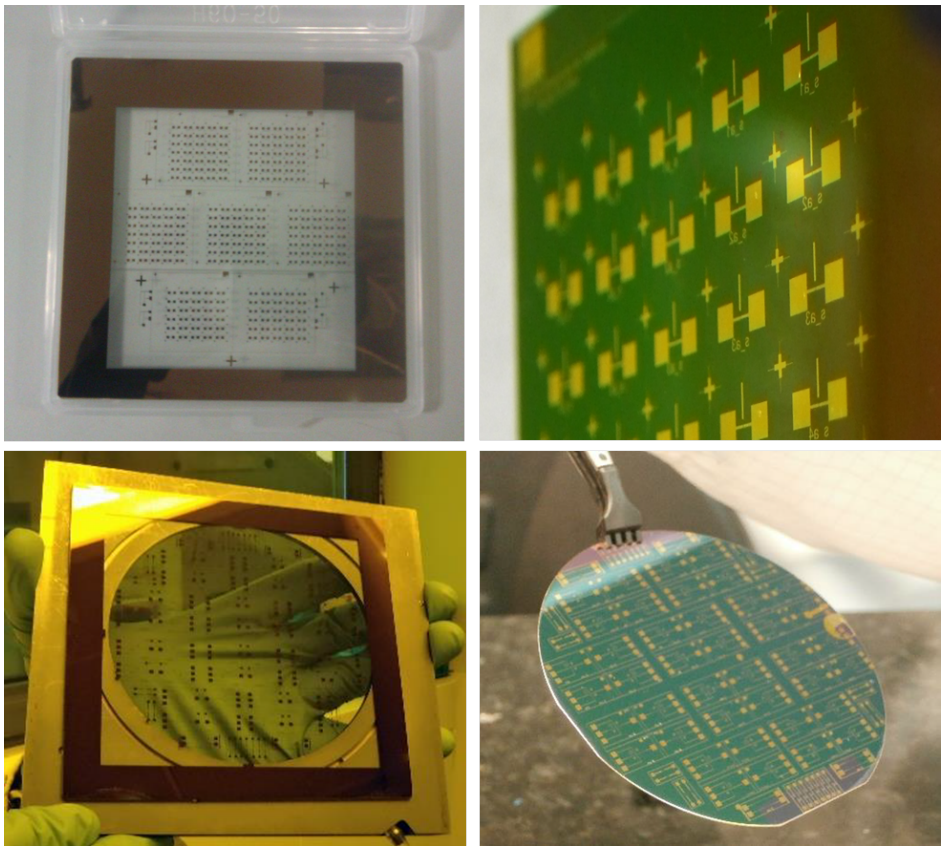

Figure 73: Pictures of chromium masks and of resulting pattern transferred on metalized substrates.

Microscopic images were taken after resist development, during following photolithographic processing, as a mean to control results for each step.

As first, optical microscopic characterization was used to evaluate line-definition of transferred pattern. Then, it has been useful to control gold and titanium etch, before resist removing, as collected in Fig. 74.

Pictures were taken by using model Eclipse L150 of Nikon Instrument Inc. Microscope available at IBEC clean room facility.

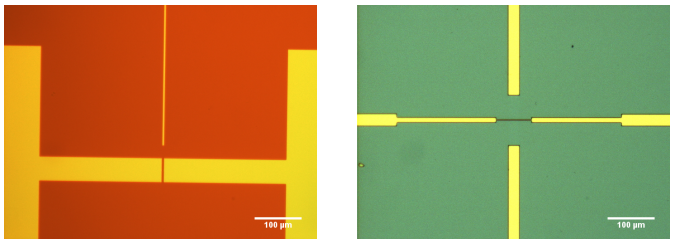

Figure 74: Bridges in the two-electrodes sensor configuration (left) and in the four electrodes one (right).

Pattern surface quality, by analysis of roughness distribution, and pattern definition through 3D mapping, was inferred by using interferometry analysis. This was performed right after resist removing which leaves the gold patterned area opened on the SiO_2 surface.

Results of this characterization are shown in the following figure Fig. 75. 3D-mapping through colored surface map, obtained by interferometry,

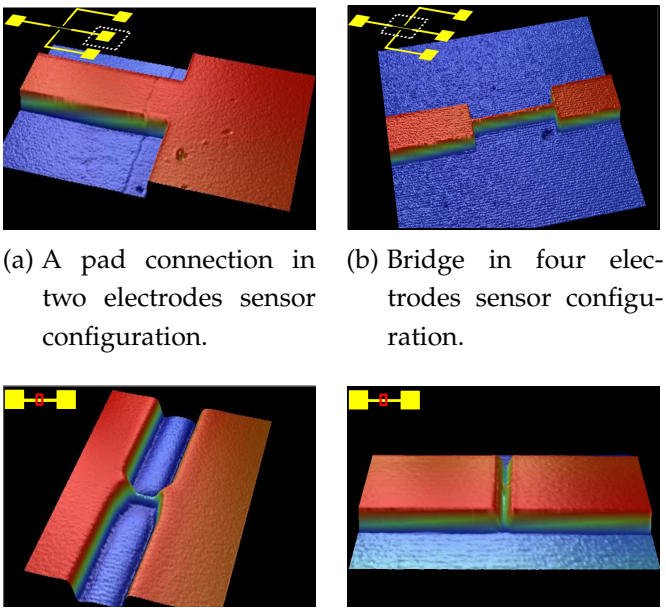

(a) A pad connection in two electrodes sensor configuration.

(b) Bridge in four electrodes sensor configuration.

(c) Bridge perspective in two electrodes configuration.

(d) Bridge frontal view in two electrodes configuration.

Figure 75: Interferometry images

show a high uniform thickness of Au (red) covering the patterned area, and an high vertical definition of depth profiles on etched area.

Following further fabrication processing, we used ellipsometry analysis in order to characterize thickness of sputtered SiO_2, after second photolithography through corresponding negative masks. By comparing the data fitting results obtained in the two different regions, Fig. 76 and Fig. 77, where respectively the material was sputtered and not, we obtained a deposited thickness value, ranging between 45 ÷55 nm. Due to the latent

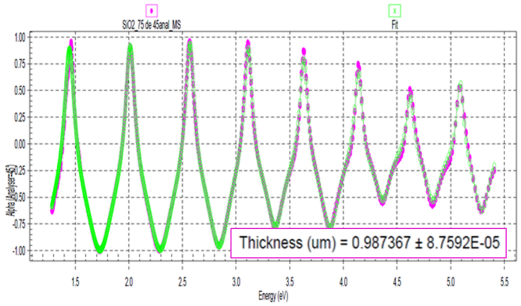

Figure 76: Experimental, and fit model, results of ellipsometry inside region of SiO_2 deposition.

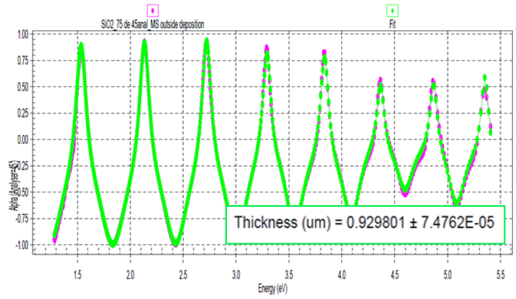

Figure 77: Experimental, and fit model, results of ellipsometry outside region of SiO_2 deposition.

directionality within the sputtering system, although sample rotation is used just to compensate this effect, we in general expect that, a greater quantity of material, could be found deposited near wafer centre.

3.4.2.2 *SEM characterization of nano-gaps*

SEM imaging at increasing magnifications, was used to characterized patterning surfaces, down micrometer scale, and to measure nano-gaps sizes. This characterization has been performed by using either SEM available at ICFO, and at IBEC clean-room facilities.

Pictures obtained are shown in Fig. 131, nano-gap sizes were then evaluated by image post-processing analysis done by using Image J software. Although variations from desired nano-gap size were detected, most of

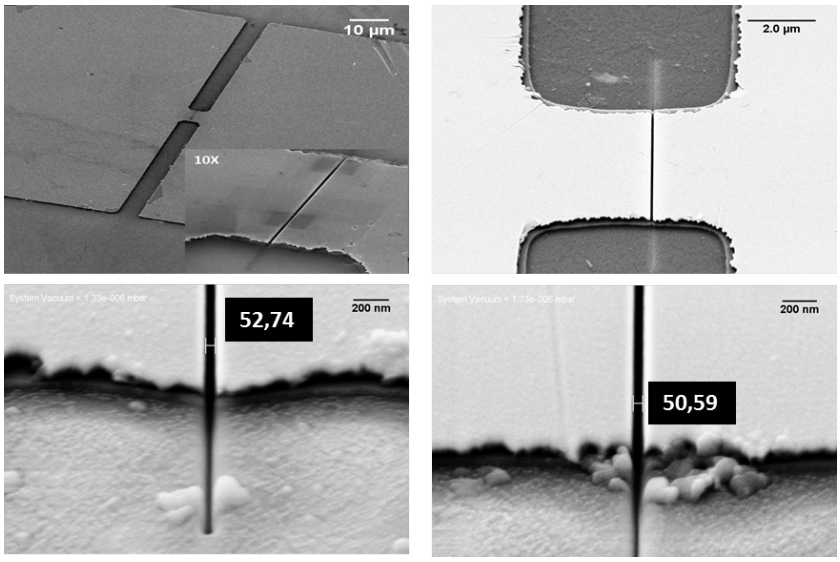

Figure 78: Some of milled nano-gaps resulting by using optimized parameters set.

nano-gaps milled fitted desired range, slight variations are observed. This is understood by considering that topography surface changes, as they can occur, working on different sample area, alter probe-surface interactions, thus affecting final outcomes.

3.4.2.3 *TOF-SIMS: nano-gap contamination*

Imaging surface analysis, on proper milled nano-gaps, was done using a primary Bi_3 ions cluster source, high image resolution was obtained using the collimated mode. Isolating behavior of SiO_2 was compensated by turning on flood gun.

Positive mode was used for the detection of metallic traces, specially those coming from Ga beam. Better gold imaging was achieved in negative mode Fig. 79. Then, depth profiling analysis operated in high mass

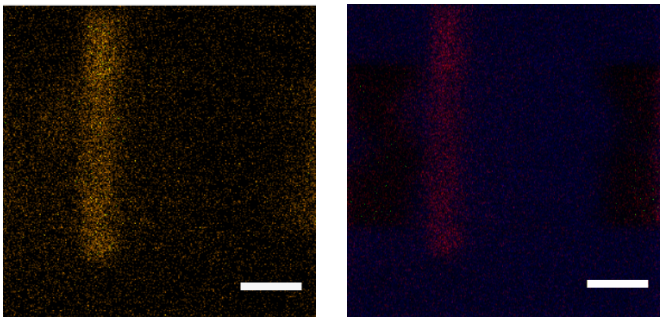

Figure 79: High resolution images: gallium ions are spotted in yellow over a dark background by SiO_2 on the left while on the right they are red colored over blu background of SiO_2 passivation layer.

resolution mode was done, detecting ionic signals found in function of reached depth. Results are plotted in Fig. 80.

Globally, traces of gallium ions are detected by TOF-SIMS analysis, although they should be not quantitatively sufficient to induce a semiconducting state in our nano-sensor. To perform this characterization, it was required to open larger nano-gaps; for this purpose, higher milling time, and intensity are applied in FIB, which could facilitate ions implantation compared to the case of smaller nano-gaps, as that used.

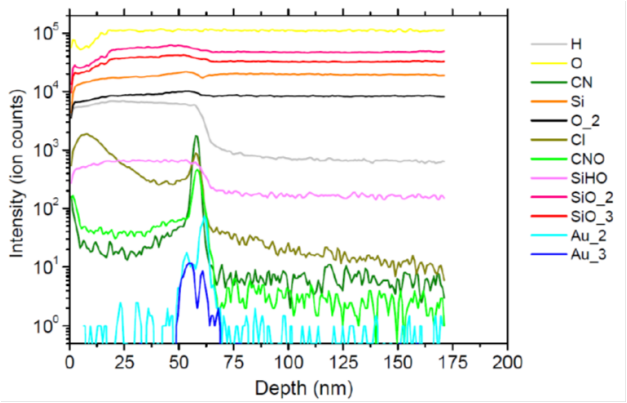

Figure 80: Ionic signal detected in function of nano-gap depth.

3.4.3 *Electric Characterization*

Nano-gap conductivity change, as result of target hybridization, providing a bridge for electron transport is the hypothesis explored as working principle of our nano-sensor. Then, DC Current-Voltage measurements were the primary investigation tool exploited throughout the work.

We studied nano-gaps electrical response by two-point contacts DC current-voltage (I/V), implemented with the set-up schematized in Fig. 81. This rather simple, and ready to use set-up, including only nano-gap

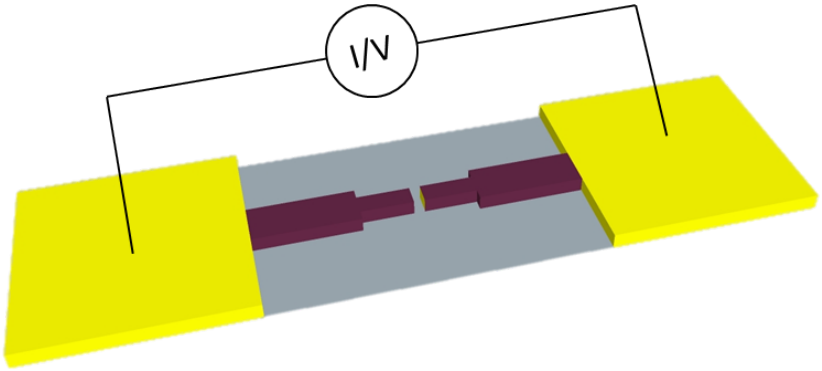

Figure 81: Scheme of the set-up used to implement nano-gap conductivity measurements. Pads connection with the measure equipment are provided by two tip probes mounted on micro-positioners for precise positioning.

electrode and a system measurement unit, a Source Meter high sensitive electrometer, resulted fruitful to face a challenging proposal, as the electrical detection of a very high resistive material by means of a standard DC measurements. We relied on the sensitivity of currently available electrometers.

Electrometers are sophisticated DC multimeter, with improved performances thanks to lower input bias currents, and higher input resistances, allowing to approach the theoretical limit of sensitivity in DC measurements.

Accurate measure of voltage from a high resistance source, as in our case, by standard digital multimeter, with input resistances ranging be-

tween 10 MΩ and 10 GΩ is limited from below by the noise, which a part from other factors is proportional to $\sqrt{R}$, where R is the input resistance.

Electrometers, with input resistances of TΩ allow sensitive measure of voltage from high resistance sources. Similarly, the low input bias current minimizes the input voltage load, increasing the resolution of low current measurements.

The electrometer used here has an input resistance for voltage measurements of 10^{16} Ω and a current resolution of 0.4 fA. Simultaneous

Figure 82: Model 6430 femto-amperometer by Keithtley, with Remote Pre-Amp Unit.

source/measure is achieved through the bi-directional amplifier 6430's Remote PreAmp, provided separately by the SMU so it can be placed near the device under test minimizing cables noise Fig. 82.

3.4.3.1 *Electrical characterization results*

In order to characterize fabricated nano-gaps we measured bare I/V curves across devices, by sourcing the voltage with a linear sweep, and measuring the current.

Single chips of about 2.5 cm^2 containing several test units were mounted on the S 1000 analytical probe station (Signatone Corporation, California, USA). Micro-positioners and tungsten probes T20-50, with 5 μm radius tip (Everbeing INTL corporation, Hsinchu, Taiwan), were employed to connect the pads to system SMU, assuring a precise and rapid control of probes positioning Fig. 83.

Chip design, locating many test units on a very reduced area, readily mounted on a probe station, facilitates this operation and test-probes can be rapidly moved on chip surface keeping the sample at same position. A general purpose interface bus (GPIB) worked out PC-SMU interface.

Data were output by LabTracer 2.0 v 2.8 software made freely available by Keithely. The software provides an easy-to-use SMU-PC dialog interface through which electrometer working parameters can be settled to run measurements and plotting data almost real-time.

Before nano-gaps characterization, we rapidly checked linearity of tip-probe response, and of overall connecting system, by running I-V measurements after contacting the two tip-probes, first between them, and then to a known resistor.

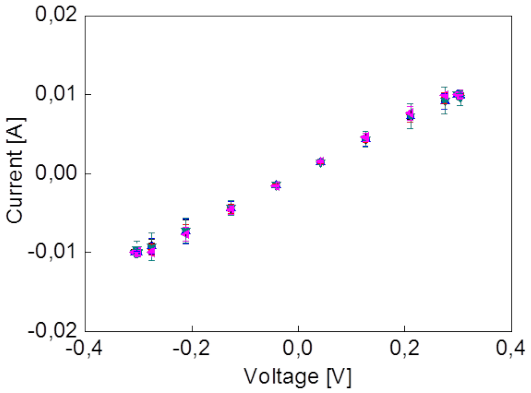

Figure 83: I-V characteristic of nano-devices before nano-gaps milling.

Before any measurement, we performed an extensive cleaning of nano-gaps according following procedure. Oxygen plasma cleaning, operated by PDC-002 Expanded Plasma Cleaner of Harrick Scientific Corporation, available in the core-facilities unit at IBEC, was done right after FIB processing.

Devices were then immersed for 1 minute in a lukewarm bath of piranha solution, a strong acid obtained by mixing H_2SO_4 and H_2O_2 in a 3:1 ratio. Piranha solution was rinsed with abundant DDI water, followed by acetone, ethanol and finally dried under a N_2 flow.

For each nano-gap, we repeated current-voltage measurements three-times by keeping the advise of performing repetitions after a time inter-

val, left in order to reduce the possibility of structural stress due to joule heating effects.

Applied voltage was limited to the range between -1 V and 1V, which yet implies a strong electric field strength ~10^7 V/m inside nano-gaps. This could constitute an issue for nano-gap safety, in particular when repeated measurements are conducted, as we could verify during preliminary optimization tests.

We considered the integrity of nano-gaps after running, at least 10 different I-V characterizations, by applying voltages included in the range of -2.5V and 2.5 V. We observed a remarkable increase of nano-gaps survival below -1V to 1V. So that analysis was limited within this range.

In order of testing conductive patterning integrity, we measured I-V response of devices before nano-gaps milling. A linear current-voltage behavior could be observed in all analyzed devices before FIB, finally validating device processing.

Data fitting by Ohm law allowed to calculate a device resistance of 30 Ω, matching the value measured by a standard digital multimeter, throughout the fabrication process, and found to be 27 Ω.

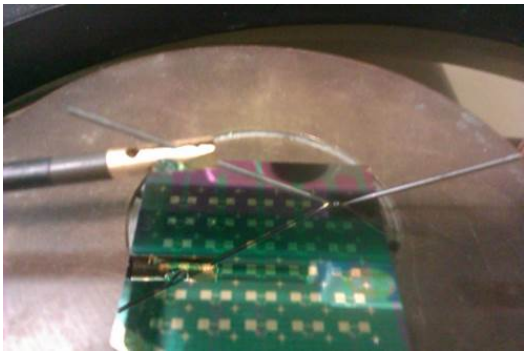

Figure 84: Scheme of the set-up used to implement nano-gap conductivity measurements. Pads connection with the measure equipment are provided by two tip probes mounted on micro-positioners for precise contact.

After milling, we tested I-V response of nano-gaps at ambient environment conditions (25°C, 40 %), and in presence of double-deionized (18 MΩ/cm) DDI water Fig. 84. Results are shown together in Fig. 85.

In both cases, we reported absence of electrical conduction which was considered a reasonable limit for their use in the low conductivity detection problem treated.

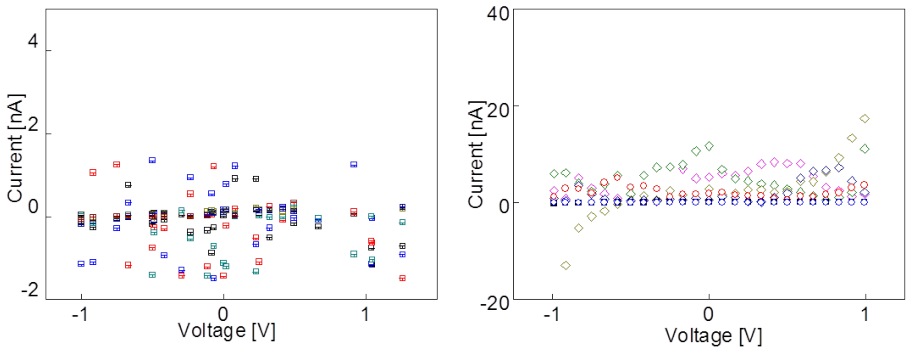

Figure 85: Current-Voltage measurements of bare nano-gaps after milling at environment conditions (left) and in presence of a milliQ water (right).

High-resistance of bare nano-gaps is a mandatory requirement for their employment in DNA detection, this was further accounted by considering the effect on bare nano-gaps conductivity of UV-ozone treatment, routinely involved to achieve molecular surface cleaning in micro and nano electronics.

UV clean works by oxidizing organic contaminants, while on SiO_2 surface it induces an hydrophilic state which can turns in temporary spurious conduction. To evaluate UV clean effect, we measured I-V response of bare nano-gaps right after the standard UV clean procedure applied, and at subsequent time intervals, Fig. 86.

According observed behavior, a slight increase of bare nano-gap conductivity follows the UV-ozone treatment, as it was already reported [125]. Although, repeating measurements after one hour resulted in 30% reduction of the current, as estimated through the ratio between maximum current's intensity one hour after UV-ozone cleaning, to the maximum value measured right after the treatment.

Recovering bare of nano-gap conductivity after 4 hours come back to initial negligible values, so that we performed bare nano-gaps electrical characterization at least that time was left from cleaning, during while

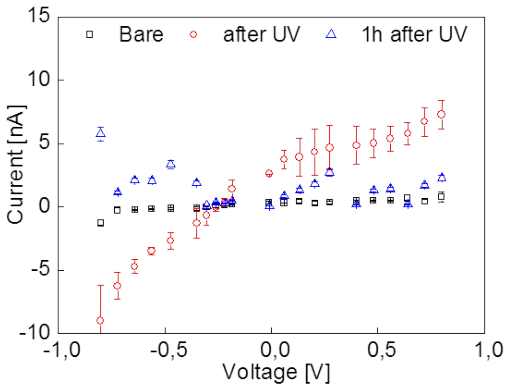

Figure 86: Current-Voltage response of bare nano-gaps right after UV ozone treatment and in the following hour.

devices were stored in a protected atmosphere to prevent environment contaminations.

3.4.4 *Test of array holder*

After array integration inside the holders system, according assembly method described in sec. we tested the viability of probes connecting arrangement for electrical characterization.

To do this, we used a 1-inch array containing several closed nano-gaps; once wired spring-probes were contacted to pad units from one side, and to SMU, we run current-voltage measurements. Results obtained are shown in Fig. 87. The overall linear response detected proves the feasibility of this chip integration to allow multiplexed electrical characterization of an array electrodes system such as we developed.

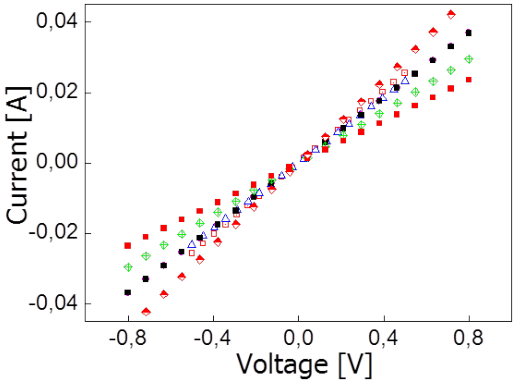

Figure 87: Current-Voltage response over closed nano-gaps belonging to distinct array's rows, through electrical connection provided by spring-probe.

3.4.5 *Electrochemical characterization*

Electrochemical methods of analysis are widely applied in life science technologies as in many industrial processing, for allowing very sensitive characterization of active species in solution and of electrode surface, through easy to implement measurements, carried out with cheap, and portable SMUs. They are compatibles with several substances, being most of known compounds, electro-actives. Electrochemical techniques are useful tools to characterize several electrode parameters, such as roughness, and active surface, among others.

Biosensor technologies have greatly took profit of electrochemical analysis based detection strategies, through which it has been possible to develop devices offering a reliable alternative to the leading applied optical based detection.

Electrochemical methods include all analysis of the chemical response to an applied electrical stimulation, of an electrochemical cell, containing a three-electrodes system, as the typical schematized in Fig. 88, including a working WE, counter CE and reference RE, immersed in an electrolyte solution. System response is analyzed by monitoring current or potential change at the electrode/solution interface, which flows under application of a continuously varied potential.

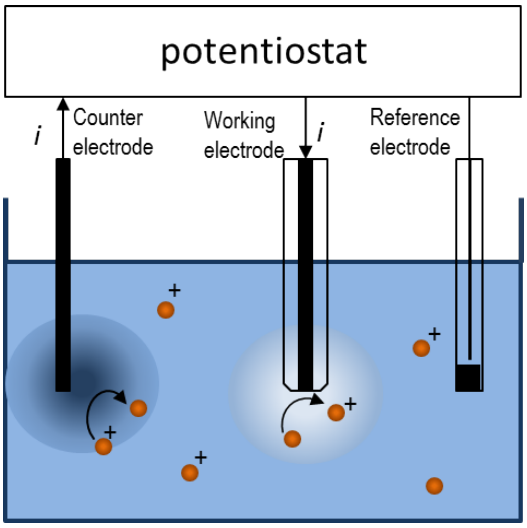

Figure 88: Schematic of an electrochemical cell: WE, RE and CE immersed in electrolyte solution.

Although there are only three parameters contributing to the analytical signal, namely, current, potential and charge, electrochemical analysis is versatile to several proposals by offering many ways of experiment arrangement [5]. But all of them derived from potentiometry, which includes conductimetry, measurements of I(V), voltamperometry, measurements of I in function of a cycling potential, and chrono-amperometry, in which I(t) measurements are used.

Electrochemical analysis is enabled by a potentiostat, which allows to control the potential difference applied between WE and RE, by injecting a current into the cell through CE. In many of electrochemical applications, the output parameter is current flowing between WE and CE.

To achieve easy electrochemical measurements in our system, two auxiliary gold micro-electrodes, a pseudo-RE and CE were provided in proximity of nano-gaps electrode surfaces, WE1 and WE2, so that after delivering of electrolyte solution, the drop-delimited, nano-metric thin-layer electrochemical cell, as that of of Fig. 134 is realized. CV was then explored to characterize nano-gaps electrode surfaces area of nano sensors and electrodes roughness. In the next chapter, CV will be applied to evaluate efficiency of immobilization strategies which we considered, thereafter,

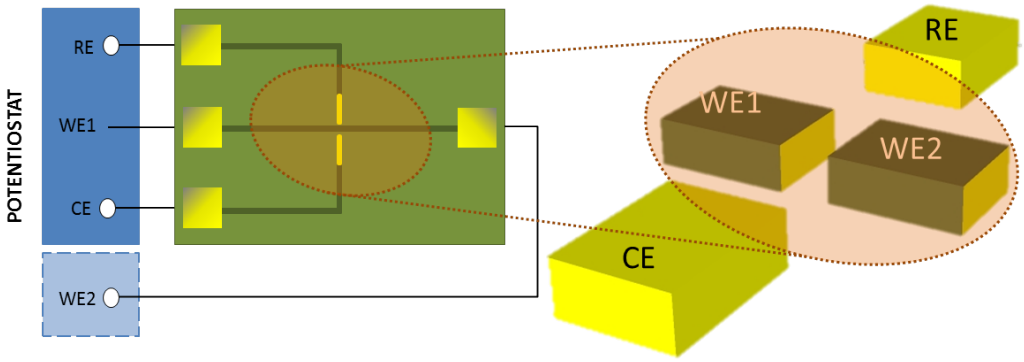

Figure 89: Electrochemical measurements set up.

to achieve selective immobilization of capture probes SAMs on nano-gap electrodes.

3.4.5.1 *Cyclic Voltammetry*

This is a voltammetry method implemented by applying a sweeping WE potential linearly in time, so to induce a current flow, which can either reduce, or oxidize, electroactive species inside the cell. Being this current

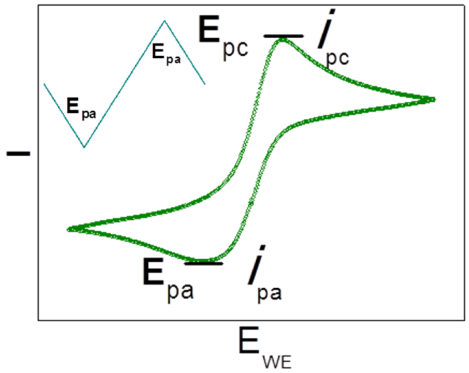

Figure 90: A Typical Cyclic Voltagram observed for a reversible redox couple.

proportional to analyte's concentration in solution, each peak in a CV corresponds to a particular analyte in solution, so that CV provides a simple qualitative, and quantitative method. CV data can be further used to access other cell parameters information, and for example, it has been largely applied to surface characterization of electrodes.

During CV, a triangular shaped potential is cyclical applied on WE, and kept constant toward RE, so that scan rate is calculated from potential slope, for a reversible redox system. Current peak shapes are equals for forward and reversed scanning, in reversible species, but are inverted due to current sign change.

To understand system response in CV, it is useful to recall Nerst equation, governing electrochemical equilibrium inside a cell :

$$E = E^{\Theta} + \frac{RT}{nF} \ln \frac{[red]}{[oxy]} \tag{18}$$

where

E and E^{Θ}	applied, and standard electrode potentials
R	the universal gas constant (8,314 J/mol K)
T	the absolute temperature (K)
n	transferred electron moles number
F	Faraday's constant (96485 C/mol)
$[red]$ $[oxy]$	concentrations of reduced and oxidized species

When potential electrode is swept from the initial value to V_p, the equilibrium position shifts from absence to full analyte reduction, generating a current flow which increases as more reactant is converted.

Current peak, and the following drop, arises as consequence of diffusion layer growth, whose thickness rises in time according $\delta \approx [Dt]^{1/2}$, where D and t are diffusion coefficient of solution analyte, and scanning time. When δ is sufficiently thick reactant diffusion toward electrode is not fast enough as required by Nerst equation, and current starts to drop.

Linear time dependence of diffusion layer thickness growth makes current peaks height related to the scan-rate, so that at higher scan rates, δ grows slowly than at lower ones, and much current can flows inside cell, before dropping down. When reversed scan is then applied, WE potential shifts to more negative values, and as result, reduced species is now oxidized, so that an opposite current, with respect forward scanning, can be detected.

In case of a reversible redox couple, this implies that, reaction formal potential satisfies the next equation:

$$E^0 = (E_{pc} + E_{pa})/2 \tag{19}$$

indeed, for a reversible redox couple, potential peaks are related by:

$$n\triangle E_{peak} = 59mV, \triangle E_{peak} = E_{pc} - E_{pa} \tag{20}$$

which provides a mean to directly verify reversibility of a redox couple by rapidly analyzing CV as E_{pc}, and E_{pa} values, can be directly read by the plot.

If electrode reaction is dominated by electrolyte diffusion, peak current is governed by the Randle-Sevcik relationship, which at room temperatures reads:

$$I_p = 0,4436nFA[C]\left(\frac{nF\nu D}{RT}\right)^{1/2} \tag{21}$$

where F is the Faraday constant (96485,34 C $mol^{-}1$), n is the number electrons moles transferred per mole of active species; A is electrode area in cm^2; D is the diffusion coefficient in cm^2/s, and ν is scan rate in V/s.

Randle-Sevcik equation is useful to extract unknown parameters by data fitting; in case that electrolyte concentration is known, it can be exploited to obtain electrode area by the slope of $(I_p, \nu^{1/2})$.

3.4.5.2 *Redox CV inside nano-gaps*

Electrochemical analysis of nano, and nano-gap electrodes, is relatively new field which is emerging, parallel to fast manufacturing technology advancements.

In particular, redox voltamperometry inside a thin-layer cell has raised only recently following the growth of applications, and interest, in nano-gap detection systems [52], [70]. Development of direct methods to analyze nano-metric surfaces modification is a relevant issue for biosensor applications, where bio-interface efficiency plays a dominant role.

Although, it has never been considered to study nano-gap electrode surfaces modification. It has been observed that current inside a nanometric thin-layer cell reaches a limiting value given by:

$$i_{lim} = nFADC/z \tag{22}$$

where z is the separation layer thickness, Fig. 91, and where n is the number of electron exchanged in the redox reaction, F the Faraday constant,

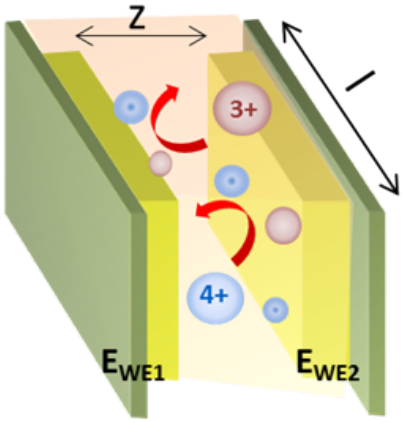

Figure 91: Schematic of a thin-layer nanometric cell.

and A is device area exposed to the solution, D the diffusion coefficient of the active species considered and C is the redox solution concentration.

3.4.5.3 *Measurements methodology*

CV measurements were carried out, at room temperature, in a solution obtained by mixing 5 mM of $K_3[Fe(CN)]_6/K_4[Fe(CN)]_6$ in 0.1 M KCl (materials by Fluka). The electrolyte used is a known reversible redox couple

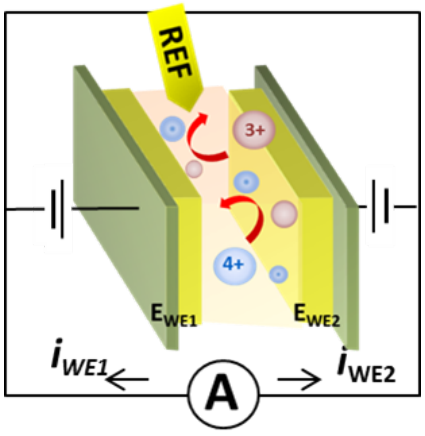

Figure 92: Electrochemical analysis of nano-gaps.

of common use, and its concentration was optimized to achieve the low-

est solution molarity, and clear redox peaks detectability, for all tested nanogaps, in the range of potential analysis fixed to -0.6 V-0.6 V.

Voltagrams were obtained by using the VMP2 Multipotentiostat of Princeton Applied Research, interfaced with PC Station through the EC-lab software, allowing to set measurement parameters, and data recordings. To enable measurements, auxiliary micro-electrodes pads RE and CE were connected to relatives Potentiostat outputs, and kept fixed. Then, one of the two WEs pad, WE1 or WE2 was alternatively connected to the equipment, and submitted to CV analysis.

Right before running CV measurements, we spotted a 20 µl redox solution droplet on the nano-gap area, this is cleaned, and substituted by a fresh one, for each CV analysis, by rinsing with abundant milliQ water and dried under an Argon flow. This could be done directly *in situ* without the need of moving sample and probes, providing fast outcomes, and increased reproducibility.

3.4.6 *Results analysis*

A sample CV obtained by applying this method, on WEs of a cleaned nano-gap is shown in Fig. 93, with schematic of WEs connections. Only

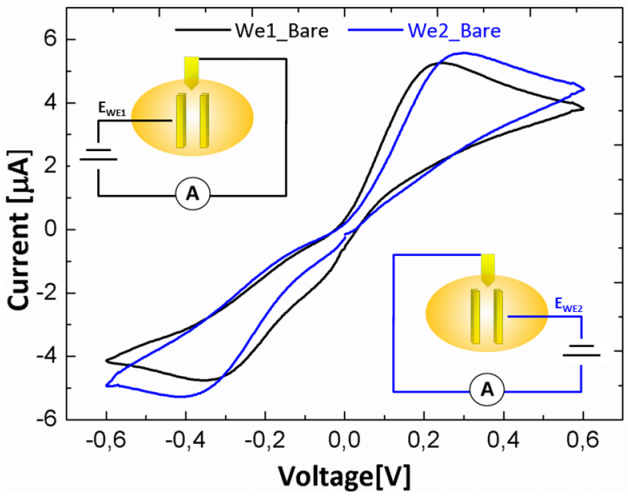

Figure 93: Cyclic Voltammetry at one, and other WE, of an analyzed nano-gap device.

slightly differences can be detected by comparing CV measured at WE1 and WE2. For both the limiting current observed is about 4 μA, greater than the value calculated by eq. (22) assuming z= 50 nm, A of $2,5 \times 10^{-9}$ cm^2 and for the diffusion coefficient $D_r = D_o = 0,700 \times 10^{-5}$ $cm^2 s^{-1}$, which results in 0.02 μA.

Since considering the measured limiting current the active area is 1.48×10^{-6} cm^2 which is related with a roughness factor of about 300 to the geometrical area. This higher active area may be related to the fabrication process, where the gold electrodes are opened by ions bombing, which do not produce a perfectly flat gold surface.

Stabilization of CV signal was rapidly achieved after 2 potential cycling, so we limited to 4 the number of registered CV for each scan rate. By keeping a low cycling number it is indeed maintained redox solution stability against evaporation, and light exposition, which by altering volume, and solution properties, could invalidate analysis. This could be enhanced at low scan rates by increased time of measurements. We prevent for this even by avoiding direct light exposition, and locating experimental set-up in a protected laboratory zone.

Accountings for these, it was possible to perform CV of each WE, at different scan rates in the range of 50 mVs^{-1} to 200 mVs^{-1}, by using initial droplet. Measurements were conducted on several nano-gaps having slightly different opening sizes.

In Fig. 94 CVs obtained, for one analyzed device, are shown at increasing scan rates in the interval between 0.05 V and 0.2 V.

Randles-Sevick plots, Fig. 95, show an overall linear peaks current dependence with the square root of potential scan rate, typical of a diffusion dominated electron transfer rate.

In this case, Randles-Sevick equation eq. (95) can be usefully exploited to determine, any of the free parameters, by a simple linear fit of $(I_p[A], \nu^{1/2}[V/s]^{1/2})$.

We used Randles-Sevick slopes to calculate active area values at each WE's of analyzed devices, which were then compared to the *nominal* or geometrical areas through the roughness factor.

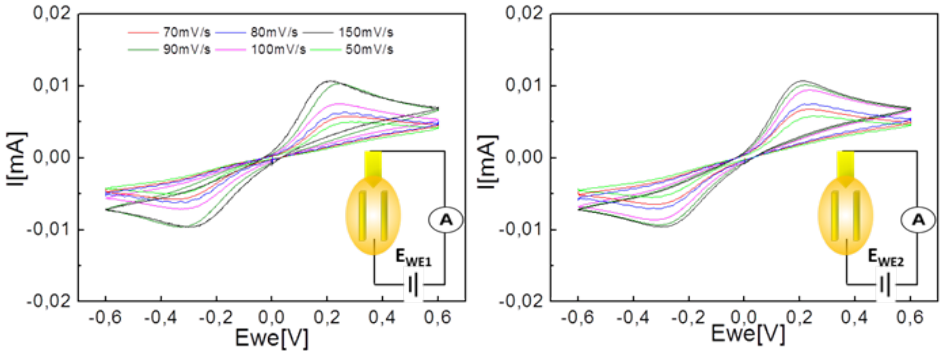

Figure 94: Cyclic Voltammetry at one, and other WE, of an analyzed nano-gap device with increasing scan rates.

From parameters obtained by Randles-Sevick fitting of peak currents from CV measurements on ten different nano-gaps we calculated a mean roughness factor value of $\rho = 102.6 \pm 47.9$.

Then, we calculated formal potentials were obtained by averaging, cathodic (forward E_{pc}) and anodic (backward E_{pa}) sweep potential values, according:

$$E^{\Theta} = (E_{PC} + E_{PA})/2 \tag{23}$$

holdings in case of a reversible redox couple, which indeed satisfies:

$$n\Delta E_{peak} = 59 \text{ mV} \tag{24}$$

where n is the number of exchanged electrons. In case of the ferrocyanide-ferricyanide redox, a standard reported value for the formal potential is $E^0 = -0,36V$, which is referenced toward an aqueous saturated calomel electrode. By averaging data extracted values, the formal potential obtained is $E^0 = -0,26 \pm 0,06$ V and $\Delta E_{peak} = 50 \pm 14$ mV.

Fulfillment of conditions given by eq. (23) and eq. (24) are also influenced by other parameters, as the ions concentration of redox solution.

Anyway experimental data are in very good agreement with thats expected from theory. From one side, this validates the reliability of fabrication process and from the other, the ability of standard CV analysis methods to account for nano-gap electrodes characterization.

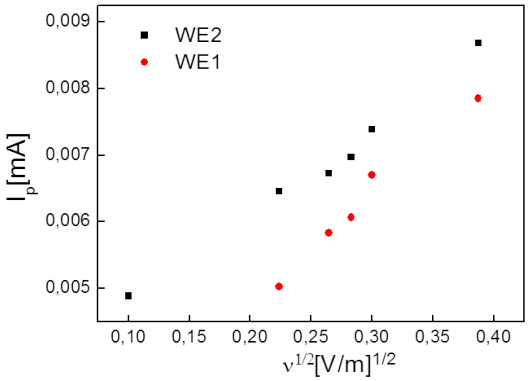

Figure 95: Randles-Sevick plots of WEs of a selected nano-gap, showing the overall expected linear parameters dependence, and high comparable behavior of WEs surface.

3.5 CONCLUSIONS

Nano-gaps electrodes are increasingly considered as a building block of nano-size devices and electrical circuit for molecular electronic applications. Providing a friendly interface for the integration of molecules with mesoscopic electronic devices, they also show great promise for biomolecules detection.

Here we presented the fabrication, and characterization, of nano-gap gold electrodes arrays further applied in DNA's hybridization electrical detection. Gold electrodes facing nano-gap at a separation distance of about 50 nm were milled by FIB lithography on gold metallized SOI wafer patterned by conventional UV-lithography, etching and sputtering processing.

A general overview on basic principles of fabrication, and characterization methods used, is given and discussed in relation with our purpose. Fabrication process was monitored throughout its development by means of several testing, mainly involving Optical Characterization. Thereafter FIB, nano-gaps were imaged by SEM.

Array design allows ready integration of nano-gap electrodes with both electric and electrochemical analysis set-up.

Current-Voltage measurements were applied in order to characterize nano-gaps electric response, being high resistivity a necessary requirement for their use in low-conducti
vity measurements.

Nano-gaps sizes forbid applications of optical detection strategies commonly applied to characterize surface modification, which pushed us to consider such alternative, suitable methodology.

Electrochemical analysis by CV measurements was then involved to provide bare electrode surface characterization, useful to control effects of following nano-gaps electrode modification by CPs specific to analyte target.

4

CAPTURE PROBES SELECTIVE ADDRESSING ON NANO-GAP ELECTRODES.

Controlled manipulation of molecules inside nano-scaled devices is a major issue for molecular electronic applications and medical devices. Precise nano-scale separation of functional interfaces in multi-sensor arrayed devices is still more relevant for biomolecules detection, where the efficiency of bio-recognition layer, at a specific test-site, plays a dominant role.

In this chapter, after giving a general overview on SAMs over gold substrates, and assembly methods, we will discuss the different methods exploited in our nano-gap device to attach specifically each CP in one of the two electrodes. Different procedures were tested and compared by electrochemical surface analysis for this purpose.

A non selective methods but easier with the direct assembling of a mixing of both CPs randomly on electrodes (adsorption from solution).

A selective immobilizing method is achieved with a stripped sacrificial layer and subsequent incubation of the desired CP (Selective SAM by electrochemical stripping). The last process explored relies on electric field application to selectively drive the CP of interest to each electrode (Selective SAM by E-field.)

4.1 SAM: A SMART BIOSENSOR INTERFACE

In the case of nucleic acids, only few years later the discovery of DNA structure, Rutter *et al*. [91] demonstrated their ability to self-associate at the surface of a metallic electrode, where they undergo a 2D condensation which gives rise to a self-assembles monomolecular layer (SAM).

This kind of (first) order phase transition uses to involve a nucleation followed by a growth process. 2D condensation is a unique property of NA; the driving forces of such transitions are the hydrogen bonds, and

the stacking base-pair, interactions. It has been also postulated that both forces, through this condensation mechanism, played an important role in the origin of life [107]. This phenomenon joined with the ability of sulfur

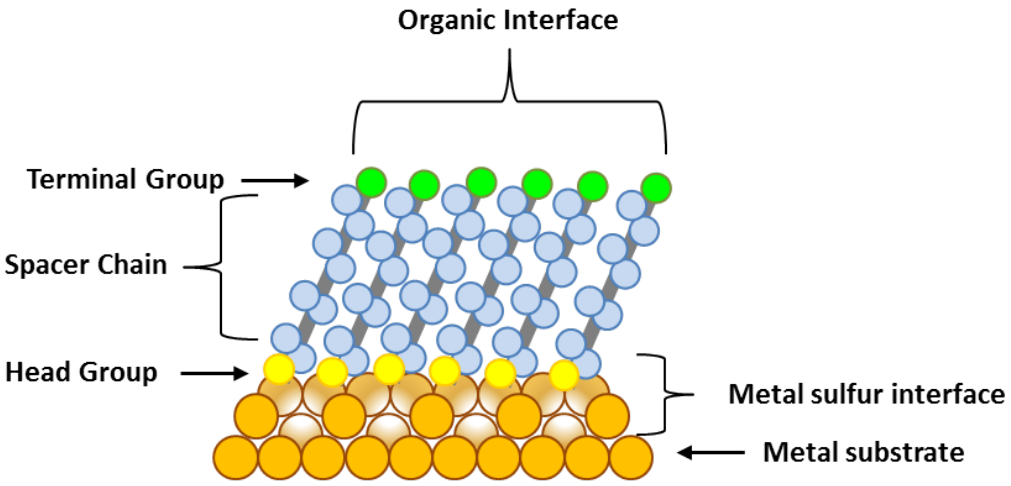

Figure 96: Structure of a self-assembled monolayer on a gold substrate.

molecules to strongly interact through a dative binding with gold, makes this technology a powerful tool for interface building.

The multiple post-immobilization modifications that can be performed on the immobilized SAM comprise a very wide range of interactions such as: intrafilm reaction, not covalent, covalent and polymeric interactions, photo, and electrochemistry reactions [20], [72]. This, and the high affinity to the sulfhydryl group shown by the gold atoms, allows the construction of alkane-thiol SAMs Fig. 96.

Spontaneous interaction of thiols molecules at metal surfaces is the phenomenon behind formation of SAM. As the name suggests, SAMs are organic assemblies of molecules resulting by the adsorption of constituents from a solution (or from the gas-phase) onto a solid (or liquid) surface.

Auto-ordering of adsorbates into a crystalline (or semicrystalline) structure gives rise to a well-defined organized surface which provides an advantageous, and controllable system, to tailor interfacial surface properties by simply immersing a substrate in dilute solution of adsorbates.

Thanks to this, SAM have been fruitfully employed in several applications: from fundamental studies to chemical sensing, corrosion protection,

wet-ability and friction control of surfaces, as well in semiconductor isolation. They are very versatile for nanotechnology applications, where they allow organizing nano-scaled clusters at fixed length-scale.

Since seminal works by Ulman, Nuzzo and Allara [90], describing the structure of alkyl-disulfide chemisorbed on gold which initiated the field, alkane-thiolate SAMs on gold, represent one of the most extensively studied SAM model.

Despite other organic assemblies obtained by distinct interfaces, the latter share high organized structures with exposed terminal groups, making it possible to arrange surface properties according desired application. In this way, solid surfaces dressed by organic chemistry functionality have been particularly fruitful for biology, as in case of cell adhesion studies, and to provide bio-recognition layer for biosensor applications.

The structure of n-thiols on gold is well-established resulting in *trans*-extended, and tilted of about 30°from the vertical [126], monolayer Fig. 96. Among the major advantages provided by alkane-thiolate SAMs on transition metals are:

- small requirement of material (1 nmol is sufficient to cover a surface about $1 cm^2$);
- allow complex organic ligands on surface
- simple preparation compatible with broad range of heterogeneous interfaces, including no-planar surfaces;
- many characterization technique can be used: surface spectroscopy, electrochemistry, physical surfaces and biophysical analysis.

Despite these, they are not thermo-mechanically stables, since at temperatures above 70°C the thiol-gold interaction is broken. No surfaces is truly atomically flat, and roughness or high curved surfaces (as for gold-nanoparticles) could prevent SAMs from order, according the same closed-packed arrangement observed for flat surfaces. SAM defects generated by following processing in certain applications could add grain boundaries and pin-holes, less is known about their influence in the electrical behavior devices enabled by SAMs.

SAM patterning tools are not integrated with standard microelectronic processing although on a micro-metric scale, micro-contact printing techniques have been successfully applied to SAM patterning. Specific patterning of biomolecules on interdigitated arrays has been shown by photolithography with biocompatible polymers [74], although its application is limited to a restricted set of materials.

Further development in this field, as represented by dip-pen nanolithography [85], enabled the delivering of molecules onto a substrate by taking the advantages of capillary transport at an AFM tip, making possible the functionalization nano-scaled devices, or in a micro-scale, inkjet printing and contact printing have been widely used in array's functionalization.

Although, all above methods are well suited to planar surface patterning and their use in other cases is not straightforward. Indeed selective area patterning requires still multiple processing through protection/deprotection of delimited surface regions.

4.2 SAM ADSORPTION FROM SOLUTION IN OUR NANO-DEVICE

Adsorption of thiols SAM from solution is the most common practice used to prepare SAM on metallic substrates.

Immersion of the gold substrate in a dilute solution of adsorbates at room temperature for few minutes, results rapidly in dense surface coverages. Reorganization process is slower requiring hours to optimize packaging with respect SAM defects (Fig. 97). Incubation times of about

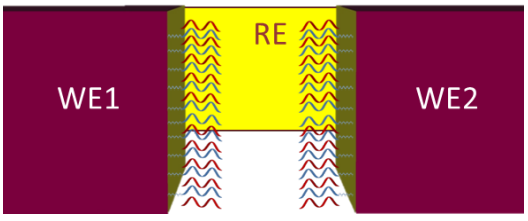

Figure 97: Method used to functionalize our nano-device.

12÷18 hours are usually observed to prepare well organized SAM with

milli-molar solution of adsorbates, being these two parameters inversely proportional.

It is estimated that 1μ mol is the minimum concentration needed to achieve a dense SAM, below this value increasing incubation times has in fact no effect on the properties of final monolayer. For this reason, working at higher concentration instead that longer incubation times is generally preferred.

We used this standard method of SAM formation in order to assemble capture probes at the nano-gap electrodes.

For this purpose we used a mixture of both CPs, CP1 and CP2 in the same incubation solution. Thus, the two CPs are immobilized in both WEs indifferently. So a certain percentage of CP1 and CP2 will be immobilized in each electrode, and there is substantially the probability to reach both CPs faced on the electrodes fro their hybridization with target.

Although by means of this method we do not have 100 % of CPs faced to its counterpart, this is an easier functionalization method for this type of device.

Electrode surfaces coverages were evaluated by means of CV analysis. Materials and protocols are given in the following subsection.

4.2.1 *Materials and Methods*

The probes molecules used in the experiments are thiolated ssDNA, 53 base length, antisymmetric each other.

Capture probes sequences, purchased at Sigma Aldrich are given in Fig. 98. All reagents were dissolved in DDI water, purified with the Millipore A10 Q-gard 1 system (18.2 MΩ/cm at 25 °C), and autoclaved before their use in our experiments. NaOH and PBS solutions used in stripping experiments were prepared with reagents provided by Sigma.

1 μM solution of either one capture-probes (CP1;CP2), or a mixture of both in 10 mM of TRIS, 1 M of NaCl, 5 mM of $MgCl_2$, and 1 mM of EDTA at pH 7,5, was added to a 1μM solution of Tris (2-carboxylethyl) phosphine hydrochloride (TCEP) with a volume ratio of 1:200 and mixed for 50 minutes at 55 °C in the Thermomixer Compact of Eppendorf. This

DNA Strand	Sequence
CP1	SH –CTTGAGGAGACGGAACG AAGGGCGTGAAGTGGTTCGTT CCGTCTCCTCAAGGG
CP2	GGGCGTGAAGTGGTGAGGAG TGGTGAAGTGCGGGCGTCCAG ACCGACTGAGCC-SH

Figure 98: CP1 and CP2 sequences.

treatment reduces the disulfide of thiolated groups which can eventually form during long-term storage.

10 µl drop of CP1 (or CP2, and CP1-CP2) was then spotted by a micro-pipette on the nano-gap region, and left incubating overnight in a wet saturated environment. Solution is removed by rinsing with PBS, to strip away unbounded molecules, followed by copious DDI water washings and finally dried under a gentle flow of N_2.

Cleaned nano-gaps were then analyzed by using CV characterization, according protocols explained in previous chapter.

4.2.2 *Electrochemical characterization of Adsorbed SAMs*

In the plots of Fig. 136 they are shown the CV obtained at one, and other WE, of one nano-gap electrode system, right after cleaning, and then after overnight incubation with the solution containing a mixture of both CPs.

We evaluated indeed storage's effects on SAM stability by repeating the same characterization two days later, as shown in the same plot, where only slight differences could be detected.

In both cases, we can appreciate a consistent reduction of the active area of WEs, following incubation. This has been quantitatively estimated in terms of the relative decrease of peak current values, with respect the

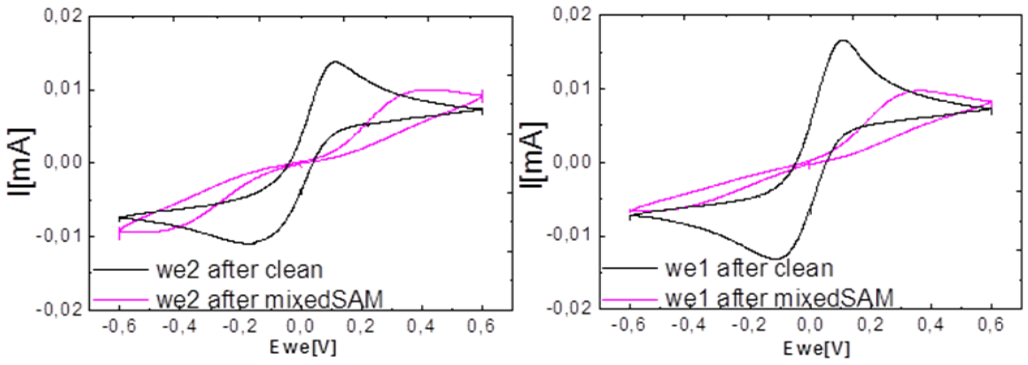

Figure 99: CV obtained at WEs of two nano-gap before and after overnight incubation with a mixed CPs solution.

maximum peak current measured on bare electrodes and considered as reference, results are shown in Fig. 137.

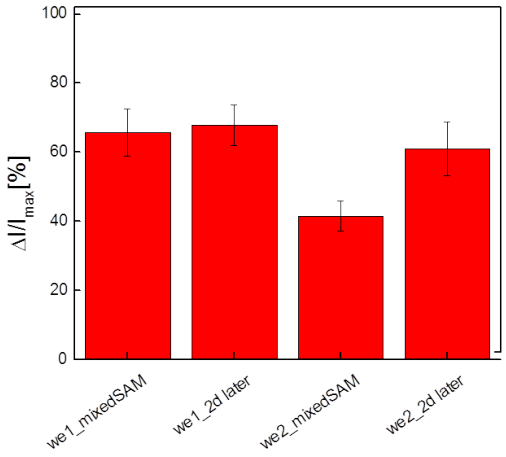

Figure 100: Relative decrease of peak current after incubation with respect the initial values, taken as reference.

Reduction of peak current values, ranging between 70% and 90%, is consistent with high degree of molecules immobilization on WE surface, which are providing an obstacle to redox solution diffusion toward electrode area, mainly helped by electrostatic repulsion of negatively charged DNA strands and the negative ferrocyanide molecule.

Results in decrease of ferrocyanide electron transfer rates are visually reflected by flattened CV shapes.

4.2.3 *TOF-SIMS Characterization of SAM*

By taking the advantages of nano-gaps fabricated with a greater separation, suitable for optical analysis, we employed them to characterized DNA functionalization inside nano-gaps by TOF-SIMS.

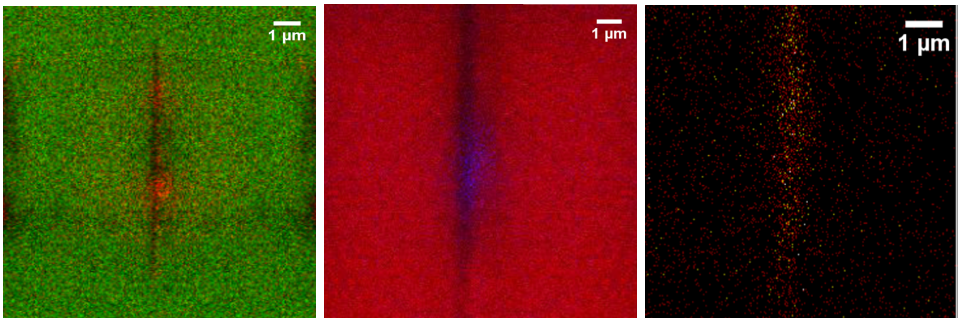

Figure 101: Results of TOF-SIMS analysis

In order to increase DNA signal inside nano-gap, considered the short size of CPs compared to a 400 nm gap, instead of using only CPs immobilized on electrodes, we hybridized them with target TW DNA 106-mer molecules incubated at 1 µm concentration in the hybridization buffer [1] obtaining two solution of CP1-TW and CP2-TW which were then used to achieve a mixed SAM assembled on nano-gap electrodes by overnight incubation.

In Fig. 101 we show results of TOF-SIMS analysis. High mass and high-resolution images confirm successful detection of DNA inside nano-gap through the PO_3 and CN ions signals specific from DNA's molecules. From this analysis it can be indeed appreciated specific molecules immobilization inside nano-gaps regions, thanks to the protection provided by SiO_2 layer.

4.3 SELECTIVE SAMS BY ELECTROCHEMICAL STRIPPING

Electrochemical desorption, of gold surface bound thiols, has been object of several studies focused to design methods enabling precise control of

1 250 mM of sodium phosphate, 15 mM of sodium citrate, 150 mM of NaCl, 1 mM of EDTA and 0.02 mM of Triton buffer at pH 7.42

regional bio-interfacial surface properties. This is obviously relevant to the development of arrays to specifically open or left free one electrode site in array, but it has been considered for many other applications, such as electro-cleaning of gold surface in order to regenerate it for further uses.

Assembling and desorption of thiolated monolayer is controlled by electrode potential, as represented in Fig. 102 where regions of SAM stability in function of electrode potential versus a standard calomel electrode (SCE) are shown.

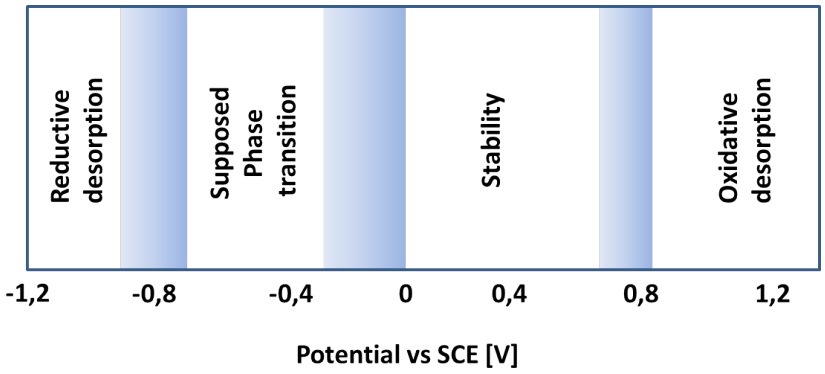

Figure 102: Regions of thiol SAM stability according electrode potential versus a SCE

Stability of thiols monolayer within the potential range between 0.2 V and 0.5 V allows self assembling of molecules, without the need for an external applied potential. This is in fact the typical open circuit potential of a gold electrode at standard conditions. Then, it is easy seen that at more negative, as well more positive applied potentials, reductive and oxidative desorption of thiols monolayer from gold electrodes could be achieved.

Depending on the kind of thiol derivative used and from metallic surface properties, effects of application of reductive potentials ranging from -0.74V to -1.2V (vs Ag/AgCl in 0.5 M KOH) [4] have been analyzed.

The process which has been postulated responsible for desorption is the next reaction:

$$R - S - Au + e^{-} \rightarrow R - S^{-} + Au \tag{25}$$

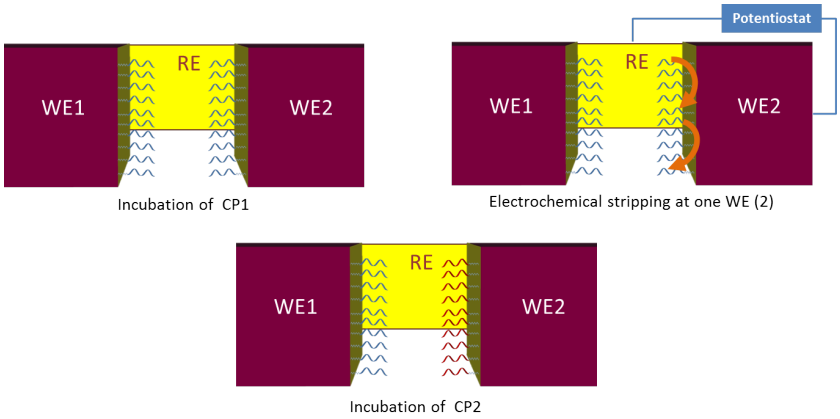

Figure 103: CV obtained at WEs of two nano-gap before and after overnight incubation with CP1 or CP2 solution.

Compared to reductive, oxidative reduction process has been less investigated, although several protocols, involving use of anodic potential sweep, or application of an oxidative DC pulse have been explored, and demonstrated useful indeed to enable following steps of assembling/desorption [18].

Electrochemical stripping was explored to selectively assemble a CP on the electrode of nano-gap sensors used in detection of DNA hybridization [93]. In this case, a single potential cycling between 0 and 1 V (vs Ag/AgCl) at a scan rate of 200 mV/s was effective to accomplish desorption from one nano-gap electrode.

Based on reported results we attempted selective desorption of one of the two CP SAM by using electrochemical stripping, by applying the protocols detailed in the following.

4.3.1 *Methods*

Selective CP's SAM by means of electrochemical stripping was attempted according the steps schematized in Fig. 103.

Nano-gaps were first overnight incubated with a solution containing either one of the CPs. This is followed by electrochemical stripping at one WE, and subsequent incubation of nano-gap with the other CP.

To strip the SAM, we applied to the selected WE a cycling potential from 0V to -1.2V in 0.05 M of NaOH, followed by rinsing with abundant PBS in order to avoid reassembling of previous stripped probes. During cycling on one WE, the opposite was keep at zero potential.

The molarity of redox solution used was established in a series of optimization steps, starting by using DDI water, and progressively increasing salt content. Final one, is the lowest at which it was possible to observe expected results. We considered then the application of a 30 s pulse of -1 V intensity towards an external Pt reference electrode, in PBS solution, as alternative stripping protocol, referred as pulse-strip in results.

4.3.2 *Electrochemical characterization of strip/adsorbed SAM*

CV analysis results of stripping processes considered, first by applying a cycling potential to one of the WE after incubation of both with a CP solution, and then by applying a DC pulse, are shown in Fig. 104.

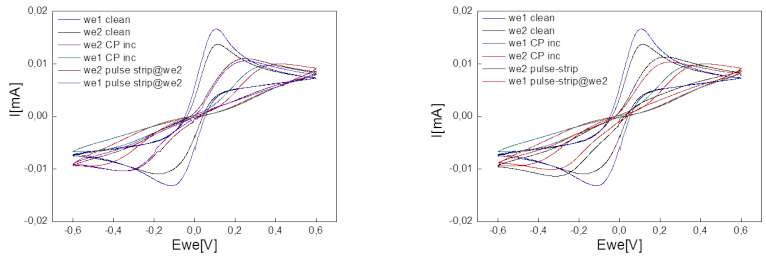

Figure 104: CV obtained at WEs of a nano-gap after each step of stripping processes, on the right after potential cycling and on left after pulse.

Voltagrams were recorded after each step on one and other WE, in order to monitor eventually effects which could arise on the opposite nano-gap electrode.

CVs in Fig. 105 show a comparison between initial WEs response, after cleaning, with that obtained respectively after CP 's incubation followed by that measured, right after stripping on WE2, and on same WE1.

As can be observed in the CV, similar behavior is detected in the stripped electrode than in the unaltered one, independently from the stripping protocol applied.

First to consider is the good immobilization of both electrodes with CP1 reducing the current ferrocyanide, although if slightly differences between these two can be appreciated. Another relevant result that we can extrapolated is that in both cases we are not removing completely the CPs from desired electrode.

As before, we calculated the relative decrease of peak current resulting after applied processes, in order to quantify outcomes. This provides indeed a fast visualization of produced effects. These results are shown in the column plots of Fig. 105.

In both cases, stripping on one WE is always accompanied by desorption of previous immobilized capture probes monolayer on the opposite WE. This observation highlights enhancement of electric field effects inside electrodes facing a nano-metric separation distance. The observed

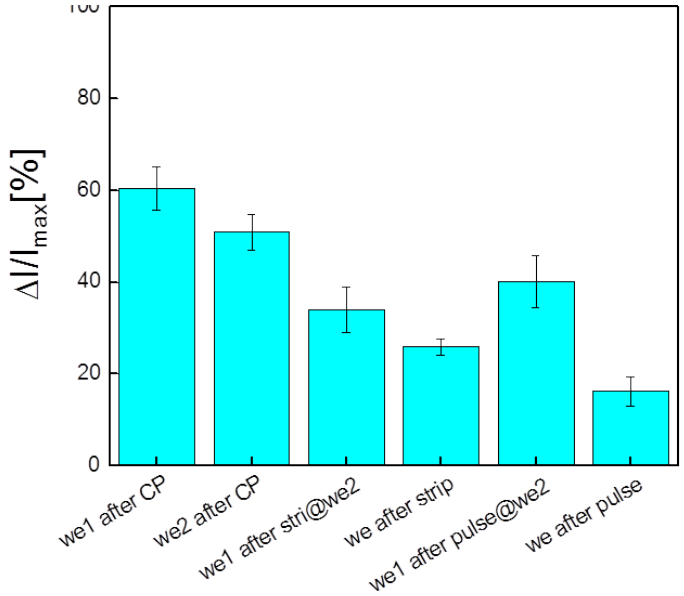

Figure 105: Relative decrease of peak current after each stripping step.

results made us deciding do not go further with the second incubation step, as explained in Fig. 103, as in any case we would end with a mixed assembled monolayer of both CPs, for which standard incubation works faster and well.

4.4 SELECTIVE SAMS BY E-FIELD

Addressing biomolecules at specific electrode-sites by using electrical fields has been largely explored in the field of microarrays [48]. Here, the selective tuning of electrical field at a given analysis spot allows gaining control over the transport, and concentration of oligo-probes for its immobilization, at the electrode surfaces, but also the driving of DNA target to specific spots resulted in increased hybridization's efficiency and stringency.

In E-field assisted microarrays, a drastic reduction of the hybridization times, from hours to seconds was observed [46], following the application of a DC positive bias, under which the negative probes migrate faster, covering successfully selected electrode surface. This is due to the force which polarizable particles (both charged and neutral) experience under a uniform electric field.

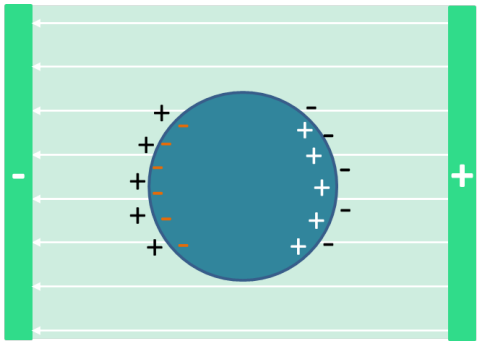

Figure 106: Polarization of a particle inside unidirectional electric field.

The electrophoretic effect induced on charged molecules, Fig. 107, has also been considered, as molecular driving tool [133], in the framework of electronic transport studies. DNA, through its unique self-assembling and recognize properties, plays the role of a versatile template for molecular electronics applications, independently from its electrical properties. For this reason, the problem of establishing solid molecule electrode contacts, enabling electron transport measurements, has been considered in system involving different kinds of DNA based molecular bridges.

Electrostatic trapping of dsDNA between nano-gaps electrodes has been explored to analyze the mechanisms of charge transport through DNA

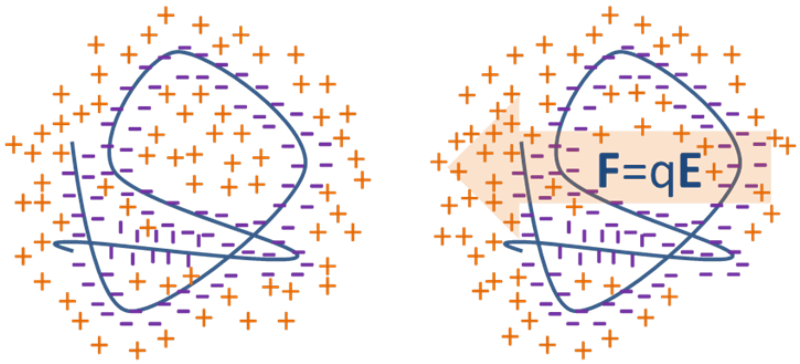

Figure 107: Polarization of a charged molecule, which is found in balance with its counter-ion field in absence of an external field (left), while it is subjected to a electrical driving force under e-field application.

molecules [86], of nano-wires obtained after metallization of DNA molecules to connect the nano-gap [15].

Immobilization of dsDNA inside adjusted nano-gap electrodes under influence of Dielectrophoretic (DEP) field has been reported [117]. More recently, prompted by engineering of complex DNA architectures, as DNA origami, DEP trapping has been used to assemble DNA origami inside nano-gaps for their electrical analysis [64].

Here we used electric field to promote electrophoretic driving of CP1 or CP2 molecules to one or other electrode. By doing this we are aimed at improving results obtained by employing above explored methods. Indeed, it should be remarked that achieving good immobilization of SAMs, by exploiting electric field stimulation not only offers an efficient method to site selective deposit the desired CP in a nano-gap device, but drastically reduce sensors assembling time from hours, as required by incubation-based methods, to few minutes.

4.4.1 *E-field assisted CP-SAMs assembly in our nano-gap*

Electrophoretic molecules driving at micro-electrodes is usually achieved under application of a uniform DC field between them, with polarity adjusted according targeting purpose. A low conductive buffer is usually

preferred in order to favor molecular polarization. In case of DNA a 50 mM histidine solution, characterized by a conductivity of 76 μS/cm, is commonly employed and reported.

Although this, throughout biosensor testing we attempted to avoid, or limit, the use of conductive buffers, in order to preserve analysis area from contaminations which could affect high-resistance nano-gap characteristics, necessary to perform a low conductivity measurements, as that required here. Nevertheless we analyzed, in a series of preliminary optimization testings, the effects of using histidine at such concentration with respect DDI water, on electrophoresis of CP to drive it to a specific electrode.

Selective CP's immobilization was attempted through a two-step electric field stimulation. First a positive charge is induced on WE1 so that

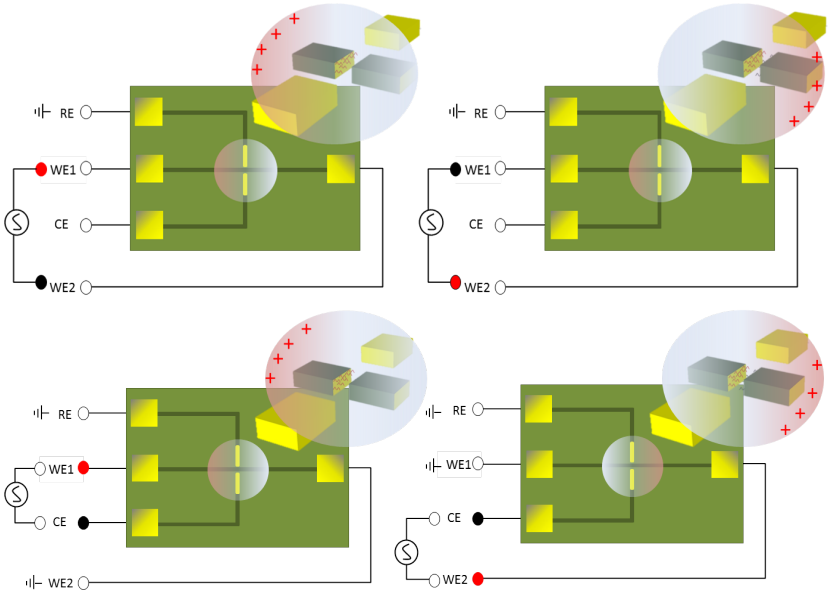

Figure 108: Steps of E-field application between WEs (left), one WE and CE (right)for selective CP'immobilization

CP1 molecules contained in the spotted solution are driven towards it. Then, WE's role is reversed while spotting second CP2 solution to trigger electrophoretic effects and attracts CP's molecules on this electrode Fig. 108.

We considered results obtained first when electrodes polarization was induced by applying a DC signal first the targeted WE, and the opposite one, and second when the signal was applied between targeted WE and CE, as schematized in Fig. 108.

DC signal was provided by the waveform Generator ww5061 of Tabor Electronics, applied between electrodes as described above while spotting a 20 µl droplet of CP1 (or CP2) solution on the analysis region.

Thereafter, drop was rapidly removed by rinsing with PBS solution, which strips away unbound molecules, followed by copious washing with DDI water, and dried under Argon flow. Then process was repeated with inverted WE's role, so to promote formation of CP2-SAM, both electrodes surfaces were characterized by means of CV, according protocols detailed in chapter 3.

4.4.2 *Results*

DC signal's intensity and time duration, were optimized to our system features starting from initial values agreed on the basis of existing reported papers.

By keeping the general advise of involving test voltages below 1 V, we tested effects of lower signals intensity in the range between 0.4 V and 1 V for 60 s on electrophoretic CP's assembly.

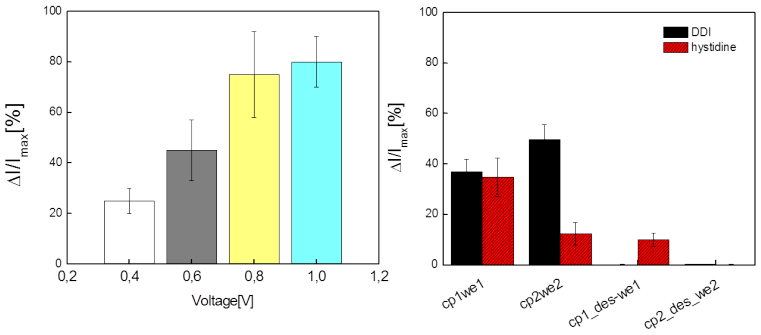

Figure 109: Relative decrease of peak currents in function of different applied DC signals intensity for 60 s (left). On the right, effects of two different buffers on immobilization under E-field stimulation.

Results of this process were quantified by considering relative decrease of peak current, following each of applied voltages, with respect initial bare WE's current peak Fig. 109, this is shown jointly with results obtained by using DDI water or 50 mM hystidine, as supporting buffer for CP's dissolution.

Percentage values in Fig. 109 are not representative of absolute surface coverages, they only constitutes percentages of comparation between each others. As it is shown on left in Fig. 109, better results both in terms of surface coverage (peak current reduction) and desorption of previous immobilized probes for second E-field application are obtained in DDI water than in histidine buffer, contrary to what is usually expected. We did not further explored the reasons and only accounted for this occurrence by choosing DDI as working buffer.

Once potential intensity was established, we evaluated electrophoretic CP's driving on selected electrode by applying first a DC signal between WE1 and WE2 of 1V for 60 s with positive polarization on WE1, followed by reversing polarity of the WE2 while using the other CP's solution.

Obtained results were analyzed by CV and they are shown in Fig. 110.

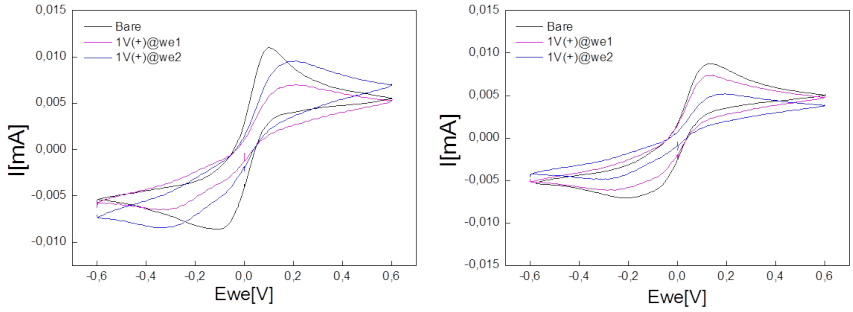

Figure 110: On the right, CV analysis of E-field driven CP immobilization on WE1, in the inset results obtained on opposite WE.

After first E-field application, which positively polarize WE1, electron transfer rate of ferrocyanide at this electrodes is reduced affecting CV shape, by an amount of about 40% as it is shown in column plot. Reduction of peak current is observed also on opposite WE presenting unspecific absorption and it results in a suppression with respect initial bare WE peak current of 15%, Fig.111. Reversing WE's polarity successfully

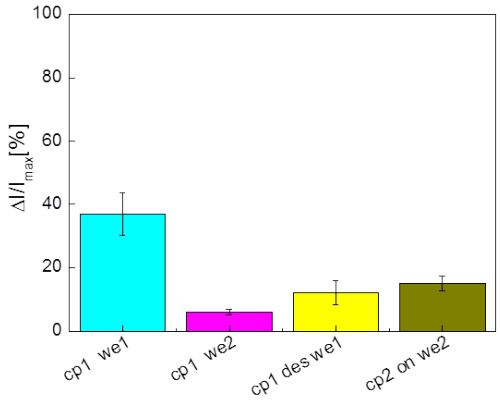

Figure 111: Surface coverages evaluated by relative decrease of peak current.

achieve driving of second CP kind toward this positive polarized electrode, with a peak current reduction almost equal to that obtained on WE1 during first E-field application, but has drastic consequences on the CP assembled on WE1 which recovers initial (bare) peak current. In order

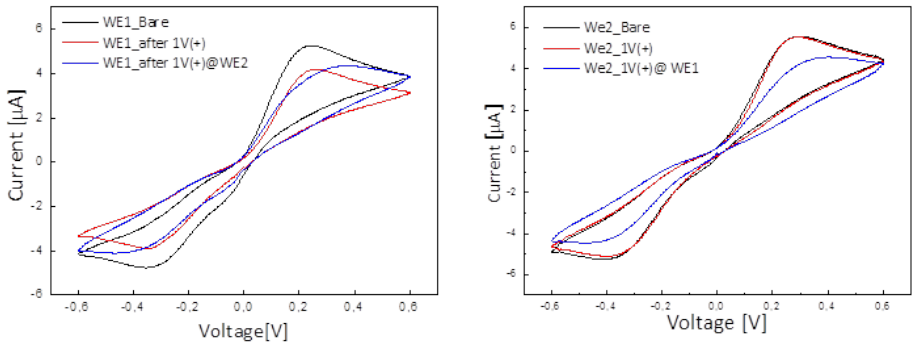

Figure 112: Results of the electrochemical analysis of the site selective deposition of CP1 in WE1 (a) and CP2 on WE2 (b).

of reducing this effect, we considered DC signal application between one WE and CE.

In Fig. 112 we show results of E-field driven immobilization of CPs, following this second procedure. According to the behavior observed here, after the application of a positive DC signal on the required WE, the current peaks of the CV, were reduced compared with the initial current of the bare electrode, which demonstrates the covering of this electrode

with the desired capture probe, with a 21 % coverage of the WE1 by CP1 monolayer.

The covering current percentage was calculated considering the starting situation of the bare electrode compared with the current after immobilization.

In this process also diffusion of the CP1 on the unconnected electrode can be observed, being undesirably non-selectively adsorbed. However, as is shown in the WE2 current peak in the inset of left plot in Fig. 112, the current observed is similar to its bare signal, supposing a negligible non-specific coverage on WE2.

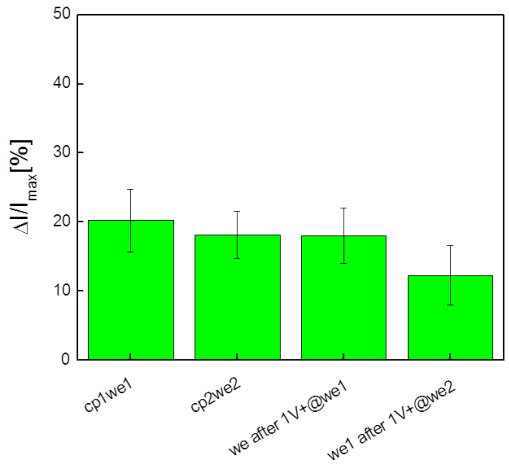

Figure 113: Relative decrease of peak current for DEP process.

Voltagrams represented on right in Fig. 112, that were measured right after inducing a positive polarization of WE2 to attract the CP2, first on WE2 and then on WE1 (in the inset) show that reversing the polarity has two effects: while the electric field created between the WE2 and CE drives negatively charged probe molecules to the WE2, resulting in a reduction of the electrode active area, it may also produce damages on the CPs already attached on the close WE1, as seen by decrease of response also at this electrode.

On one side, the successfully drive of CP2 to the WE2 is demonstrated by the decrease of current observed in the CV characterization, which is related to 18% of surface coverage Fig. 113. On the other, a low decrease

of coverage is observed also in WE1, and the voltagram recorded on this electrode has an increased area after the second immobilization step.

Although, being only 4% of CP1 coverage affected by the application of electric field on the neighboring electrode, this method demonstrates potentiality as tool for the selective addressing of molecular probes in nano-gaps devices. In general, lower surface coverages are obtained following this latter process, but a drastic reduction of immobilization times, from overnight incubation, required by all previous methods, to the overall 5 minutes which are necessary to accomplish electrophoretic driving of capture probes, is achieved. To improve rate of specific absorption asso-

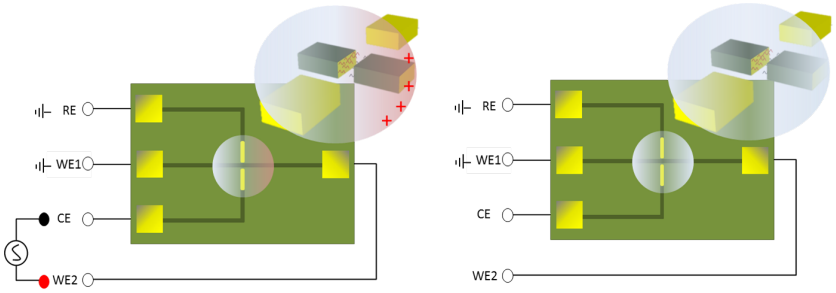

Figure 114: Steps involved in the last proved method, E-field is applied on WE2 to attract CP2 followed by incubation of nano-gaps with CP1

ciated to this process we considered a last method involving a first E-field immobilization step of one CP's kind to a WE, followed by standard standard SAM adsorption incubation, as it is schematized in the following Fig. 114.

Results obtained by applying this last methods are shown in Fig. 115.

According obtained results, this strategy is useful to increase specific adsorption of selected CP on targeted electrode, as well it is useful to reduce not specific adsorption on both electrodes. Of course, in this case we loose the advantage of very reduced assembling times required by applying electrophoresis as discussed above.

4.5 CONCLUSIONS

SAM provides a bio-interface flexible to many applications according the functionality expressed by terminal groups. In particular, they offer a

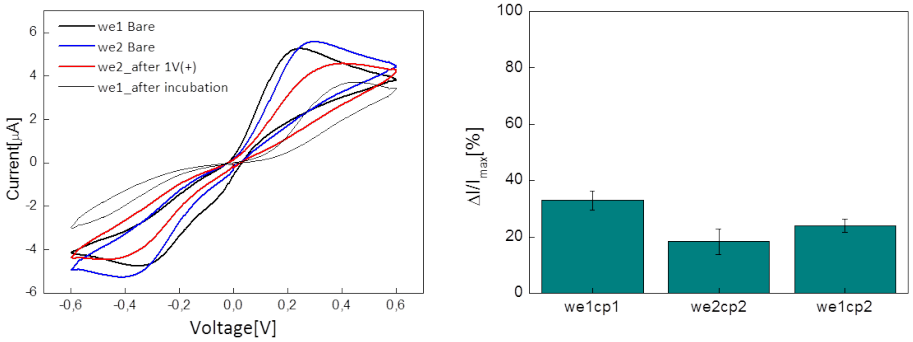

Figure 115: Cv analysis following step of last immobilization method, and effects on peak current intensity

fast and effective route to functionalize surface electrodes by a molecular coating, as required for biosensor applications.

Compared to the standard methods used to the same purpose and based on Langmuir-Blodgett process, SAMs offer numerous advantages such as easy processing, low defects degree, and better stability in water and other solvents. For this reason, since their introduction, SAMs on different substrates have been object of many studies, and are widely employed to build versatile bio-interface for targeted applications.

However in multifunctionalizing surface on array or nano-gap, where a Langmuir-Blodgett and SAM'adsorption from solution, do not give a selective functionalization of electrodes, other methods need to be considered.

We used adsorption of a mixture of CP1 and CP2, electrochemical stripping, and E-field assisted CP's immobilization strategies to functionalize the two nano-gap electrodes, and we evaluated their effects on SAM formation by applying CV analysis.

Comparing the two E-field driving methods and according our results, electrochemical stripping although effective to remove a previous SAM on a selected electrode, is altering the monolayer assembled on opposite electrode. This is especially important in our nano-gap configuration, facing the electrodes at nano-metric proximity. This is not surprising to occur because low applied voltages implies high electric field strength on such nano-metric distances.

In light of this, whenever the method is useful to recover electrode surface for its regeneration, it is not well suited to our application. By giving rise to a final mixed SAM it is not convenient compared to SAM adsorption from solution, which requires only one overnight incubation process.

Aimed at improving these results, we attempted selective assembling of CPs assisted by E-field application under which charged probe molecules are attracted toward a given polarized electrode. Globally, this strategy was useful to achieve selective adsorption of CPs, but compared to monolayer assembled by overnight incubation, the amount of surface coverage is consistently lower.

A complementary optical characterization of DNA molecules assembly inside nano-gap with suitable separation size, was indeed provided by means of TOF-SIMS analysis.

5

DNA DETECTION IN THE NANO-GAP SENSOR

This chapter describes experiments performed to demonstrate the feasibility of developing nano-gap electrodes system as a DNA biosensor enabling direct electrical detection of DNA's hybridization and SNP.

Nano-gap electrodes modified with CPs assembled monolayers specific to the analyte target are used to specifically trap the complementary DNA. Current voltage measurements are applied in order to detect presence of hybridized DNA inside nano-gaps, which closes the electrical circuit and provides the bridge for charge conduction. Recovering of initial biosensor response after a denaturalization process, and its capability to quantitative measurements tested by adding different target concentrations are also analyzed. Results obtained are analyzed and discussed.

5.1 ELECTRICAL DETECTION OF DNA'S HYBRIDIZATION

5.1.1 *Methodology*

Electrical detection of DNAhybridization is achieved by monitoring nano-gaps response by means of current-voltage measurements, which were performed according methodology discussed in section of chapter 3.

Electrical characterization of nano-gaps was performed after initial bare, clean nano-gaps analysis, during following steps of device assembling with molecular probes, and finally after addition of target analyte, which closes the circuit by bridging nano-gap electrodes through specific complementary DNA base-pair recognition. Hybridization is expected to affect nano-gaps electrical response, leading to current increase supported by charge migration on the formed DNA bridge.

To demonstrate the selectivity of detection by means of DNA mediated long range electron transfer (LoRET) the complementary hybridization is compared with the signal obtained with SNP. To this purpose, we em-

ployed two mutated probe oligonucleotides that were chosen so as to have one single base mismatch at the 5′ and 3′ end respectively which are involved in target capture by hybridization.

Bare nano-gaps are cleaned and characterized, afterwards they are immobilized with SAM CPs followed by electric and electrochemical characterization, as it was explained in previous chapters. Then, 1 μ M of the target sequence in the hybridization buffer (250 mM of sodium phosphate, 15 mM of sodium citrate, 150 mM of NaCl, 1 mM of EDTA and 0.02 mM of Triton buffer at pH 7.42.) was deposited on the electrodes, and left incubating for 1 h in a humid saturated environment.

Thereafter, nano-gaps were thoroughly rinsed and dried with N_2 to remove the non-attached probes before electrical measurements. These latter were performed using Keithley sub-femtoAmp Remote Source meter, Model 6430 connected to probe station, as described in chapter 3, at room atmospheric conditions (referred to as the *out of solution* environment with an average temperature of 24°C ±1°C and 55% relative humidity, r.h.), and *in solution* in autoclaved DDI water, purified with the Millipore A10 Q-gard 1 system (18.2 MΩ/cm at 25°C).

In order to fill the gap with liquid, a drop of water was delivered to the region between gold pads by means of a micro-pipette. Each measurement were repeated three times, each run was fast enough to prevent the evaporation of water drop, also even during further repetitions and to avoid system stress during application of long during test potentials.

5.1.2 *Hybridization in E-field and adsorbed CPs assembled nano-gaps*

According results obtained in previous chapter, we used for electrical detection experiments nano-gaps modified by CPs under E-field application, giving rise to better selectivity outcomes, and that assembled by adsorption from a mixed solution containing both CPs.

In Fig. 138 we show the increase of current after target hybridization which were measured, in air, on nano-gaps selectively modified by E-field application, and on randomly funcionalized nano-gaps. Currents values were normalized with respect bare signal, measured before hybridization.

Following observed results, target hybridization at mixed SAM produces always a higher current increase compared with the response obtained on nano-gaps selectively functionalized.

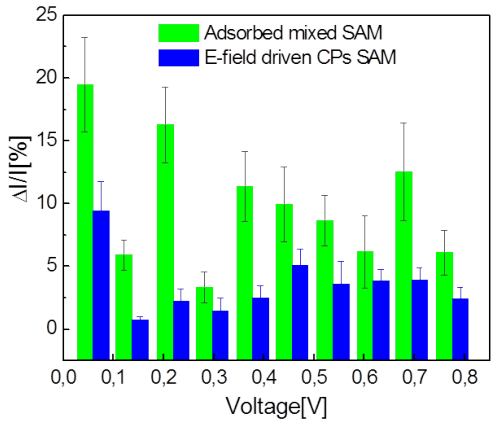

Figure 116: Increase of current after target hybridization on mixed SAM assembled nano-gaps and E-field driven selectively modified devices.

Although this is principle counterintuitive, we postulated that it could arise in virtue of the poor surface coverage achieved by adopting such immobilization strategy. Indeed, as it will clearer from further SEM analysis of hybridized nano-gaps, which results will be commented in the following, DNA inside nano-gaps hybridizes by forming bundles which connects the nano-gap edges so that a denser CP SAM could be more likely to favor such cross-linked structures by than by a more ordered one.

This result made us to consider for further optimization experiments only nano-gaps modified by adsorbed mixed SAM, which will be treated in the following.

5.1.3 *Hybridization detection in adsorbed SAM nano-gap*

Nano-gaps achieving best detection performances in first comparative analysis considered were thereafter used to validate the working principle of the biosensor and to establish its feasibility for the targeted application.

This was done by considering nano-gap hybridization response under different conditions, as it is detailed further.

As first, we studied biosensor selectivity to SNP by analyzing nano-gap response after hybridization of target DNA on well matched, and mismatched, CPs modified nano-gaps, whose SAMs were assembled by adsorption from solution.

In Fig. 117 we show current-voltage response of well-matched, and mismatched CPs functionalized nano-gaps after target hybridization, measured at room conditions. Experiments were done by using 10 nano-gaps having an average size of $52,02 \pm 5,90$ nm and with an error of 1σ.

The voltage range applied [-0.8 V; +0.8 V] was chosen to exclude counterions contribution to the measurements [106]. Such a contribution can arise both from polarization and faradaic processes. These latter are unlikely to occur within this potential window because they require higher voltages for the exchange of electrons between counterions and the molecu le, through reduction and/or oxidation processes.

Voltages included in this range are also well-suited to prevent the breakdown of air molecules in the inter-electrode nano-gap region and the electrodes reorganization, which can result in a larger gap [2]. Bare nano-gaps

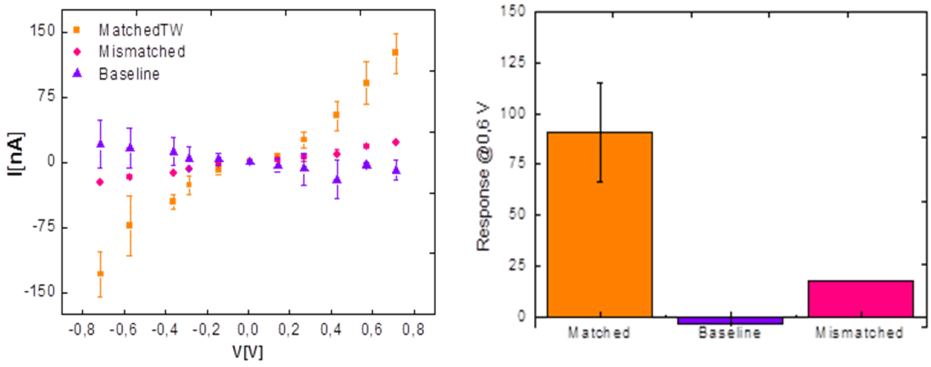

Figure 117: Detection of DNA hybridization, under complementary and mismatched conditions. The column plot represents the response at 0,6 V.

and CPs modified ones produced almost the same electrical signal. The difference between these signals is shown as the Baseline in plot of Fig.

117. This normalization was adopted in order to take account of the errors introduced by differences in the nano-gap features.

In the same graph, we also show the measurements obtained after 1 h of incubation with the well-matched target segment (Matched TW, synthetic 109-mer, with 62% of G:C), and the same sequence hybridized at mismatched DNA-Thiol-Probes (Mismatched; CP2mut and CP1mut, synthetic 53-mer, with 58.5% and 64.2 % of G:C, respectively). The signals were normalized as before.

The curves obtained resemble those typically observed for semiconductor materials, with a smoothed non-linearity with respect that commonly found in standard semiconductors. We observed a clear increase in current after hybridization of the DNA target. At the highest positive voltage applied, we measured a current of 125 ± 23 nA, corresponding to a high rate of charge migration of about $8 \times 10^{11} e^{-} s^{-1}$ in standard laboratory conditions, and accounts for a 98% increase in the nano-gap current after the hybridization of the target.

We retained of interest to compare the results obtained by observing *in solution* and *out of solution* data, so to compare DNA conduction measurements in air and in low conductivity solution, as DDI water. In fact in the case of DNA molecule, it is very relevant the environment contribution to the overall conductivity has been stressed in the literature. This environment is indeed more probable to assure molecule stability with respect temperature increase induced by voltages application.

In the case of *insolution* measurements a lower increment of the nano-gaps current after the hybridization of well-matched target, is detected Fig. 118. In fact, although the maximum current was 135 ± 30 nA, the relative increment accounted respect the baseline was only 65% compared with the 98% obtained in air measurements.

This lower current increment is result of the higher contribution of the DDI water background, so that this higher baseline signal made *out of solution* detection more sensitive. We did not observe an exponential dependence of DNA conductivity on the r.h., as reported elsewhere [132], [2] by which it was concluded that, the water layer absorbed by DNA from environment humidity was the major contributor to conductivity at room atmospheric conditions.

It has recently been proposed [8] that the unbinding of π electrons, triggered by DNA hydration, induces band-gap narrowing, from the value of 8 eV in case of dry DNA to about 3 eV for hydrated DNA, which for sufficient wet, is characterized by the B-form. According to our results,

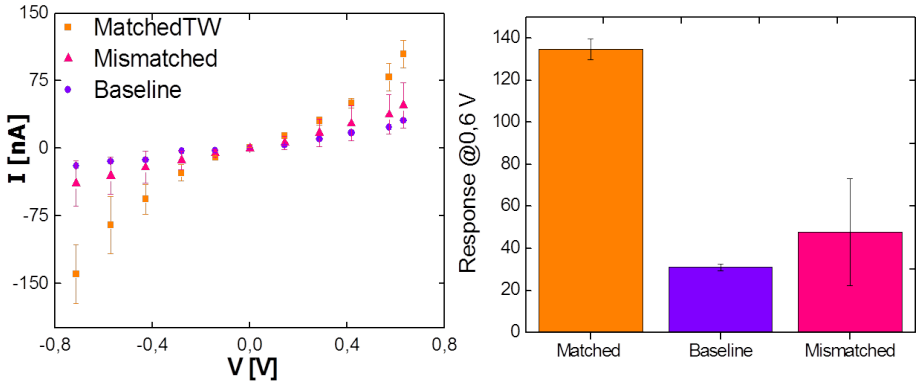

Figure 118: DNA's hybridization detection under complementary and mismatched conditions. The column plot represents the response at 0.6 V.

and in light of above observations, we postulate that DNA's hydration at ambient conditions is necessary to trigger the conductivity of DNA, by stabilizing its structure.

This conclusion is along with previous reports in which it was postulated that the strict, non-physiological conditions, required by some direct conductance experimental set ups, were at the origin of corresponding negative reports on dry [36] and frozen DNA [79].

In contrast to the hybridization with well-matched target, we did not observe significant current changes at devices whose nano-gap electrodes were functionalized with single-base mismatched probes.

The maximum current in this case was $22,8 \pm 0,3$ nA out of solution and $37,8 \pm 12,2$ nA in solution. At 0,6 V, resistance for the mismatched strand, calculated assuming ohmic linear behavior, is 83% greater than for the complementary strand *out of solution*; in case of *in solution* measurements the increment is only 52%.

This result is in good agreement with reported observations about the sensitivity of DNA-mediated charge migration to single-base mismatches,

as already proved in electron transfer-based electrochemical platforms [105], where a single mismatch in a 100-mer chain was found to give rise to a shift in the cathodic and anodic peaks of cyclic voltamperometry, corresponding to a decrease of almost 47% and 50% of the well-matched signal, respectively.

The agreement found is indicative of DNA electron transport sensitivity to base mismatching. Furthermore, the sharp decrease in current observed in the presence of mismatches ensures that the transport is through the DNA stack and not contributed by surroundings, indeed solution effect is negligible.

5.1.4 *Reusability of the DNA sensor*

The wide-scale application of DNA analysis requires the implementation of highly sensitive methods on inexpensive platforms. In order to reduce the cost of these devices an important issue is to achieve sensor regeneration.

Design of our biosensor allows assessment of capture probes reusability by simply denaturalizing the hybridized DNA. In order to achieve

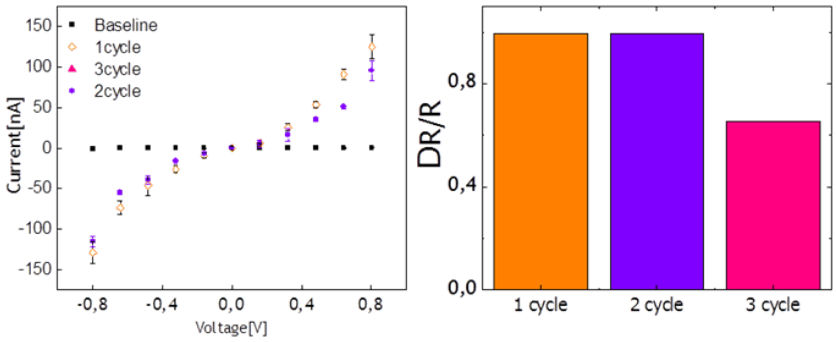

Figure 119: Currents measured after denaturalization and further incubation with the complementary target. Out of solution data are shown.

this, the molecular device was exposed to a solution 10 mM NaOH for 2 min. After extensively washing the array with abundant DDI water

and drying it with a nitrogen flux, we measured the I-V characteristics of de-hybridized/hybridized gaps during various cycles.

The results are shown in Fig. 119. As in previous analysis each signal was normalized with respect the corresponding baseline. Shown baseline was averaged over the three results, obtained after each denaturalization step.

Device's reusability up to 3 cycles, suppression of the current after DNA's denaturation, and the subsequent increase after incubation with the target, not only demonstrate reusability of modified nano-gaps electrodes but indeed remark that hybridized DNA is the bridge enabling nano-gaps conductivity.

In case of a deeper reusability to use different CPs sequences, the design of this nano-device permits the stripping of immobilized CPs SAMs, as it was explained in previous chapter for the complete reusability of the nano-gap sensors.

5.1.5 *Quantitative measurements*

In order to prove biosensor capability for quantitative measurements, we studied the possible dependence of the nano-gap currents on a range of target sequence concentrations, results of this experiment are shown in Fig. 120.

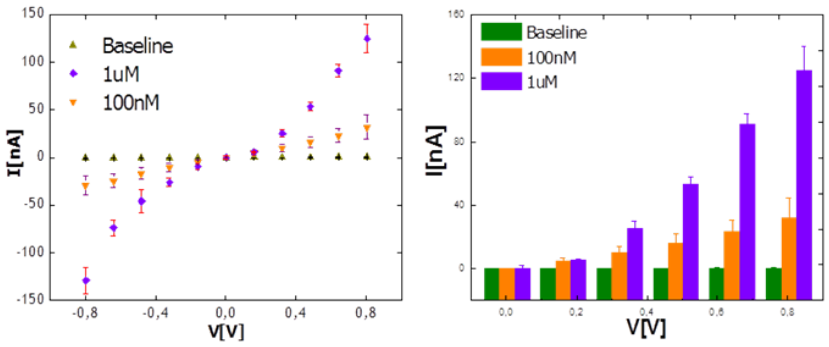

Figure 120: Sensor response at different TW concentrations. Out of solution data are shown.

Higher concentrations caused a greater nano-gap current according to observed results, which we attribute to the possibility that increasing target concentrations augment the probability of nano-gaps connections by molecular bridges resulting in higher current from target hybridization.

However, this quantitative measurements is just a proof of concept to elucidate the quantitative ability of this device, but further concentration measurements need to be performed in order to obtain a calibration curve and a limit of detection.

5.2 SEM CHARACTERIZATION OF HYBRIDIZED NANO-GAPS DEVICE

According electrical characterization with considered controls, it is clear the feasibility of the sensing principle enabling our platform and based long-range electron transport along DNA. However, for a deeper study of our nano-device we considered SEM characterization of nano-gaps.

The SEM picture in Fig. 121 shows shining nano-gap edges in the hybridized nano-gap, due to the presence of the CPs SAMs attached on the gold electrodes, on each side of the nano-gap.

Hybridized DNA bridging nano-gaps electrodes can be observed in inside it, highlighting that bundles of hybridized DNA, rather than single molecules bridges, are most likely to be trapped inside the sensor. From this analysis, we postulate that the hybridization of complementary

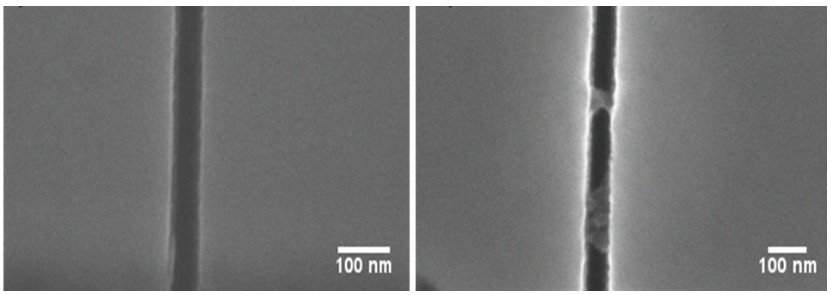

Figure 121: SEM pictures of one of the devices used, before (left) and after (right) the hybridization of the target DNA.

strands inside the nano-gap can also take place through the formation of cross-linked patterns.

In the DNA bundles observed with the SEM, we measured a lateral surface of about 200 nm, which is much greater than the cross-section value of a DNA molecule, of about 2 nm. In this case, it is expected that the intra-molecular interactions between DNA also play a relevant role, contributing to the increase of charge transport on the bridge of ssDNA, where the ssDNA molecules support only weak currents [92]. Probably the formation of such bundles is facilitated by random absorption of the two CPs on nano-gaps electrodes.

5.3 ANALYSIS OF CURRENT-VOLTAGE CHARACTERISTICS

Electrical transport through a molecular system depends from several parameters such as the electronic structures of the molecule, the type of molecule-electrode coupling, and the position HOMO-LUMO relative to the Fermi energy of the electrodes, just to list some.

In general, in order to establish the exact conduction mechanism by I-V characteristics analysis, more parameters than thats here measured should be considered such as, for example, variable-temperature dependent data (pure tunneling is, for example, temperature independent) or molecular length-dependent data, by means of which many mechanisms could be ruled out. It was not the aim of this tesis to face this problem, nevertheless, by using standard analysis methods found in literature we attempted to provide reliable data fitting to interpret obtained results.

The growing number of current-voltage data of different molecular systems, from vacuum nano-electronics [9] to molecular electronics [1], [7], [22], has been analyzed by applying the Simmons model [102], [103], [104], which was originally derived to describe the off resonant tunneling of charges.

Inherent limitations of Simmons model application has been extensively discussed by Vilan [119] which also studied the possibilities of its application to fit molecular I-V data in absence of molecular length-dependent, and temperature-dependent data.

In particular, Vilan demonstrated by considering the scaling and the linearization of the Simmons model, that the magnitude of the current, characterized by the equilibrium conductance $G_0(\Omega^{-1})$ and the I-V shape

factor, ρ, defined as the ratio between width and height of the barrier, can be used as phenomenological parameters to describe molecular junction transport.

In Fig. 122 plot of conductance for considered sequences obtained by simply applying the relationship $G = I/V$ to the experimental I-V data are shown.

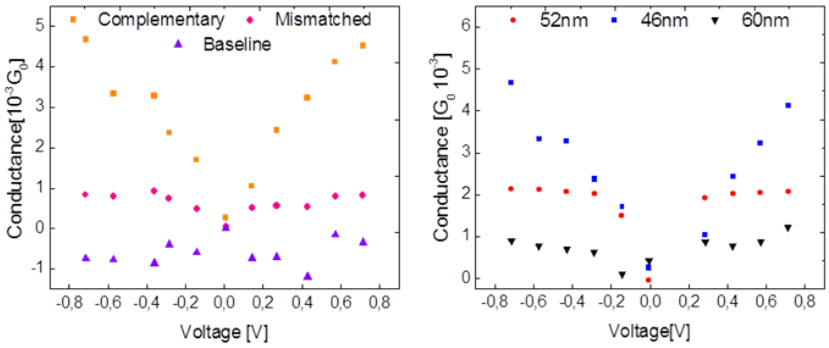

Figure 122: Conductance for analyzed sequences, in terms of the conductance quantum (left) and Plot of $G(G_0) - V$ in function of three different gap sizes (right).

From their analysis it is seen that for V>0,25 V the conductance increases linearly with an almost constant slope of $2,5 \times 10^{-4} G_0$ (with G_0 the fundamental conductance quantum, representing the value of zero bias conductance). Linearity persists over all the potential range explored, without showing potential polarity dependence, nor no saturation, as it has been observed in the case of MWNT [115].

In the Fig. 122 a $G(G_0)V$ plot for three different molecular lengths is shown.

Molecular lengths are accounted by the nano-gap sizes, and as consequence this could imply a different bending of the molecule trapped inside the gap. Although our data are not sufficient to provide insight on the dependence of electrical behavior by molecular conformation inside nano-gaps.

In general, it is interesting to observe that despite the approximations considered in both cases, these conductance values are very similar to that obtained by involving the phenomenological model exposed in chapter 2.

Following analysis exposed by Vilan [119], we will consider the polynomial approximation of the Simmons model given by:

$$\frac{I}{V} \approx G_0(1 + CV^2) \tag{26}$$

where $C \approx \frac{\rho^2}{96}$, in order to get a linear representation of the I-V (when it is possible, this will provide the range for which the application of the Simmons model is relevant to the data set); and to extract the functional parameters in eq. (26).

The slight asymmetry in the $I/V vs V^2$ plot between forward and reverse bias data, is taken in account by fitting the data on two different bias ranges, separately. The fit coefficients can be translated into barrier parameters if the contact area is known, and under the assumption that molecular length is equal to the potential width [119].

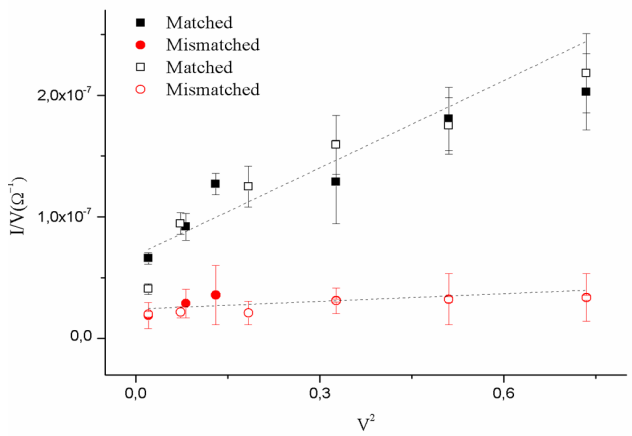

Figure 123: Plot of the integral conductance against the squared bias providing the linear representation of I-V data according eq. (26) (empty dots are for reverse bias data and dot lines are linear fit to data.)

By assuming for the contact area, the value $400nm^2$, obtained from the SEM analysis of the nano-gaps, and by considering the gold work function value ($E_f = 5.0\,eV$), it is possible to give an estimation of the HOMO-LUMO energy gap for our system, under the well-matched and mismatched hybridization conditions. By doing so, the calculated energy gap values fall in the range $2.2 \div 4.6\,eV$, in good agreement with the postulated ones, expected to be within the range $3 \div 4\,eV$ [16].

The other parameter of fit G_0, the equilibrium conductance, has been widely used as characteristic parameters applied to discuss transport problems. Although this, it just reflects the current magnitude value and it does not give insight on the specific conduction mechanism. However, it is useful to know in order to compare the results obtained here with that already present in the literature.

To this end, we recalculated the values of equilibrium conductance fitting the low bias range ($\pm 0.4V$) of the I-V, for the matched and mismatched targets, to the equilibrium relation $I \approx G_0 V$.

By assuming the contact area value of $400\,nm^2$ and a nano-gap length of 52.02±5.90 nm (on the basis of SEM characterization of Fig. 121), we estimated the corresponding resistivity values, given in Table 4. The values

DNA strand	$R(\Omega)$	$\rho(\Omega/m)$
Complementary	$\approx 3M\Omega$	$\approx 2,4\Omega m$
Mismatched	$\approx 100M\Omega$	$\approx 0,2\Omega m$

Table 4: Resistivity and conductivity values calculated

found are in general agreement with those reported for similar platforms.

In case of a poly(dG)-poly(dC) of 50 nm of self-assembled DNA networks [17] a resistivity value of $1\Omega cm$ was found by means of STM analysis.

A resistivity of of about $2\Omega m$ was reported by Wang [121] which used ac impedance measurements on a random λ DNA bundle 20 nm in width and 25-30 nm in height. In case of a 15-mer sequence bridging a carbon nanotube gap, a resistance of $1M\Omega$ was observed [42], this value was shown to increase with the length of DNA considered, and it was observed a value of 25-40 GΩ when a 80-base pair sequence bridged a carbon nanotube [92].

We found overall agreement with comparable reported results also for the decrease of conductivty observed in presence of a G-A mismatch on one side and of a G-T mismatch on the opposite. We calculated a a four-fold increase in the resistance of mismatched sequence with respect to the fully complementary strand.

It has bee postulated that resistance increase arises for the decreased stability of the hydrogen bond for the on-site changing of the ionization potential, and for the alterations of π stack structure [50].

Theoretical calculations [50] established that hydrogen bond destabilization plays a minor role in the suppression of DNA conductivity while π stack distortions, and the change of on-site energy, came out to be the determinant factors. Indeed, when the donor and acceptor lie on the same strand the site-dependence to mismatch shifting is negligible.

In order to account for this, it is useful to observe that in case of G-A and G-T mismatching, sequence's integrity is affected only in one strand, while the other is unaltered. By involving DNA metallization, it was possible to show exponential increase of resistance in function of occurring mismatching [84]. By means of the same experimental set up, it was also observed that G-T mismatch has a lower influence (accounting for an increase of 1.02 MΩ) on conductivity change with respect to a G-A mismatch, with an increase of 1.20 MΩ in resistance, and then that mismatch position is irrelevant as long as sequence length is below that of electronic coherence [50].

5.4 CONCLUSIONS

In this chapter we presented and discussed results of experiments done to demonstrate the feasibility of our biosensor platform for label-free direct electrical detection of DNA's hybridization and SNP, based on LoRET supported by DNA.

We compared results obtained by current-voltage characterization of nano-gap electrodes during the following stages of devices assembling with specific oligo-probes for the target DNA. Measurements were carried at room atmospheric conditions, and in DDI water providing a more physiological environment for DNA. Although, given the relatively higher background signal of bare nano-gaps electrodes in DDI water, *out of solution* detection was more sensitive.

By modifying nano-gap electrodes with mutated CPs we were able to show the selectivity of detection based on DNA LoRET with respect SNP. Indeed, this can be considered a useful control experiments confirming

that changes in electrical response of nano-gaps arose for the presence of DNA molecules. This is further proved by results obtained in quantitative, and denaturalization-re-hybridization and assays.

We detected a signal distinguishable from that of the control at a target concentration of 100 nM. This is the lowest detection limit reached, compared with existing platforms that rely on long-range electron transfer combined with proper labeling (4μM [130] [129]; 25 μM [105]), the limit of detection being higher (0.5 nM) only in [130], in a labeled system. We stress that, on the contrary, in our platform the detection was achieved in a total, label and reagent-free fashion, as it was based on the robustness of charge migration along DNA.

Finally, by using a standard denaturalization process, we showed reusability of CP's modified nano-gap electrodes up to 3 cycles, after incubation with the target DNA.

From proposed model analysis we were able to extract conductance and resistivity values associated with molecular entities in our system. Results found are in general agreement with thats already reported in literature and obtained by considering similar experimental conditions, indeed we highlight an excellent agreement between conductance values estimated by means of the phenomenological model proposed at the end of second chapter, and that derived by employing experimental data according discussed modeling.

6

GENERAL CONCLUSIONS

The aim of this tesis was to explore the possibility of exploiting electrical properties of DNA molecules in order to detect a specific DNA sequence, and single nucleotide polymorphism (SNP) point-base mutation, in a conductance-based nano-sensor with a free-label detection scheme.

This objective faced several scientific and technological issues mainly related with the general challenge of understanding molecular electronic transport properties, and to design experimental systems suitable for their analysis.

A preliminary study of current understanding of electrical properties of DNA, by a deep review of existing experimental and theoretical results, allowed us to establish a reliability context for the platform from the conceptual point of view and then to optimize design, physical realization and testing of the system.

We developed a phenomenological model, based on standard picture of long range DNA charge migration, which assumes multi-hopping of charges through intermediate steps characterized by super exchange transfer rates, to obtain a rough estimation of charge of rate transfer for the molecular bridge considered, between donor and acceptor states represented by electrodes. This was then exploited to evaluate conductance of the molecule, under the hypothesis of wire-like conduction, in order to fix the bounds of observability of experimental parameters.

Based on our analysis, we conceived the nano-sensor platform such to have two gold nano electrodes face-to-face nano-gap edges at a separation distance adjusted to fit the size of involved molecules, including DNA as part of the electrical circuit, which is closed thereafter the specific interaction between a target (bridge) DNA and two antisymmetric capture probes. Target's hybridization, by switching off nano-gap electric circuit, triggers its own detection through increase of the current across the nano-gap, monitored by standard electrical measurement.

Lay-out design was optimized in order to maximize the analytical performances with respect cost and sophisticate processing, having nano-gaps easily accessibles to both electrical and electrochemical measurements, which we applied to characterize nano-gap electrode surfaces where optical based analysis are limited.

Nano-gaps with high-resistance and reproducible features where obtained by combining standard photolithography and FIB lithography. By involving of several characterization techniques we validated this fabrication processing as useful to achieve the sensitivity required for low conductivity measurements, and an overall efficient method exploitable for large production. Array design shares the possibility for high dense patterning and multiplexed detection in a deliverable system such as the prototype holdings structure tested.

Further assembly of device, deal with the problem of control molecular probe positioning inside nano-gap.

We applied three different strategies of immobilizations, standard adsorption of thiolated probes from solution, electrochemical stripping and E-field driven, and compared results by means of CV characterization, which was been shown to provide and effective framework of analysis to fit our investigation problem. According obtained results, we used in electrical detection experiments nano-gap modified by random CPs assembly through adsorption from solution, and E-field funcionalized CPs.

We measured I-V response of nano-gaps after DNA's hybridization achieved by incubating CPs modified nano-gaps with target solution, in order to validate the hypothesis of current increase supported by bridging molecules. We observed clear current increase following target hybridization in randomly assembled nano-gaps which then were chosen for the subsequent sensor optimizations experiments.

We proved nano-sensor selectivity with respect SNP by analyzing the I-V response of nano-gaps funcionalized with well-matched and mismatched CPs after target hybridization. Observed decrease of current is compatible with reduced efficiency of DNA for charge transport due to alteration of the π stack structure introduced by mutation.

Then, we considered regenerability and sensitivity to different target concentrations. Positive obtained results demonstrate the feasibility of the system developed for application as a DNA sensor.

7

RESUMEN EN CASTELLANO

7.1 INTRODUCCIÓN

Todos somos iguales a menos de unos 1% de variaciones que afectan el acoplamiento de una, entre las bases, de la secuencia de adn que constituye el genoma de cada individuo. Estas diferencias, o polimorfísmo de un solo nucleótido (SNP) como suelen ser llamadas, se suponen ser a la base de la respuesta de cada individuo a desarrollar enfermedades especificas, o la reacciones a tratamientos terapéuticos así como al ataque por parte de virus u otros organismos patógenos.

Determinar los mecanismos a través de los cuales los SNPs manifiestan estos efectos es una de las cuestiones principales a la cual actualmente se enfrentan genética clínica, genética molecular, biología molecular y fundamental. La detección de hibridación de cadenas de ADN es un reto relevante científicamente e tecnológicamente, que puede aprovechar de las posibilidades proporcionadas por los alcances en los procesos de nano fabricación y caracterización, inspiradores de la idea de una medicina en el punto de atención.

El debate científico [116], [30] sobre las propriedades eléctricas del ADN, animado por la intrigante idea que pueda actuar como un molecular wire, se originó en seguida a la conquista de su estructura por Watson and Crick en los 50. Se adelantó la hipótesis que el superposición de los orbitales π entre las bases pudiera actuar como un canal por el transporte de carga [108].

El tema ha sido recientemente sujeto de nuevo interés en seguida a la descubierta de que el comportamiento eléctrico del ADN puede ser implicado en los mecanismos de daño y reparación, a partir de la observación de la propagación del daño oxidativo de una guanina a distancias grandes del oxidante [56]. Esta observación confirma la original idea, seguida el estudio de los fenómenos de mutation y reparación en la molécula, de

que el transporte de carga en el ADN puede soportar una llave para la comprensión de las dinámicas funcionales del ADN, comprometidas en algunas enfermedades.

Este aspecto, unidamente a dos peculiaridades de la molécula, es decir el acoplamiento especifico entre las secuencia, y la capacidad de auto asemblaje, hacen del ADN un candidato adecuado en la electrónica molecular, y muy interesante como componente activo de sistemas nano-métrico [118].

7.2 OBJECTIVOS

El propósito de este trabajo es lo de establecer un sistema de detección de hibridación de ADN, y SNP, basado en la medida eléctrica de la resistencia de un nano-gap funcionalizado con el DNA target, gracias a las propriedades eléctricas del ADN.

Diferentes objetivos específicos se han llevado a cabo por el desarrollo y test del sistema:

- Un estudio preliminar de la literatura relacionada con las proprie dades eléctricas del ADN se ha conducido con la finalidad de establecer el marco de factibilidad del proyecto. De acuerdo con los resultados de este estudio ha sido posible idear el sistema y optimizar su eficacia respeto a las experiencias reportadas.

- Fijar una estrategia de fabricación de los dispositivos capaz de proveer nano-gap aptos a la medida de conductividad muy baja, según una rutina de fácil implementación y con alta reproducibilidad de los resultados. Estos se han caracterizados mediante el utilizo de diferentes técnicas basadas primariamente en métodos de detección Optica y Eléctrica/Electro-química.

- Obtener la bio-funcionalización selectiva de los electrodos en el nano-gap testando y caracterizando métodos diferentes.

- Probar el principio de funcionamiento del sistema a través de la medida de la conductividad en los nano-gap durante las diferentes etapas de funcionalización con los bio-receptores y el DNA target.

- Optimizar el sensor testando su selectividad respeto a la presencia de mutaciones, la sensibilidad a medir diferentes concentraciones del target, y finalmente la posibilidad de regeneración del dispositivo después desnaturalización del ADN hibridado.

7.3 METODOLOGIA GENERAL

El sistema propuesto es constituido por dos electrodos de oro enfrentados en un nano-gap con una abertura de alrededor 50 nm, Fig. 128. Las partes del dispositivo no interesada en el proceso de detección son protegida por un espesor de SiO_2 que limita las fuentes de ruido en la señal de detección, y detiene la inmovilización de los bio-receptores y del ADN target fuera del nano-gap. En la plataforma, los bio-receptores utilizados

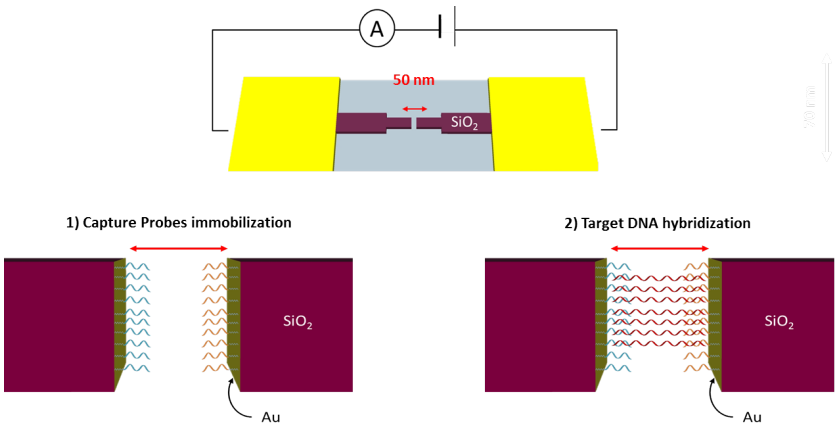

Figure 124: Esquema del sistema propuesto.

son dos sondas de ADN, funcionalizadas con moléculas de tioles por su inmovilización en los electrodos del nano-gap. Las sondas de ADN, anti-simétricas entre ellas, son complementaria en la parte terminal a la secuencia de ADN que se desea detectar. En esta manera, la formación del compuesto sondas-ADN target desencadena el cierre del nano-gap haciendo posible la detección de la hibridación mediante medida de la conductividad del sistema.

En comparación con sistemas parecidos, previamente propuestos [94], [101], la configuración adoptada en este trabajo, con los electrodos enfrentados uno al otro, favorece la orientación ordenada de los orbitales π

así que se incrementa el transporte de carga a lo largo de la molécula que puede ser detectada mediante una medida directa que no se basa en el utilizo de procesos de amplificación de la señal.

7.4 FABRICACIÓN Y CARACTERIZACIÓN DE LOS DISPOSITIVOS

7.4.1 *Fabricación*

La estrategia de procesamiento de los nano-sensores ha sido establecida con el objetivo general de optimizar la eficacia vs la accesibilidad de los procesos utilizados en función de los conocimientos corrientes de las diferentes técnicas de fabricación y caracterización de nano-sistemas, y respeto a la facilidad de accesos a estas tecnologías con gastos reducidos y procesamiento propia.

Los nano-sensores, constituidos por una pareja de electrodos de oro a una distancia de alrededor 50 nm, han sido fabricados mediante fotolitografía y nano-litografía a través FIB sobre una oblea de Silicio (SOI) metalizada por un espesor nano-métrico de oro, 70 nm, adherido sobre 10 nm de titanio.

La fotolitografía de las obleas se ha finalizado según la rutina representada en Fig. 125.

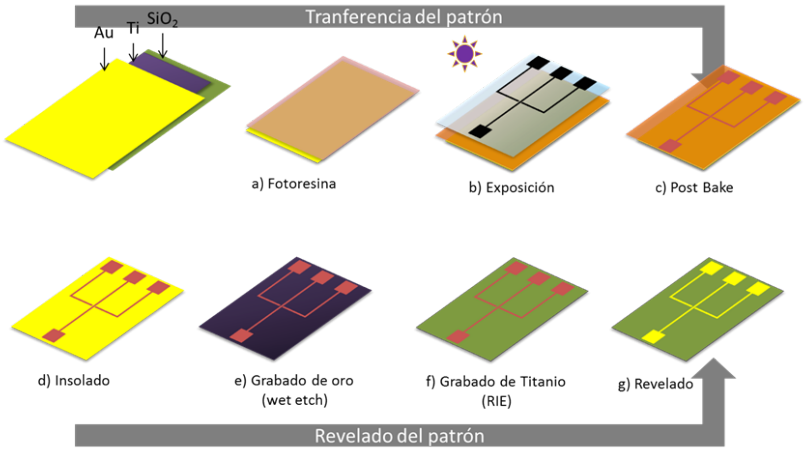

Figure 125: Etapas típicas en un proceso de foto-litografía.

La fotolitografía, mediante lo cual es posible transferir un patrón con definición micro-métrica, es uno de lo standard en la procesamiento de dispositivos micro-electronicos a escala industrial. Este proceso, inspirado por el mismo principio de la litografía, se basa sobre el utilizo de una fuente de luz ultra-violada (UV) y las propiedades de las resinas foto-sensibles adaptadas por esta aplicación. Estas se obtienen a partir de polímeros capaces de alterar sus propriedades físicos-químicas después la exposición luminosa.

En particular, las resinas normalmente aplicadas en micro y nano-fabrica tion, son tales que bajo luz UV, de intensidad y potencias ajustadas, se vuelven accesibles, o menos, al ataque por parte de disolventes. De esta manera, es posible transferir el patrón desde la mascara concretada a un substrato recubierto de la foto-resina ,y definir finalmente las estructuras curando el substrato expuesto, y eliminando, o depositando, en seguida las capas de materiales necesarias por obtener el grabado final.

En el caso tratado, ha sido utilizada por transferir sobre la oblea los patrones eléctricos representados con las correspondientes máscaras de campo oscuro, que se han considerado en la fase inicial Fig. 126, y luego, en la optimización de las caracterización de los nano-sensores Fig. 127.

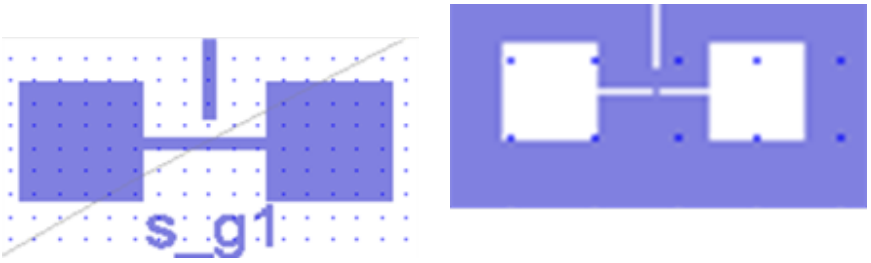

(a) Mascara de campo claro (b) Mascara de campo oscuro

Figure 126: Mascaras utilizadas por el primer patrón (mask1)

La definición requerida por el diseño es compatible con los limites de aplicación de la fotolitografía, impuestos por el fenómeno de difracción de la luz.

En acuerdo con la mascara de campo claro, se ha empleado una foto-resina de tipo negativo (AZ) que después la exposición permite disolver las partes non expuestas en un baño químico del reactivo correspondiente,

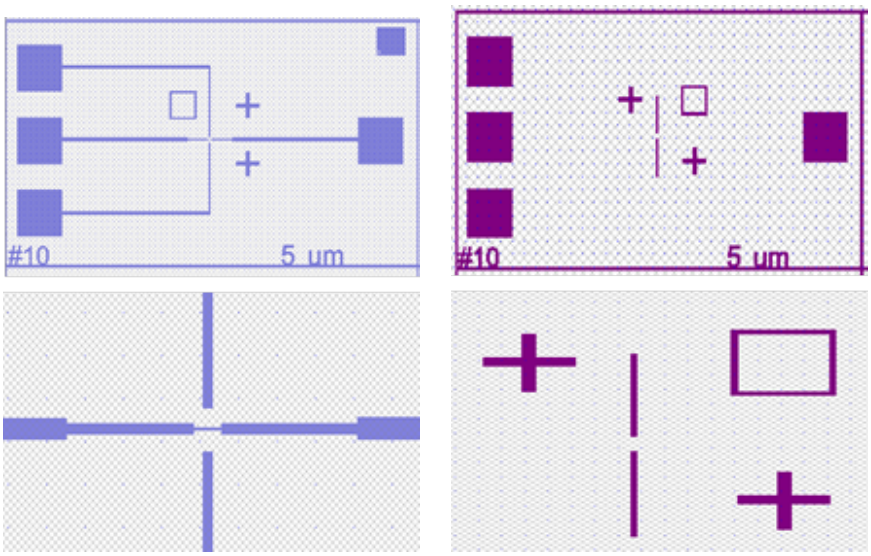

(a) Mascara de campo claro (b) Mascara de campo oscuro

Figure 127: Mascaras utilizadas por el patrón de optimización (mask2)

así de quedar accesibles a los siguientes procesos necesarios por definir el patrón de oro sobre el soporte de SOI.

Estos consisten en el ataque de los espesores nano-métricos de oro y titanio conseguidos aplicando respectivamente un baño químico ("wet etching") e un plasma de iones ("dry etching"/ "reactive ion etching (RIE)) y que permiten conseguir el grabado de oro según el patrón, como ilustrado en Fig. 128.

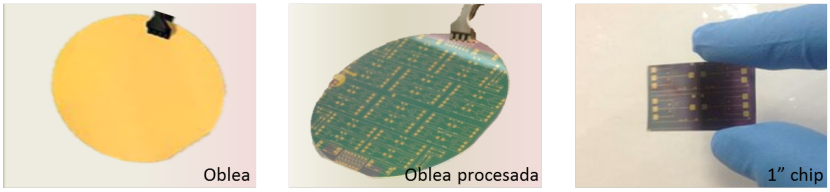

Figure 128: Una oblea antes y después la fabricación.

Sucesivamente, se han procesado las obleas con una segunda fotolitografía a través de las mascaras de campo oscuro. Esto permite asegurar protección de las áreas non expuestas durante la pasivación del patrón eléctrico, mediante cual conseguir la reducción de corrientes parásitas y

maximizar la señal procedente por el ADN hibridado al interior del nano-gap.

La pasivación ha sido obtenida depositando un espesor nano-métrico de SiO_2 mediante sputtering, la obertura final de los pads por las conexiones con los aparatos de medida, se consigue con un ataque químico de la resina (no expuesta) que disolvendose provoca la eliminación del oxido depositado encima . Los nano-gaps son finalmente abiertos con el tamaño establecido mediante FIB.

Durante las diferentes etapas de desarrollo del proceso los resultados se han caracterizados empleando métodos basados en detección óptica (Microscopio Optica, Interferometría, Elipsometría, TOF-SIMS), SEM, analysis eléctrica y electro-química, como presentado en los siguientes párrafos.

7.4.2 *Caracterización Optica*

Las diferentes técnicas de caracterización óptica utilizadas, Microscopia Optica, Interferometria y Ellipsometria son todas basadas en el utilizo de una sonda de luz, con parámetros adaptados según el tipo de analysis aplicado.

En microscopia óptica un haz colimado de luz visible, combinado con un sistema de lentes, permite detectar y magnificar la imagen resultante de la interacción sonda-muestra, por esta razón se considera este como un medio por potenciar las capacidades de la visión humana. E nuestro caso, el objetivo de la caracterización microscópica ha sido lo de controlar y evaluar el éxito de los procesos foto-litograficos en conseguir la transferencia de los patrones con las características preestablecidas.

Algunas de las imágenes obtenida se muestran e Fig.129.

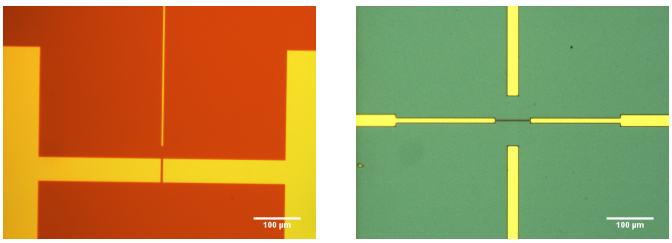

Figure 129: Puente en la configuración de dos (a) y tres electrodos (3).

Al contrario, las otras dos técnicas pese a que siempre se basan sobre una sonda de la misma naturaleza, proporcionan un tipo de caracterización diferente, y de hecho se aplican mas bien por obtener informaciones respeto a los materiales presentes en la superficie analizada.

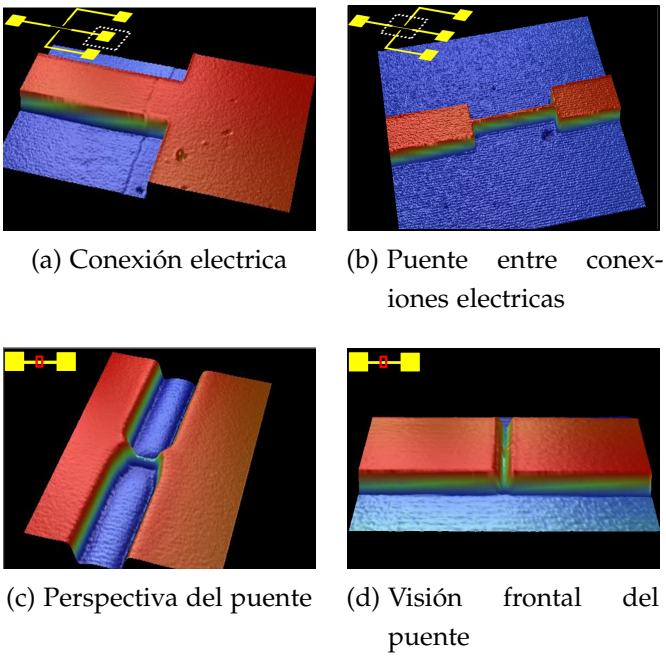

(a) Conexión electrica

(b) Puente entre conexiones electricas

(c) Perspectiva del puente

(d) Visión frontal del puente

Figure 130: Caracterización interferometrica.

En particular, la interferometria permite caracterizar la rugosidad de una superficie a través del análisis de la interferencia entre una señal de luz blanca usada como referencia, y la señal detectada luego que la sonda ha interactuado con la superficie examinada. Gracias al desarrollo de programas de reconstrucción de imágenes poderosos, los interferometros modernos ofrecen mucha sensibilidad y también la posibilidad de realizar reconstrucciones tridimensionales.

Este tipo de análisis ha sido utilizada por monitorear la calidad de la superficie durante el desarrollo del proceso de fabricación.

Algunos de los resultados conseguidos se enseñan en Fig. 130.

Los colores, indicando materiales diferentes, muestran en superficie una alta uniformidad del espesor de oro (en rojo) que recubre el patrón, además gracias a la perspectivas ofrecidas por la reconstrucción tridi-

mensional se puede también apreciar la alta definición de la geometría obtenida.

Respeto a las técnicas anteriores, la elipsometría se basa en el empleo de luz laser que ilumina puntualmente una zona de la superficie y permite, mediante el análisis del index de refracción, establecer los materiales y los espesores correspondientes que se encuentran en una muestra, con precisión de decenas de Å.

Sin embargo, hay que tener en cuenta que el análisis es limitado a la región iluminada por el spot del haz laser, en consecuencia no es una técnica adapta al estudio de grandes superficies.

En nuestro caso, la caracterización elipsometrica ha sido util en evaluar los resultados del proceso de sputtering. Comparando el index de refracción en una zona de la muestra pasivada con el espesor de SiO_2, y fuera, ha sido posible establecer el valor depositado igual a

Esta primera fase de caracterización del proceso de fabricación ha permitido controlar los diferentes estadios del desarrollo, y mediante el análisis de las propriedades ópticas del patrón de validar la eficacia de la rutina operada.

Después la abertura de los nano-gaps este tipo de caracterización es intrínsecamente limitada siendo el gap de medida inferior a la resolución posible con sistemas ópticos. Por esta razón, en la fase posterior a la abertura de los nano-gaps microscopia por escaneo de electrones (SEM) y análisis eléctrica/electro-química han sido aplicados por evaluar los resultados de la nano-litografía FIB, sea comprobando el tamaño de los gaps obtenidos a través procesamiento de las imágenes del SEM Fig. 131, que validando la funcionalidad de los sistemas por la aplicación diseñada, es decir la medida de conductividad muy baja mediante caracterización eléctricas y electro-químicas, como se detallará en el siguiente párrafo.

Con este mismo propósito también se ha considerado el utilizo de TOF-SIMS por investigar la contaminación del gap por implantación de iones de Galio del FIB u otros residuos de fabricación. Por esta análisis, basada como las anteriores en detección óptica, fue necesario fabricar gaps de tamaño mayor, en los cuales se ha detectado presencia de tales iones, pero en concentraciones no suficientes a dopar la superficie de SiO_2 y alterar sus propriedades de conducción. Además, cabe tener en cuenta que por

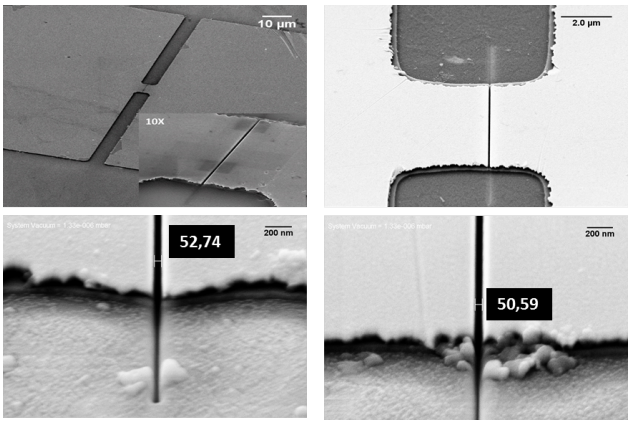

Figure 131: Imágenes SEM de algunos nano-gaps fabricados.

fabricar gaps de abertura mas grande, el haz de iones se aplica con intensidades mayores y durante tiempos mas largos, que pueden favorecer la contaminación.

7.4.3 *Caracterización eléctrica*

Caracterizar la respuesta eléctrica de los nano-gaps es el método principal sobre el cual se basa la demostración del sistema propuesto. Por esta razón medidas de la características corriente-tensión (I-V) de los nano-gaps se han conducido sistemáticamente durante las diferentes fases de producción, y sucesivamente a lo largo de inmovilización de las sondas de ADN y finalmente por detectar la hibridación del target. Las medidas se pueden finalizar fácilmente mediante el uso de una mesa de puntas y gracias a la sensibilidad del equipo utilizado en el orden de femto-ampere.

Un esquema del sistema experimental es representado en la Fig.132. Un

Figure 132: Imágenes SEM de algunos nano-gaps fabricados.

test preliminar de conductividad del patrón se ha conducido antes del abertura de los nano-gaps, útil a establecer la integridad de los circuitos eléctricos, los resultados se muestran juntos a los otros obtenidos después abertura de los nano-gaps en Fig. 133.

El comportamiento linear observado confirma la funcionalidad eléctrica del circuito. El valor de la resistencia calculado fiteando los datos mediante la ley de Ohm provee un valor de 30 Ω en acuerdo con el valor rápidamente testado por uso de un normal multimetro.

La respuesta obtenida en los sistemas con el gap abierto es prácticamente menospreciable en las dos condiciones consideradas, es decir en aire y en agua DDI. En este ultimo caso, un fondo de un order de magnitud mas alto caracteriza la respuesta de los sistemas. Por ultimo, se

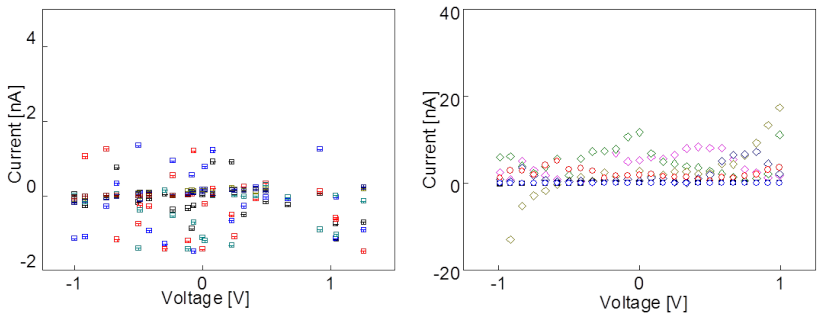

Figure 133: Características I-V en aire (izquierda) y en agua DDI (derecha)

ha considerado el efecto sobre la conductividad debido al tratamiento de limpieza a través del exposición a UV-Ozone, usualmente aplicado en micro y nano-electronica, y que ha sido indicado como posible fuente de conductividad, debida al incremento de la hidro-filicidad de la superficie después la exposición a la radiación [125].

La misma medida, repetida a distancia de solo una hora, muestra el consistente recupero de la respuesta inicial con un fondo prácticamente menospreciable detectado en el cabo de 4 horas luego el UV-Ozone. Esta observación se ha tenido en cuenta operando la caracterización eléctrica a distancia de tiempo suficiente desde el tratamiento.

7.4.3.1 *Caracterización electro-química*

Este tipo de caracterización ha sido considerada con el objetivo de superar las limitaciones de los sistemas de basados en medidas ópticas de las propriedades superficiales, y validar una rutina alternativa por estudiar la funcionalización de los electrodos con las sondas de ADN en sistemas de nano-gaps.

La voltamperometría cíclica, que mide la corriente al electrodo de trabajo bajo la aplicación de un potencial cíclico en una celda de tres electrodos, ha sido largamente utilizada en la caracterización de las superficies de micro-electrodos y de su funcionalización con bio-moleculas.

La presencia de moléculas inmovilizadas sobre una superficie altera la dinámica de la reacción de transferencia de electrones al electrodo de trabajo. De esta manera, operando los micro-electrodos por analizar como electrodos de trabajo, en una apropiada celda electro-química, se puede caracterizar la superficie.

En el caso de nano-sistemas, y especialmente en los de nano-gaps, la voltamperometría está siendo solo recientemente considerada gracias al creciente interés por el utilizo de este tipo de sistema en la detección de bio-moleculas [70], [52].

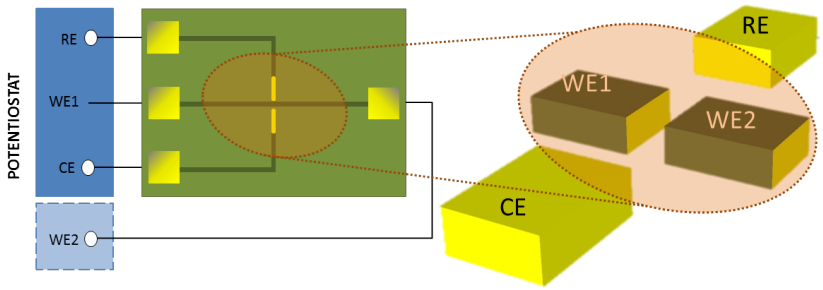

Figure 134: Esquema de la celda electro-química con las conexiones al potentiostato.

Sin embargo, el utilizo de esta metodología por caracterizar la superficie de electrodos en un nano-gap no ha sido todavía discutido. Para finalizar esta tarea se ha adaptado el patrón eléctrico de los nano-gaps proporcionando dos electrodos auxiliares en su proximidad de manera

que la celda electro-química de Fig. 134 es facilmente obtenida depositando un microvolumen del electro-litro usado.

Las conexiones con el potentiostato, a través los micro-posicionadores de la mesa de puntas, se han operado manteniendo inalterada la posición de los electrodos de referencia y auxiliar, y intercambiando la conexión del electrodo de trabajo en función del electrodo WE1, o WE2 que se quiere caracterizar.

Un ejemplo de los resultados obtenidos, donde se representa el voltagrama medido a uno y otro electrodos de trabajo, según ahora explicado, es en Fig. 135. La similaridad de la respuesta confirma la reproducibilidad entre las dos superficie de los electrodos.

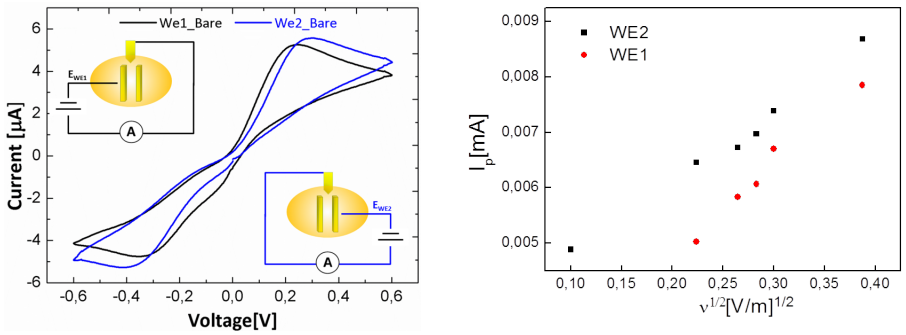

(a) Resultados CV (b) Randles-Sevcick plot

Figure 135: CV medidos a los WEs a 50 mV/s, y ejemplo de linearización de datos aplicando el modelo de Randles-Sevick

Midiendo los voltagramas a valores crecientes de scan-rate del potencial cíclico, es posible calcular aplicando el modelo de Randles-Sevcick el valor del area efectiva del electrodo de trabajo.

El modelo se aplica en el caso de un proceso dominado por la difusión de la solución de análisis hacía el electrodo de trabajo.

La validez de esta hypotesis se contrasta averiguando la linearidad del pico de la corriente catódica en función de la raíz cuadrada del scan-rate, como se puede apreciar en la Fig.135 que representa uno de los resultados obtenidos conduciendo esta análisis. Empleando el modelo de Randles-Sevcick por fitear los datos, ha sido posible estimar el valor del area activa,

y utilizando el valor del area geométrica, obtener el valor del coeficiente de rugosidad de los electrodos de los nano-gaps $\rho = 102.6 \pm 47.9$.

La mayor area resultante puede ser debida al hecho que las superficies resultantes de la fabricación no sean perfectamente planas, si no que proporcionan una rugosidad mayor dando lugar a una area efectiva mas grande que la geométrica.

7.5 FUNCIONALIZACIÓN SELECTIVAS DE LOS ELECTRODOS

La funcionalización de superficies mediante bio-moleculas que permiten así complementar las propriedades del substrato con aquella de una interficie orgánica, es un aspecto de primaria importancia en el desarrollo de bio-sensores. La calidad y las características de los bio-receptores inmovilizados sobre el substrato de análisis, contribuye incrementado la respuesta y la especificidad del sistema global di detección. En general, es un tema de interés también por otros campos de aplicaciones, como en Ingeniería Celular, donde obtener superficies bio-mimeticas es uno de los primeros pasos que se pone por el siguiente desarrollo.

El fenómeno de absorción espontánea de moléculas orgánicas a la superficie de los metales, ha sido a la base del siguiente desarrollo de métodos de funcionalización de superficies a través del auto-asemblaje de mono-capas de moléculas, noto como SAM. Este proceso ha sido particularmente estudiado en el caso de la absorción de tioles sobre oro realizada por la afinidad entre el oro y los sulfures de los tioles [126]. Los tioles sobre oro dan origen a una momo-capa altamente ordenada con una ligera inclinación de las moléculas respeto al eje perpendicular, debida al interbalance electrostático de las cargas entre las moléculas y con la superficie. El ordenamiento de la mono-capa y su regularidad respeto a defectos aumentan con el tiempo de incubación, sin embargo poco minutos resultan ya suficientes en adsorbir las moléculas a la superficie y normalmente 12 h de incubación son consideradas suficientes por conseguir una mono-capa ordenada.

De esta manera, el método de SAM provee un mecanismo muy simple por expresar las propriedades de los tioles sobre una superficie como el oro, especialmente adapta por aplicación electrónicas. De hecho ha sido

largamente aplicado en la funcionalización de electrodos como alternativa mas eficiente al tradicional método basado en Langmuir-Blodgett.

Sin embargo, sea el SAM por incubación que las mono-capas depositadas por Langmuir-Blodgett, son de difícil adaptación a la modificación selectiva de areas delimitadas del substrato de análisis.

En el caso de micro-electrodos y nano-electrodos con superficies planas, métodos como el micro-contact printing (μP) [95] y la nano-litografía "dip-pen" [85] pueden ser implementados por conseguir la modificación selectiva de la superficie. Su aplicación es, al contrario, evidentemente limitada al considerar un sistema de nano-electrodos en la configuración utilizada en el caso tratado. Por esta razón, se han desarrollado y testado diferentes estrategias de inmovilización de las sondas de ADN por conseguir la funcionalización selectiva de cada electrodo en el nano-gap.

Los métodos empleados y los resultados obtenidos se comentan en seguida.

- Adsorción por incubación en una solución de una mixtura de los dos CPs.

- Inmovilización selectiva mediante electro-chemical stripping obtenida mediante incubación del sistema con una solución de una sola sonda, seguida por strip electro-químico operado mediante aplicación de un potencial a uno de los electrodos por conseguir la reducción del ligazón entre oro-tioles y incubación del sistema con una solución de la otra sonda.

- Inmovilización selectiva mediante aplicación de un campo eléctrico, conseguida mediante aplicación de un pulso con polaridad positiva sobre uno de los electrodos por atraer electroforeticamente las sondas de un tipo contenida en la solución de trabajo, seguida por la aplicación de un segundo pulso con polaridad opuesta respeto al anterior por promover la absorción de las sondas en la solución de trabajo hacia este electrodo.

Los resultados obtenidos según los diferentes métodos se han evaluado estudiando el recubrimiento de la superficie de oro de los electrodos a través voltamperometría cíclica, como explicado en el párrafo anterior, y

comparando los valores relevados después la incubación de los nano-gaps con aquellos de los nano-gaps limpios.

Una primera consideración que se pudo establecer, a través de esta análisis, es que la absorción de moléculas a la superficie del electrodo altera su respuesta voltamperometrica, resultando en una reducción de los picos de corriente y de la transferencia de electrones, como se deduce de la reducción total del area de la curva, que se observa en los CVs de la Fig. 136. Esta compara los CV medidos en un nano-gap, a uno y otro

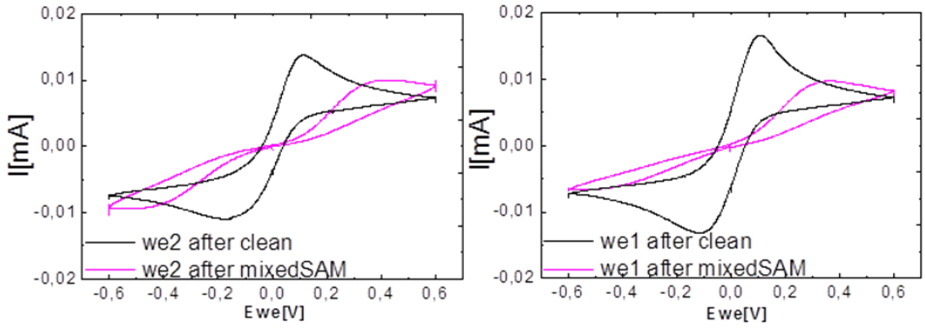

Figure 136: CV medidos a los electrodo de los nano-gaps después incubación de las sondas de ADN.

electrodo de trabajo, después incubación de la mono-capa mixta de sondas (mixed SAM). Resultados cuantitativos se han obtenido calculando el decremento relativo del pico catódico de la corriente después las inmovilización de las sondas, representados en la Fig. 137, juntos con aquellos medidos a distancia de dos días de la primera caracterización, por valorar la estabilidad de las mono-capas. Luego, se han evaluados los efectos de los métodos de inmovilización selectiva mediante la medida de los CV a los electrodos de trabajo después cada fase de los protocolos de inmovilización. A través de esta sistemática caracterización ha sido posible estudiar los efectos producidos sobre el electrodo opuesto a lo utilizado como electrodo de trabajo, durante los experimentos.

Desde el análisis de los datos, se ha llegado a la conclusión general que el tamaño nano-métrico del gap amplifica los efectos debidos al aplicación de los voltages experimentales produciendo efectos en la absorción/desorción de moléculas inmovilizadas sobre la superficie del electrodo. Este efecto es particularmente relevante cuando se considera la

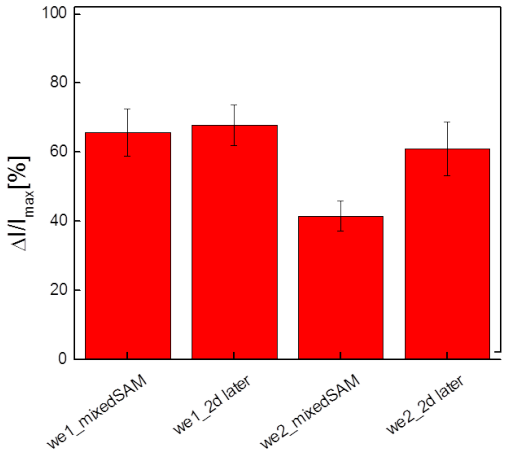

Figure 137: Decremento relativo de la corriente en los electrodos de trabajos después inmovilización de sondas mixta (mixed SAM)

aplicación de un potencial electro-químico por conseguir la desorción selectiva de moléculas desde un electrodo.

Comparativamente mejor resultados se obtienen, al contrario, conside rando la inmovilización selectiva por aplicación de un potencial electro-foreticos oportunamente polarizado a la superficie del electrodo, entre este ultimo y uno de los electrodos auxiliares, por atraer las moléculas cargadas negativamente. Pese a este, una reducción de la corriente medida en el electrodo opuesto a lo utilizado por la electro-foresis persiste, por lo cual el método mas eficaz ha sido luego obtenido a través de la inmovilización por electro-foresis de un tipo de sonda sobre un electrodo, seguida por la incubación de todo el sistema con la solución de la otra sonda.

Este ultimo método, junto con la absorción no selectiva por incubación, se ha aplicado por funcionalizar los electrodos de los nano-gaps empleados en los experimentos de detección de hibridación y SNP.

7.6 DETECCIÓN DE HIBRIDACIÓN DE ADN Y SNP

El principio de trabajo del nano-sensor propuesto, es decir el transporte de carga a través del puente de ADN formado después la hibridación del ADN target con las sondas previamente inmovilizadas a loes electrodos

de los nano-gaps, ha sido testado en una serie de experimentos, basados principalmente en la medida de las características tensión-corriente de los nano-gaps.

La respuesta de los nano-gaps después 1h de incubación con el ADN target ha sido comparada con aquella medida en ausencia del puente hibridado. Un primer test ha permitido caracterizar cual sistema de inmovilización de las sondas, entre los dos probados, favorecía la detección del ADN.

Los resultados obtenidos son representado en Fig. 138 en la cual se enseña el incremento relativo de corriente, después hibridación complementaria en los sistemas inmovilizados por incubación, y por adsorción selectiva.

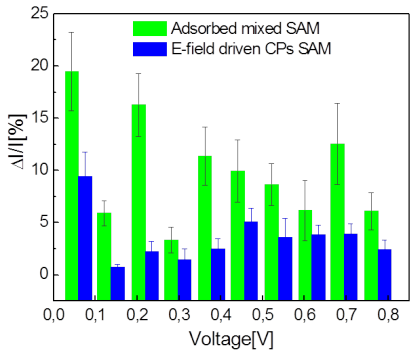

Figure 138: Incremento relativo de corriente registrado después hibridación complementaria en nano-gaps con inmovilización selectiva y non.

Como se puede observar en la gráfica, el incremento de corriente siguiente la hibridación de ADN es mayor en los nano-gaps modificados por una SAM mixta de las sondas, a través del proceso no selectivo de absorción por incubación, respeto a lo que se obtiene en los sistemas con inmovilización selectiva de las sondas.

Se ha postulado que esto ocurre debido al hecho que el sistema no selectivo proporciona una mono-capa mas ordenada y compacta que favorece la hibridación del ADN en el nano-gap, pese a que no sea selectivamente optimizada. Esta hypotesis ha sido valorada por la posterior análisis de los nano-gap hibridados mediante SEM. En la imagen obtenida en un nano-gap antes y después hibridación, que se enseña en la Fig. 139, se

pueden apreciar aglomerados de ADN que conectan los electrodos con caminos de hibridación ínter-cruzados.

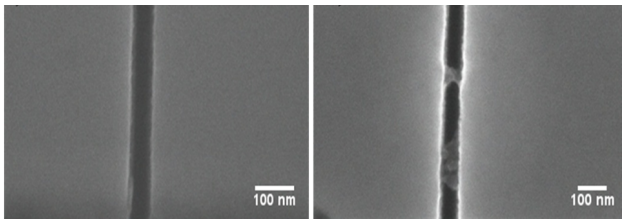

Figure 139: Imágenes SEM de un nano-gap antes y después hibridación.

En acuerdo con cuanto establecido en esta primera análisis, los ulteriores experimentos de validación del nano-sensor se han llevado a cabo utilizando los nano-gaps con inmovilización no selectiva de las sondas.

Por comprobar le especificidad del principio de trabajo del nano-sensor se han comparado las señales medidas después hibridación en nano-gaps con sondas complementarias, y mutadas.

En Fig. 140 se representan los resultados de las medidas obtenidas a condiciones ambientales, la respuesta medida en agua DDI se representa a través del incremento relativo de corriente después hibridación a un voltaje fijo. En ambos casos la señal indicada como "baseline" es la diferencia entre la corriente medida después inmovilización de las sondas, menos el fondo medido en los nano-gaps limpios.

El mismo tipo de normalización se ha adoptado también por los otros señales, es decir la corriente medida después hibridación complementaria y en presencia de SNP. El consistente incremento de la corriente de los nano-gap sigue la hibridación complementaría, sin embargo debido a un fondo mayor de las medidas en agua DDI, se consigue una detección mas eficaz a condiciones ambientales.

En el caso de hibridación con sondas mutadas el incremento es marcadamente inferior, en acuerdo con la hypothesis de sensibilidad del transporte de carga en presencia de mutaciones, que permite testar la selectividad del nano-sensor, y al mismo tiempo comprobar que es el ADN que media el transporte de carga en el nano-gap.

El principio de trabajo ha sido ulteriormente validado en los estudios siguientes, mirados a optimizar la plataforma de detección, y en los cuales

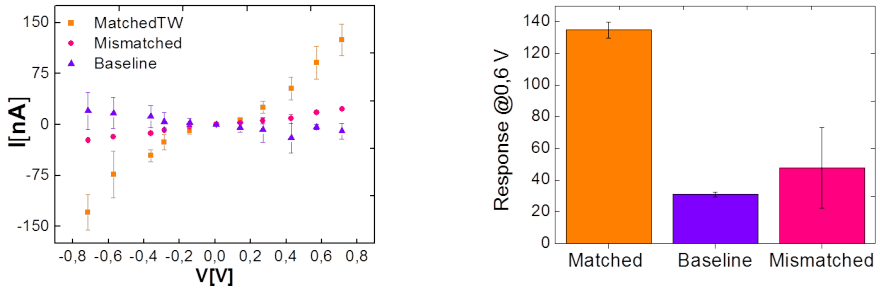

(a) [Detección de hibridación (b) Detección de hibridación, agua DDI

Figure 140: Características eléctricas de los nano-gaps después hibridación con ADN complementario, y en presencia de SNP.

se han considerados la sensibilidad a diferentes concentraciones del target, y la regeneración del nano-sensor después ciclos de desnaturalización/re-hibridación del ADN hibridado. Los resultados siguen en Fig. 141.

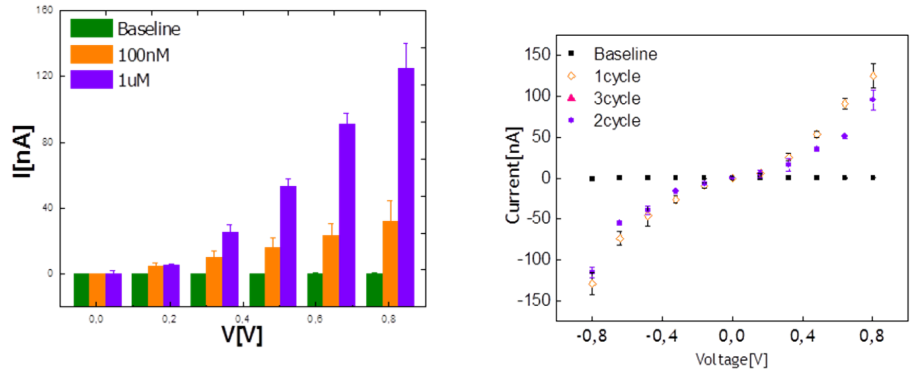

(a) Respuesta a diferentes concentraciones de ADN (b) Regeneración del nano-sensor después desnaturalización

Figure 141: Resultados de los ensayos de sensibilidad a concentraciones diferentes y regeneración del dispositivo.

Desde el análisis de las características I-V de los nano-gaps en los dos casos analizados se concluye que, el nano-sensor desarrollado es sensible a concentraciones diferentes de target, todavía un estudio mas profundo es necesario por obtener una curva de calibración del sistema y consecuentemente el limite de detección. Mientras que los resultados de las

pruebas de regeneración del sensor se ve que es posible volver al estado inicial de respuesta del sensor luego tres ciclos de aplicación de la rutina desnaturalización/ hibridación.

El conjunto de los resultados obtenidos demuestra la factibilidad de este sistema de detección de hibridación de ADN basado en las propriedades eléctricas del ADN. Las diferentes caracterización operadas han permitido de probar: la selectividad del principio de funcionamiento respeto a la presencias de SNP, como esperado desde el análisis de las propriedades eléctricas del A, que el transporte de cargas se realiza a través la molécula, como demuestran sea la sensibilidad a diferentes concentraciones de target que la regeneración del dispositivo después desnaturalización.

BIBLIOGRAPHY

[1] Hylke B Akkerman, Ronald C G Naber, Bert Jongbloed, Paul a van Hal, Paul W M Blom, Dago M de Leeuw, and Bert de Boer. Electron tunneling through alkanedithiol self-assembled monolayers in large-area molecular junctions. *Proceedings of the National Academy of Sciences of the United States of America*, 104(27):11161–6, July 2007. ISSN 0027-8424. doi: 10.1073/pnas.0701472104. URL http://www.pubmedcentral.nih.gov/articlerender.fcgi?artid=1899190&tool=pmcentrez&rendertype=abstract.

[2] N P Armitage, M Briman, and G Gr. Charge Transfer and Charge Transport on the Double Helix. *arXiv:cond-mat/0309360v1*, 2003. URL http://arxiv.org/pdf/cond-mat/0309360.pdf.

[3] McCarty M. Averin OT, MacLeod CM. Studies on the chemical nature of the substance inducing trans- formation of pneumococcal types. *J Exp Med*, 7:137–160, 1944.

[4] Shankar Balasubramanian, Alexander Revzin, and Aleksandr Simonian. Electrochemical Desorption of Proteins from Gold Electrode Surface. *Electroanalysis*, 18(19-20):1885–1892, October 2006. ISSN 10400397. doi: 10.1002/elan.200603627. URL http://doi.wiley.com/10.1002/elan.200603627.

[5] A. J. Bard and L. R. Faulkner. *Electrochemical Methods: Fundamentals and Applications.*, volume 2nd edition of *ISBN 978-0-471-04372-*. Wiley, 2001.

[6] Jacqueline K Barton, Eric D Olmon, and Pamela a Sontz. Metal Complexes for DNA-Mediated Charge Transport. *Coordination chemistry reviews*, 255(7-8):619–634, April 2011. ISSN 0010-8545. doi: 10.1016/j.ccr.2010.09.002. URL http://www.pubmedcentral.nih.gov/articlerender.fcgi?artid=3105778&tool=pmcentrez&rendertype=abstract.

[7] Jeremy Beebe, BongSoo Kim, J. Gadzuk, C. Daniel Frisbie, and James Kushmerick. Transition from Direct Tunneling to Field Emission in Metal-Molecule-Metal Junctions. *Physical Review Letters*, 97 (2):026801, July 2006. ISSN 0031-9007. doi: 10.1103/PhysRevLett.97.026801. URL http://link.aps.org/doi/10.1103/PhysRevLett.97.026801.

[8] Julia Berashevich and Tapash Chakraborty. How the surrounding water changes the electronic and magnetic properties of DNA. *The journal of physical chemistry. B*, 112(44):14083–9, November 2008. ISSN 1520-6106. doi: 10.1021/jp806143x. URL http://www.ncbi.nlm.nih.gov/pubmed/18844404.

[9] Sudeep Bhattacharjee, Manoj K. Harbola, Avradip Pradhan, and Atanu Modak. Coexistence of tunneling and displacement currents in a nanogap driven with ac fields. *Applied Physics Letters*, 100(15): 153104, 2012. ISSN 00036951. doi: 10.1063/1.3702454. URL http://link.aip.org/link/APPLAB/v100/i15/p153104/s1&Agg=doi.

[10] Abhijit Biswas, Ilker S. Bayer, Alexandru S. Biris, Tao Wang, Enkeleda Dervishi, and Franz Faupel. Advances in top–down and bottom–up surface nanofabrication: Techniques, applications amp; future prospects. *Advances in Colloid and Interface Science*, 170(1–2):2 – 27, 2012. ISSN 0001-8686. doi: http://dx.doi.org/10.1016/j.cis.2011.11.001. URL http://www.sciencedirect.com/science/article/pii/S0001868611001904.

[11] M. Bixon and Joshua Jortner. Energetic Control and Kinetics of Hole Migration in DNA. *The Journal of Physical Chemistry B*, 104(16):3906–3913, April 2000. ISSN 1520-6106. doi: 10.1021/jp9936493. URL http://pubs.acs.org/doi/abs/10.1021/jp9936493.

[12] M Bixon, B Giese, S Wessely, T Langenbacher, M E Michel-Beyerle, and J Jortner. Long-range charge hopping in DNA. *Proceedings of the National Academy of Sciences of the United States of America*, 96(21): 11713–6, October 1999. ISSN 0027-8424. URL http://www.ncbi.nlm.nih.gov/pubmed/20203015.

[13] M Bixon, Joshua Jortner, and Tel Aviv. Electronic Coupling for Charge Transfer and Transport in DNA. (C):9740–9745, 2000.

[14] Elizabeth M Boon, Alison L Livingston, Nikolas H Chmiel, Sheila S David, and Jacqueline K Barton. DNA-mediated charge transport for DNA repair. *Proceedings of the National Academy of Sciences of the United States of America*, 100(22):12543–7, October 2003. ISSN 0027-8424. doi: 10.1073/pnas.2035257100. URL http://www.pubmedcentral.nih.gov/articlerender.fcgi?artid=240652&tool=pmcentrez&rendertype=abstract.

[15] E Braun, Y Eichen, U Sivan, and G Ben-Yoseph. DNA-templated assembly and electrode attachment of a conducting silver wire. *Nature*, 391(6669):775–8, February 1998. ISSN 0028-0836. doi: 10.1038/35826. URL http://www.ncbi.nlm.nih.gov/pubmed/9486645.

[16] M Briman, N P Armitage, E Helgren, and G Gru. Dipole Relaxation Losses in DNA. pages 1–4, 2004.

[17] Lintao Cai, Hitoshi Tabata, and Tomoji Kawai. Self-assembled DNA networks and their electrical conductivity. *Applied Physics Letters*, 77(19):3105, 2000. ISSN 00036951. doi: 10.1063/1.1323546. URL http://link.aip.org/link/APPLAB/v77/i19/p3105/s1&Agg=doi.

[18] Christie a Canaria, Jonathan So, James R Maloney, C J Yu, Jeffrey O Smith, Michael L Roukes, Scott E Fraser, and Rusty Lansford. Formation and removal of alkylthiolate self-assembled monolayers on gold in aqueous solutions. *Lab on a chip*, 6(2):289–95, February 2006. ISSN 1473-0197. doi: 10.1039/b510661c. URL http://www.ncbi.nlm.nih.gov/pubmed/16450040.

[19] M T Castañeda, a Merkoçi, M Pumera, and S Alegret. Electrochemical genosensors for biomedical applications based on gold nanoparticles. *Biosensors & bioelectronics*, 22(9-10):1961–7, April 2007. ISSN 0956-5663. doi: 10.1016/j.bios.2006.08.031. URL http://www.ncbi.nlm.nih.gov/pubmed/17010599.

[20] Nirmalya K Chaki and K Vijayamohanan. Self-assembled monolayers as a tunable platform for biosensor applications. *Biosensors*

& bioelectronics, 17(1-2):1–12, January 2002. ISSN 0956-5663. URL http://www.ncbi.nlm.nih.gov/pubmed/11742729.

[21] Zhihong Chen, Joerg Appenzeller, Joachim Knoch, Yu-ming Lin, and Phaedon Avouris. The role of metal-nanotube contact in the performance of carbon nanotube field-effect transistors. *Nano letters*, 5(7):1497–502, July 2005. ISSN 1530-6984. URL http://www.ncbi.nlm.nih.gov/pubmed/16178264.

[22] Seong Ho Choi, Chad Risko, M Carmen Ruiz Delgado, Bongsoo Kim, Jean-Luc Brédas, and C Daniel Frisbie. Transition from tunneling to hopping transport in long, conjugated oligo-imine wires connected to metals. *Journal of the American Chemical Society*, 132(12): 4358–68, March 2010. ISSN 1520-5126. doi: 10.1021/ja910547c. URL http://www.ncbi.nlm.nih.gov/pubmed/20218660.

[23] G Cuniberti and A Rodriguez. Tight-binding modeling of charge migration in. pages 1–21.

[24] Ralf Dahm. Friedrich miescher and the discovery of {DNA}. *Developmental Biology*, 278(2):274 – 288, 2005. ISSN 0012-1606. doi: http://dx.doi.org/10.1016/j.ydbio.2004.11.028. URL http://www.sciencedirect.com/science/article/pii/S0012160604008231.

[25] P. de Pablo, F. Moreno-Herrero, J. Colchero, J. Gómez Herrero, P. Herrero, a. Baró, Pablo Ordejón, José Soler, and Emilio Artacho. Absence of dc-Conductivity in λ-DNA. *Physical Review Letters*, 85(23):4992–4995, December 2000. ISSN 0031-9007. doi: 10.1103/PhysRevLett.85.4992. URL http://link.aps.org/doi/10.1103/PhysRevLett.85.4992.

[26] Jafar Ezzati Nazhad Dolatabadi, Omid Mashinchian, Baharak Ayoubi, Ali Akbar Jamali, Ahmad Mobed, Dusan Losic, Yadollah Omidi, and Miguel de la Guardia. Optical and electrochemical DNA nanobiosensors. *TrAC Trends in Analytical Chemistry*, 30 (3):459–472, March 2011. ISSN 01659936. doi: 10.1016/j.trac.2010.11.010. URL http://linkinghub.elsevier.com/retrieve/pii/S0165993611000033.

[27] Narváez A. Domínguez E1, Rincón O. Electrochemical dna sensors based on enzyme dendritic architectures: an approach for enhanced sensitivity. *Analytical chemistry*, 76(11):3132–8., 2004.

[28] T Gregory Drummond, Michael G Hill, and Jacqueline K Barton. Electrochemical DNA sensors. *Nature biotechnology*, 21(10):1192–9, October 2003. ISSN 1087-0156. doi: 10.1038/nbt873. URL http://www.ncbi.nlm.nih.gov/pubmed/14520405.

[29] Lev Dykman and Nikolai Khlebtsov. Gold nanoparticles in biomedical applications: recent advances and perspectives. *Chem. Soc. Rev.*, 41:2256–2282, 2012. doi: 10.1039/C1CS15166E. URL http://dx.doi.org/10.1039/C1CS15166E.

[30] Rrp Singh Endres, R G DL Cox and R G Endres. Colloquium : The quest for high-conductance DNA. *Review of Modern Physics*, 76 (January), 2004.

[31] a N Enyashin, S Gemming, and G Seifert. DNA-wrapped carbon nanotubes. *Nanotechnology*, 18(24):245702, June 2007. ISSN 0957-4484. doi: 10.1088/0957-4484/18/24/245702. URL http://stacks.iop.org/0957-4484/18/i=24/a=245702?key=crossref.3bac6f351dab8306daad37ff1527d594.

[32] Walt Epstein, Biran. Fluorescent based nucleic acid detction and microarray. *Analytical Chemical Acta*, 469:3–36, 2002.

[33] Chunhai Fan, Kevin W Plaxco, and Alan J Heeger. Electrochemical interrogation of conformational changes as a reagentless method for the sequence-specific detection of DNA. *Proceedings of the National Academy of Sciences of the United States of America*, 100(16):9134–7, August 2003. ISSN 0027-8424. doi: 10.1073/pnas.1633515100. URL http://www.pubmedcentral.nih.gov/articlerender.fcgi?artid=170884&tool=pmcentrez&rendertype=abstract.

[34] H W Fink and C Schönenberger. Electrical conduction through DNA molecules. *Nature*, 398(6726):407–10, April 1999. ISSN 0028-0836. doi: 10.1038/18855. URL http://www.ncbi.nlm.nih.gov/pubmed/10201370.

[35] Zhiqiang Gao, Ajay Agarwal, Alastair D Trigg, Navab Singh, Cheng Fang, Chih-Hang Tung, Yi Fan, Kavitha D Buddharaju, and Jinming Kong. Silicon nanowire arrays for label-free detection of DNA. *Analytical chemistry*, 79(9):3291–7, May 2007. ISSN 0003-2700. doi: 10.1021/ac061808q. URL http://www.ncbi.nlm.nih.gov/pubmed/20563793.

[36] Joseph C Genereux, Amie K Boal, and Jacqueline K Barton. DNA-mediated charge transport in redox sensing and signaling. *Journal of the American Chemical Society*, 132(3):891–905, January 2010. ISSN 1520-5126. doi: 10.1021/ja907669c. URL http://www.pubmedcentral.nih.gov/articlerender.fcgi?artid=2902267&tool=pmcentrez&rendertype=abstract.

[37] Andrey L Ghindilis, Maria W Smith, Kevin R Schwarzkopf, Kristian M Roth, Kia Peyvan, Sandra B Munro, Michael J Lodes, Axel G Stöver, Karen Bernards, Kilian Dill, and Andy McShea. CombiMatrix oligonucleotide arrays: genotyping and gene expression assays employing electrochemical detection. *Biosensors & bioelectronics*, 22 (9-10):1853–60, April 2007. ISSN 0956-5663. doi: 10.1016/j.bios.2006.06.024. URL http://www.ncbi.nlm.nih.gov/pubmed/16891109.

[38] Bansal M Ghosh A. A glossary of dna structures from a to z. *Acta Cryst D*, 59:620–626, 2003.

[39] B. Nagel / H. Dellweg / L. M. Gierasch H. Dellweg / L. M. Gierasch. Glossary for chemists of terms used in biotechnology (iupac recommendations 1992). *Pure and Applied Chemistry*, 64(1):143–168, 2009.

[40] B Giese, J Amaudrut, a K Köhler, M Spormann, and S Wessely. Direct observation of hole transfer through DNA by hopping between adenine bases and by tunnelling. *Nature*, 412(6844):318–20, July 2001. ISSN 0028-0836. doi: 10.1038/35085542. URL http://www.ncbi.nlm.nih.gov/pubmed/11460159.

[41] Harry B Gray and Jack Halpern. Distant charge transport. *Proceedings of the National Academy of Sciences of the United States of America*, 102(10):3533, March 2005.

ISSN 0027-8424. doi: 10.1073/pnas.0501035102. URL http://www.pubmedcentral.nih.gov/articlerender.fcgi?artid=553342&tool=pmcentrez&rendertype=abstract.

[42] Xuefeng Guo, Alon a Gorodetsky, James Hone, Jacqueline K Barton, and Colin Nuckolls. Conductivity of a single DNA duplex bridging a carbon nanotube gap. *Nature nanotechnology*, 3 (3):163–7, March 2008. ISSN 1748-3395. doi: 10.1038/nnano.2008.4. URL http://www.pubmedcentral.nih.gov/articlerender.fcgi?artid=2747584&tool=pmcentrez&rendertype=abstract.

[43] Jong-in Hahm and Charles M. Lieber. Direct Ultrasensitive Electrical Detection of DNA and DNA Sequence Variations Using Nanowire Nanosensors. *Nano Letters*, 4(1):51–54, January 2004. ISSN 1530-6984. doi: 10.1021/nl034853b. URL http://pubs.acs.org/doi/abs/10.1021/nl034853b.

[44] Martel R Derycke V Appenzeller J Avouris Ph. Heinze S, Tersoff J. Carbon nanotubes as schottky barrier transistors. *Phys Rev Lett*, 89: 106801–106804, 2002.

[45] Michael J Heller. DNA microarray technology: devices, systems, and applications. *Annual review of biomedical engineering*, 4:129–53, January 2002. ISSN 1523-9829. doi: 10.1146/annurev.bioeng.4.020702.153438. URL http://www.ncbi.nlm.nih.gov/pubmed/12117754.

[46] Michael J Heller and Anita H Forster. Active microelectronic chip devices which utilize controlled electrophoretic fields for multiplex DNA hybridization and other genomic applications Nucleic acids. pages 157–164, 2000.

[47] P T Henderson, D Jones, G Hampikian, Y Kan, and G B Schuster. Long-distance charge transport in duplex DNA: the phonon-assisted polaron-like hopping mechanism. *Proceedings of the National Academy of Sciences of the United States of America*, 96(15):8353–8, July 1999. ISSN 0027-

8424. URL http://www.pubmedcentral.nih.gov/articlerender.fcgi?artid=17521&tool=pmcentrez&rendertype=abstract.

[48] R Hintsche, B Elsholz, G Piechotta, R Woerl, C G J Schabmueller, J Albers, V Dharuman, E Nebling, C Paulus, M Schienle, and R Thewes. Fully Electrical Microarrays. 1(05), 2005. doi: 10.1016/S1871-0069(05)01006-2.

[49] K W Hipps. Molecular electronics. It's all about contacts. *Science (New York, N.Y.)*, 294(5542):536–7, October 2001. ISSN 0036-8075. doi: 10.1126/science.1065708. URL http://www.ncbi.nlm.nih.gov/pubmed/11641487.

[50] Sun-Yong HWANG. Conductivity of DNA with a Single Base Pair Mismatch. *Journal of the Korean Physical Society*, 58(6):1682–1687, 2011.

[51] Watson J.D. and Crick F.H.C. A structure for deoxyribose nucleic acid. *Nature*, 171:737–738, 1953.

[52] Shuo Kang, Ab F. Nieuwenhuis, Klaus Mathwig, Dileep Mampallil, and Serge G. Lemay. Electrochemical single-molecule detection in aqueous solution using self-aligned nanogap transducers. *ACS Nano*, 7(12):10931–10937, 2013. doi: 10.1021/nn404440v. URL http://dx.doi.org/10.1021/nn404440v. PMID: 24279688.

[53] a Y Kasumov, M Kociak, S Guéron, B Reulet, V T Volkov, D V Klinov, and H Bouchiat. Proximity-induced superconductivity in DNA. *Science (New York, N.Y.)*, 291(5502):280–2, January 2001. ISSN 0036-8075. doi: 10.1126/science.291.5502.280. URL http://www.ncbi.nlm.nih.gov/pubmed/11209072.

[54] S O Kelley, E M Boon, J K Barton, N M Jackson, and M G Hill. Single-base mismatch detection based on charge transduction through DNA. *Nucleic acids research*, 27(24):4830–7, December 1999. ISSN 1362-4962. URL http://www.pubmedcentral.nih.gov/articlerender.fcgi?artid=148785&tool=pmcentrez&rendertype=abstract.

[55] Shana O. Kelley, R. Erik Holmlin, Eric D. a. Stemp, and Jacqueline K. Barton. Photoinduced Electron Transfer in Ethidium-Modified DNA Duplexes: Dependence on Distance and Base Stacking. *Journal of the American Chemical Society*, 119(41):9861–9870, October 1997. ISSN 0002-7863. doi: 10.1021/ja9714651. URL http://pubs.acs.org/doi/abs/10.1021/ja9714651.

[56] Shana O. Kelley, R. Erik Holmlin, Eric D. a. Stemp, and Jacqueline K. Barton. Photoinduced Electron Transfer in Ethidium-Modified DNA Duplexes: Dependence on Distance and Base Stacking. *Journal of the American Chemical Society*, 119(41):9861–9870, October 1997. ISSN 0002-7863. doi: 10.1021/ja9714651. URL http://pubs.acs.org/doi/abs/10.1021/ja9714651.

[57] Kagan Kerman, Dilsat Ozkan, Pinar Kara, Arzum Erdem, Burcu Meric, PeterâE. Nielsen, and Mehmet Ozsoz. Label-Free Bioelectronic Detection of Point Mutation by Using Peptide Nucleic Acid Probes. *Electroanalysis*, 15(7):667–670, May 2003. ISSN 10400397. doi: 10.1002/elan.200390084. URL http://doi.wiley.com/10.1002/elan.200390084.

[58] Kagan Kerman, Yasutaka Morita, Yuzuru Takamura, Eiichi Tamiya, Kenzo Maehashi, and Kazuhiko Matsumoto. Peptide Nucleic Acid – Modified Carbon Nanotube Field-Effect Transistor for Ultra-Sensitive Real-Time Detection of DNA Hybridization. (4):65–70, 2005. doi: 10.1385/Nano.

[59] Yann-Vaï Kervennic and Sergey Kubatkin. Fabrication of clean nanogaps using a combined electrochemical-chemical method. *Small (Weinheim an der Bergstrasse, Germany)*, 5(22):2541–4, November 2009. ISSN 1613-6829. doi: 10.1002/smll.200900908. URL http://www.ncbi.nlm.nih.gov/pubmed/19714734.

[60] Ju-Hyun Kim, Hanul Moon, Seunghyup Yoo, and Yang-Kyu Choi. Nanogap electrode fabrication for a nanoscale device by volume-expanding electrochemical synthesis. *Small (Weinheim an der Bergstrasse, Germany)*, 7(15):2210–6, August 2011. ISSN 1613-6829.

doi: 10.1002/smll.201002103. URL http://www.ncbi.nlm.nih.gov/pubmed/21608123.

[61] Sang Nyon Kim, James F Rusling, and Fotios Papadimitrakopoulos. Carbon Nanotubes for Electronic and Electrochemical Detection of Biomolecules. *Advanced materials (Deerfield Beach, Fla.)*, 19(20):3214–3228, October 2007. ISSN 1521-4095. doi: 10.1002/adma.200700665. URL http://www.pubmedcentral.nih.gov/articlerender.fcgi?artid=2564812&tool=pmcentrez&rendertype=abstract.

[62] S. Komineas, G. Kalosakas, and a. Bishop. Effects of intrinsic base-pair fluctuations on charge transport in DNA. *Physical Review E*, 65(6):061905, June 2002. ISSN 1063-651X. doi: 10.1103/PhysRevE.65.061905. URL http://link.aps.org/doi/10.1103/PhysRevE.65.061905.

[63] B. Kouchmeshky, W. Aquino, J. C. Bongard, and H. Lipson. Co-evolutionary algorithm for structural damage identification using minimal physical testing. *International Journal for Numerical Methods in Engineering*, 69(5):1085–1107, January 2007. ISSN 00295981. doi: 10.1002/nme.1803. URL http://doi.wiley.com/10.1002/nme.1803.

[64] Anton Kuzyk, Bernard Yurke, J Jussi Toppari, Veikko Linko, and Päivi Törmä. Dielectrophoretic trapping of DNA origami. *Small (Weinheim an der Bergstrasse, Germany)*, 4(4):447–50, April 2008. ISSN 1613-6829. doi: 10.1002/smll.200701320. URL http://www.ncbi.nlm.nih.gov/pubmed/18350556.

[65] Sang Kyu Kim, Hyunmin Cho, Hye-Jung Park, Dohyoung Kwon, Jeong Min Lee, and Bong Hyun Chung. Nanogap biosensors for electrical and label-free detection of biomolecular interactions. *Nanotechnology*, 20(45):455502, November 2009. ISSN 1361-6528. doi: 10.1088/0957-4484/20/45/455502. URL http://www.ncbi.nlm.nih.gov/pubmed/19822932.

[66] F. D. Lewis. Distance-Dependent Electron Transfer in DNA Hairpins. *Science*, 277(5326):673–676, August 1997. ISSN 00368075. doi:

10.1126/science.277.5326.673. URL http://www.sciencemag.org/cgi/doi/10.1126/science.277.5326.673.

[67] Charles M Lieber. Nanowire nanosensors. (April):20–28, 2005.

[68] Kemp M. The monnalisa of science. *Nature*, 421:416–420, 2003.

[69] Kenzo Maehashi, Kazuhiko Matsumoto, Kagan Kerman, Yuzuru Takamura, and Eiichi Tamiya. Ultrasensitive Detection of DNA Hybridization Using Carbon Nanotube Field-Effect Transistors. *Japanese Journal of Applied Physics*, 43(No. 12A):L1558–L1560, November 2004. ISSN 0021-4922. doi: 10.1143/JJAP.43.L1558. URL http://jjap.ipap.jp/link?JJAP/43/L1558/.

[70] Klaus Mathwig and Serge G. Lemay. Mass transport in electrochemical nanogap sensors. *Electrochimica Acta*, 112:943 – 949, 2013. ISSN 0013-4686. doi: http://dx.doi.org/10.1016/j.electacta.2013.05.142. URL http://www.sciencedirect.com/science/article/pii/S0013468613011006.

[71] Sheng Meng and Efthimios Kaxiras. Interaction of DNA with CNTs : Properties and Prospects for Electronic Sequencing. pages 67–96, 2009.

[72] Vladimir M Mirsky. New electroanalytical applications of self-assembled monolayers. *TrAC Trends in Analytical Chemistry*, 21(6-7):439–450, June 2002. ISSN 01659936. doi: 10.1016/S0165-9936(02)00601-5. URL http://linkinghub.elsevier.com/retrieve/pii/S0165993602006015.

[73] S; Sundaresan A; Chen H; Jacobsen SE; Ecker JR (January 2005). Mockler, TC; Chan. Applications of dna tiling arrays for whole-genome analysis. *Genomics*, 85(1):1–15.

[74] Ioanis Katakis. Monica Mir, Srujan Kumar Dondapati, Maria Viviana Darte, Margarita Chatzichristidi, Konstantino Misiakos, Panagiola Petrou, Sotirios E. Kakabakos, Panagiotis Argitis. Electrochemical biosensor microarray funcionalized by means of biomolecules

friendly photolitography. *Biosensors and Bioelectronics*, 25(9):2115–2121, 2010.

[75] Takashi Nagase, Tohru Kubota, and Shinro Mashiko. Fabrication of nano-gap electrodes for measuring electrical properties of organic molecules using a focused ion beam. *Thin Solid Films*, 438-439:374–377, August 2003. ISSN 00406090. doi: 10.1016/S0040-6090(03)00772-7. URL http://linkinghub.elsevier.com/retrieve/pii/S0040609003007727.

[76] P. R. Nair and M. a. Alam. Performance limits of nanobiosensors. *Applied Physics Letters*, 88(23):233120, 2006. ISSN 00036951. doi: 10.1063/1.2211310. URL http://link.aip.org/link/APPLAB/v88/i23/p233120/s1&Agg=doi.

[77] Pradeep R Nair and Muhammad a Alam. Screening-limited response of nanobiosensors. *Nano letters*, 8(5):1281–5, May 2008. ISSN 1530-6984. doi: 10.1021/nl072593i. URL http://www.ncbi.nlm.nih.gov/pubmed/18386914.

[78] Abraham Nitzan and Mark a Ratner. Electron transport in molecular wire junctions. *Science (New York, N.Y.)*, 300(5624):1384–9, May 2003. ISSN 1095-9203. doi: 10.1126/science.1081572. URL http://www.ncbi.nlm.nih.gov/pubmed/12775831.

[79] M.A. O'Neill and J.K. Barton. Dna-mediated charge transport requires conformational motion of the dna bases: Elimination of charge transport in rigid glasses at 77 k. *J. Am. Chem. Soc.*, 126:13234–13235, 2004.

[80] Emil Palec. Electroactivity of Proteins : Possibilities in Biomedicine and Proteomics. 2005. doi: 10.1016/S1871-0069(05)01019-0.

[81] Emil Paleček. Fifty Years of Nucleic Acid Electrochemistry. *Electroanalysis*, 21(3-5):239–251, February 2009. ISSN 10400397. doi: 10.1002/elan.200804416. URL http://doi.wiley.com/10.1002/elan.200804416.

[82] Posthieglova I. Palecek E, Jelen F. Adsorptive transfer stripping voltammetry offers new possibilities in dna research. *Stud Biophys*, 130:51–54, 1989.

[83] So-Jung Park, T Andrew Taton, and Chad a Mirkin. Array-based electrical detection of DNA with nanoparticle probes. *Science (New York, N.Y.)*, 295(5559):1503–6, February 2002. ISSN 1095-9203. doi: 10.1126/science.1067003. URL http://www.ncbi.nlm.nih.gov/pubmed/11859188.

[84] Peng-Chung Jagjian, Tzeng-Feng Liu, Chuan-Mei Tsai, Mei-Yi Li, Ming-Shih Tsai, Shin-Hua tseng, Tsai-Mu Cheng and Chia-Ching Chang. DNA Mismatch Detection by Metal Ion Enhanced Impedance Analysis. *Chinese journal of physics vol. 47, no. 5 october 2009*, 47(5):740–747, 2009.

[85] Richard D Piner, Jin Zhu, Feng Xu, and Seunghun Hong. "Dip-Pen" Nanolithography. 283(May 1998):661–664, 1999.

[86] D Porath, a Bezryadin, S de Vries, and C Dekker. Direct measurement of electrical transport through DNA molecules. *Nature*, 403 (6770):635–8, February 2000. ISSN 0028-0836. doi: 10.1038/35001029. URL http://www.ncbi.nlm.nih.gov/pubmed/10688194.

[87] S Priyadarshy, S M Risser, and D N Beratan. S. Priyadarshy, â S. M. Risser, â¡ and D. N. Beratan* ,â . 2(96):17678–17682, 1996.

[88] Franklin R. and Gosling R.G. Molecular configuration in sodium thymonucleate. *Nature*, 171:740–741, 1953.

[89] Wilson R. The use of gold nanoparticles in diagnostics and detection. *Chem. Soc. Rev.*, 37(9):2028–2045, 2008.

[90] David L. Allara Ralph G. Nuzzo. Adsorption of bifuncional organic disulfides on gold surfacw. *Journal of American Chemical Society*, 105 (13):4481–4483, 1983.

[91] J.Jursa Retter U., Vetterl V. On the sability of condensed adsorbcion films. *Journal of Electroanalitycal Chemistry*, 274:1–9, 1989.

[92] Somenath Roy, Harindra Vedala, Aparna Datta Roy, Do-Hyun Kim, Melissa Doud, Kalai Mathee, Hoon-kyu Shin, Nobuo Shimamoto, Viswanath Prasad, and Wonbong Choi. Direct electrical measurements on single-molecule genomic DNA using single-walled carbon nanotubes. *Nano letters*, 8(1):26–30, January 2008. ISSN 1530-6984. doi: 10.1021/nl0716451. URL http://www.ncbi.nlm.nih.gov/pubmed/18052084.

[93] Somenath Roy, Xiaojun Chen, Mo-Huang Li, Yanfen Peng, Franklin Anariba, and Zhiqiang Gao. Mass-produced nanogap sensor arrays for ultrasensitive detection of DNA. *Journal of the American Chemical Society*, 131(34):12211–7, September 2009. ISSN 1520-5126. doi: 10.1021/ja901704t. URL http://www.ncbi.nlm.nih.gov/pubmed/19655794.

[94] Somenath Roy, Xiaojun Chen, Mo-Huang Li, Yanfen Peng, Franklin Anariba, and Zhiqiang Gao. Mass-produced nanogap sensor arrays for ultrasensitive detection of DNA. *Journal of the American Chemical Society*, 131(34):12211–7, September 2009. ISSN 1520-5126. doi: 10.1021/ja901704t. URL http://www.ncbi.nlm.nih.gov/pubmed/19655794.

[95] SA Ruiz and CS Chen. Microcontact printing: a tool to pattern. *Soft Matter*, 2007. doi: 10.1039/b613349e. URL http://pubs.rsc.org/en/content/articlepdf/2007/sm/b613349e.

[96] J. J. Sakurai. *Modern Quantum Mechanics.* Addison-Wesley, 1993.

[97] G B Schuster. Long-range charge transfer in DNA: transient structural distortions control the distance dependence. *Accounts of chemical research*, 33(4):253–60, April 2000. ISSN 0001-4842. URL http://www.ncbi.nlm.nih.gov/pubmed/10775318.

[98] Claus a. M. Seidel, Andreas Schulz, and Markus H. M. Sauer. Nucleobase-Specific Quenching of Fluorescent Dyes. 1. Nucleobase One-Electron Redox Potentials and Their Correlation with Static and Dynamic Quenching Efficiencies. *The Journal of Physical Chemistry*, 100(13):5541–5553, January 1996. ISSN 0022-3654. doi:

10.1021/jp951507c. URL http://pubs.acs.org/doi/abs/10.1021/jp951507c.

[99] Fangwei Shao, Katherine Augustyn, and Jacqueline K Barton. Sequence dependence of charge transport through DNA domains. *Journal of the American Chemical Society*, 127(49):17445–52, December 2005. ISSN 0002-7863. doi: 10.1021/ja0563399. URL http://www.ncbi.nlm.nih.gov/pubmed/16332096.

[100] C.F. shaw. Gold-based therapeutic agents. *Chemical reviews*, 99:2589–2600, 1999.

[101] Wei Shen, Huimin Deng, Yuqian Ren, and Zhiqiang Gao. An electronic sensor array for label-free detection of single-nucleotide polymorphisms. *Biosensors & bioelectronics*, 43:165–72, May 2013. ISSN 1873-4235. doi: 10.1016/j.bios.2012.12.025. URL http://www.ncbi.nlm.nih.gov/pubmed/23306071.

[102] John G. Simmons. Low-Voltage Current-Voltage Relationship of Tunnel Junctions. *Journal of Applied Physics*, 34(1):238, 1963. ISSN 00218979. doi: 10.1063/1.1729081. URL http://link.aip.org/link/JAPIAU/v34/i1/p238/s1&Agg=doi.

[103] John G. Simmons. Generalized Formula for the Electric Tunnel Effect between Similar Electrodes Separated by a Thin Insulating Film. *Journal of Applied Physics*, 34(6):1793, 1963. ISSN 00218979. doi: 10.1063/1.1702682. URL http://link.aip.org/link/JAPIAU/v34/i6/p1793/s1&Agg=doi.

[104] John G. Simmons. Electric Tunnel Effect between Dissimilar Electrodes Separated by a Thin Insulating Film. *Journal of Applied Physics*, 34(9):2581, 1963. ISSN 00218979. doi: 10.1063/1.1729774. URL http://link.aip.org/link/JAPIAU/v34/i9/p2581/s1&Agg=doi.

[105] Jason D Slinker, Natalie B Muren, Sara E Renfrew, and Jacqueline K Barton. DNA charge transport over 34 nm. *Nature chemistry*, 3(3):228–33, March 2011. ISSN 1755-4349. doi: 10.1038/nchem.

982. URL http://www.pubmedcentral.nih.gov/articlerender.fcgi?artid=3079570&tool=pmcentrez&rendertype=abstract.

[106] Ma Song-Shan, Xu Hui, Wang Huan-You, and Guo Rui. Characteristics of alternating current hopping conductivity in DNA sequences. *Chinese Physics B*, 18(8):3591–3596, August 2009. ISSN 1674-1056. doi: 10.1088/1674-1056/18/8/076. URL http://stacks.iop.org/1674-1056/18/i=8/a=076?key=crossref.9ae25b6d5a3227e3a9a79ca8fa057fd4.

[107] S J Sowerby, N G Holm, and G B Petersen. Origins of life: a route to nanotechnology. *Bio Systems*, 61(1):69–78, June 2001. ISSN 0303-2647. URL http://www.ncbi.nlm.nih.gov/pubmed/11448527.

[108] D I Spivey. Semiconductivity of Organic Substances. pages 1–5, 1961.

[109] Steen Steenken and Slobodan V Jovanovic. How Easily Oxidizable Is DNA ? One-Electron Reduction Potentials of Adenosine and Guanosine Radicals in Aqueous Solution. 7863(20):617–618, 1997.

[110] a. J. Storm, J. van Noort, S. de Vries, and C. Dekker. Insulating behavior for DNA molecules between nanoelectrodes at the 100 nm length scale. *Applied Physics Letters*, 79(23):3881, 2001. ISSN 00036951. doi: 10.1063/1.1421086. URL http://link.aip.org/link/APPLAB/v79/i23/p3881/s1&Agg=doi.

[111] Gemma Rius Suñé. Electron beam lithography for Nanofabrication. (January), 2008.

[112] Ya-Ping Sun, Kefu Fu, Yi Lin, and Weijie Huang. Functionalized carbon nanotubes: properties and applications. *Accounts of chemical research*, 35(12):1096–104, December 2002. ISSN 0001-4842. URL http://www.ncbi.nlm.nih.gov/pubmed/12484798.

[113] Shigeori Takenaka. Threading Intercalators as Redox Indicators. 1 (05), 2005. doi: 10.1016/S1871-0069(05)01010-4.

[114] M. L. Trouwborst, S. J. van der Molen, and B. J. van Wees. The role of Joule heating in the formation of nanogaps by electromigration. *Journal of Applied Physics*, 99(11):114316, 2006. ISSN 00218979. doi: 10.1063/1.2203410. URL http://link.aip.org/link/JAPIAU/v99/i11/p114316/s1&Agg=doi.

[115] Makusu Tsutsui, Shota Mitsuya, Shu Kurokawa, and Akira Sakai. Conductance versus bias voltage characteristics of multi-walled carbon nanotubes. *Nanotechnology*, 16(9):1863–1867, September 2005. ISSN 0957-4484. doi: 10.1088/0957-4484/16/9/074. URL http://stacks.iop.org/0957-4484/16/i=9/a=074?key=crossref.814abb6a99a1fff6509cd4f39ee2ed7d.

[116] N. J. Turro and Jacqueline K. Barton. Paradigms, supermolecules, electron transfer and chemistry at a distance. What's the problem? The science or the paradigm? *Journal of Biological Inorganic Chemistry*, 3(2):201–209, April 1998. ISSN 0949-8257. doi: 10.1007/s007750050222. URL http://www.springerlink.com/openurl.asp?genre=article&id=doi:10.1007/s007750050222.

[117] S. Tuukkanen, a. Kuzyk, J. J. Toppari, V. P. Hytönen, T. Ihalainen, and P. Törmä. Dielectrophoresis of nanoscale double-stranded DNA and humidity effects on its electrical conductivity. *Applied Physics Letters*, 87(18):183102, 2005. ISSN 00036951. doi: 10.1063/1.2117626. URL http://link.aip.org/link/APPLAB/v87/i18/p183102/s1&Agg=doi.

[118] Massimiliano Di Ventra and Michael Zwolak. DNA Electronics Proof ' s Only. 2.

[119] Ayelet Vilan. Analyzing Molecular Current-Voltage Characteristics with the Simmons Tunneling Model : Scaling and Linearization. *Journal of Physical Chemistry C*, 111(11):4431–4444, 2007.

[120] Alexander a. Voityuk, Joshua Jortner, M. Bixon, and Notker Rösch. Electronic coupling between Watson–Crick pairs for hole transfer and transport in desoxyribonucleic acid. *The Journal of Chemical Physics*, 114(13):5614, 2001. ISSN 00219606. doi: 10.1063/1.1352035.

URL http://link.aip.org/link/JCPSA6/v114/i13/p5614/s1&Agg=doi.

[121] Jiaxiong Wang. Electrical conductivity of double stranded DNA measured with ac impedance spectroscopy. *Physical Review B*, 78(24): 245304, December 2008. ISSN 1098-0121. doi: 10.1103/PhysRevB.78.245304. URL http://link.aps.org/doi/10.1103/PhysRevB.78.245304.

[122] Joseph Wang. Towards Genoelectronics: Electrochemical Biosensing of DNA Hybridization. *Chemistry - A European Journal*, 5 (6):1681–1685, June 1999. ISSN 0947-6539. doi: 10.1002/(SICI)1521-3765(19990604)5:6<1681::AID-CHEM1681>3.0.CO;2-U. URL http://doi.wiley.com/10.1002/(SICI)1521-3765(19990604)5:6<1681::AID-CHEM1681>3.0.CO;2-U.

[123] Joseph Wang. Nanoparticle-based electrochemical DNA detection. *Analytica Chimica Acta*, 500(1-2):247–257, December 2003. ISSN 00032670. doi: 10.1016/S0003-2670(03)00725-6. URL http://linkinghub.elsevier.com/retrieve/pii/S0003267003007256.

[124] Joseph Wang, Ronen Polsky, and Danke Xu. Silver-Enhanced Colloidal Gold Electrochemical Stripping Detection of DNA Hybridization. *Langmuir*, 17(19):5739–5741, September 2001. ISSN 0743-7463. doi: 10.1021/la011002f. URL http://pubs.acs.org/doi/abs/10.1021/la011002f.

[125] Leifer K Strømme M. Welch K, Blom T. Enabling measurements of low-conductance single molecules using gold nanoelectrodes. *Nanotechnology*, 22:125707, 2011.

[126] George M Whitesides, Jennah K Kriebel, and J Christopher Love. Molecular engineering of surfaces using self-assembled monolayers. *Science progress*, 88(Pt 1):17–48, January 2005. ISSN 0036-8504. URL http://www.ncbi.nlm.nih.gov/pubmed/16372593.

[127] Takano T Broka C Tanaka S Itakura K Dickerson R (1980). Wing R, Drew H. Crystal structure analysis of a complete turn of b-dna. *Nature*, 287(5784):755–8, 1980.

[128] Elicia L S Wong and J Justin Gooding. Charge transfer through DNA: A selective electrochemical DNA biosensor. *Analytical chemistry*, 78(7):2138–44, April 2006. ISSN 0003-2700. doi: 10.1021/ac0509096. URL http://www.ncbi.nlm.nih.gov/pubmed/16579591.

[129] Elicia L.S. Wong, Freya J. Mearns, and Justin J. Gooding. Further development of an electrochemical DNA hybridization biosensor based on long-range electron transfer. *Sensors and Actuators B: Chemical*, 111-112:515–521, November 2005. ISSN 09254005. doi: 10.1016/j.snb.2005.03.072. URL http://linkinghub.elsevier.com/retrieve/pii/S0925400505003229.

[130] Elicia L.S. Wong, Freya J. Mearns, and Justin J. Gooding. Further development of an electrochemical DNA hybridization biosensor based on long-range electron transfer. *Sensors and Actuators B: Chemical*, 111-112:515–521, November 2005. ISSN 09254005. doi: 10.1016/j.snb.2005.03.072. URL http://linkinghub.elsevier.com/retrieve/pii/S0925400505003229.

[131] Jie J.S. Fan X. Zapien J.A. Leung L.B. Luo L.B. Wang P.F. Lee C.S. Lee S.T. Yuan G.D., Zhang W.J. p-type zno nanowire arrays. *Nanoletters*, 8(8):2591, 2008.

[132] Yong Ju Yun, Han Young Yu, and Dong Han Ha. Measurement of electrical transport along stretched λ-DNA molecules using the four-probe method. *Current Applied Physics*, 11(5):1197–1200, September 2011. ISSN 15671739. doi: 10.1016/j.cap.2011.02.019. URL http://linkinghub.elsevier.com/retrieve/pii/S1567173911000976.

[133] Lifeng Zheng, Shengdong Li, Peter J Burke, and James P Brody. Towards Single Molecule Manipulation with Dielectrophoresis Using Nanoelectrodes. 00(3):1–4.

[134] Xiaoli Zhu, Kun Han, and Genxi Li. Magnetic nanoparticles applied in electrochemical detection of controllable DNA hybridization. *Analytical chemistry*, 78(7):2447–9, April 2006. ISSN 0003-2700. doi: 10.1021/ac051962x. URL http://www.ncbi.nlm.nih.gov/pubmed/16579633.